2006

Effects Of Atmospheric Turbulence On The Propagation Of Flattened Gaussian Optical Beams

Doris Cowan
University of Central Florida

EFFECTS OF ATMOSPHERIC TURBULENCE ON THE PROPAGATION OF FLATTENED GAUSSIAN OPTICAL BEAMS

by

DORIS COWAN
B.S. Indiana University, 1970
M.S. Butler University, 1973
M.S. University of Central Florida, 2004

A dissertation submitted in partial fulfillment of the requirements
for the degree of Doctor of Philosophy
in the Department of Mathematics
in the College of Sciences
at the University of Central Florida
Orlando, Florida

Fall Term
2006

Major Professors:
Larry C. Andrews
Cynthia Y. Young

ABSTRACT

In an attempt to mitigate the effects of the atmosphere on the coherence of an optical (laser) beam, interest has recently been shown in changing the beam shape to determine if a different power distribution at the transmitter will reduce the effects of the random fluctuations in the refractive index. Here, a model is developed for the field of a flattened Gaussian beam as it propagates through atmospheric turbulence, and the resulting effects upon the scintillation of the beam and upon beam wander are determined. A comparison of these results is made with the like effects on a standard TEM_{00} Gaussian beam. The theoretical results are verified by comparison with a computer simulation model for the flattened Gaussian beam.

Further, a determination of the probability of fade and of mean fade time under weak fluctuation conditions is determined using the widely accepted lognormal model. Although this model has been shown to be somewhat optimistic when compared to results obtained in field tests, it has value here in allowing us to compare the effects of atmospheric conditions on the fade statistics of the FGB with those of the lowest order Gaussian beam.

The effective spot size of the beam, as it compares to the spot size of the lowest order Gaussian beam, is also analyzed using Carter's definition of spot size for higher order Gaussian beams.

for Rex,
the wind beneath my wings.

ACKNOWLEDGMENTS

Funding for this research was provided by NASA through a fellowship from the Florida Space Grant Consortium.

I wish to express my sincere appreciation to Dr. Larry Andrews and to Dr. Cynthia Young for their many efforts on my behalf throughout my studies at the University of Central Florida.

TABLE OF CONTENTS

LIST OF FIGURES

LIST OF SYMBOLS

$\overline{f(x)}$	The mean of the function $f(x)$
$\langle \cdot \rangle$	Ensemble average
*	Complex conjugate
A_0	Beam amplitude
$A_n(r)$	$\sum_{n=0}^{N}\left\{\left[\frac{2iL}{k\left(1+i\alpha_N L\right)}\right]^n \frac{1}{W_{N0}^{2n}} L_n\left[\frac{ikr^2}{2L\left(1+i\alpha_N L\right)}\right]\right\}$
B_n	$\left\{\left[\frac{2iL}{k\left(1+i\alpha_N L\right)}\right]^n \frac{1}{{W_{N0}}^{2n}}\right\}$
C_n^2	Refractive index structure parameter
$d\nu\left(\mathbf{K}, z\right)$	Random amplitude of the refractive index flux
$\mathbf{E}\left(\mathbf{R}\right)$	Vector amplitude of propagating electromagnetic wave
$E_m\left(\mathbf{r}_1, \mathbf{r}_2\right), m = 1,2,3$	Second order statistical moments of the Rytov approximation
$\mathrm{erf}\,(x)$	Error function
$\exp\left(x\right)$	Exponential function
${}_1F_1\left(x\right)$	Confluent hypergeometric function
${}_2F_1\left(x\right)$	Hypergeometric function

F_0	Phase front radius of curvature at the transmitter
$F_n\left(\mathbf{K},\left\|z-z'\right\|\right)$	Two dimensional spectral density of the index of refraction
F_T	Fade threshold parameter
FGB	Flattened Gaussian beam
FSO	Free space optical system
$G\left(\mathbf{s},\mathbf{r},z\right)$	Green's function
$H_m(x)$	Hermite polynomial of order m
$I\left(x,y,z\right)$	Irradiance of the field at a point in space $\left(x,y,z\right)$
i	Imaginary unit
$J_0\left(x\right)$	Bessel function of the first kind of order zero
$\mathbf{K}$	Three dimensional wave vector defined as $\left(\mathrm{K}_x,\mathrm{K}_y,0\right)$ with $\mathrm{K}_z=0.$
k	Optical wave number, equivalent to $2\pi/\lambda$
L_0	Outer scale eddy size
l_0	Inner scale eddy size
L	Propagation distance to the receiver
$L_n\left(x\right)$	Laguerre polynomial
$n\left(\mathbf{R}\right)$	Index of refraction
$n_1\left(\mathbf{R}\right)$	Random fluctuation in the index of refraction
$p\left(L\right)$	Propagation parameter equal to $1+i\alpha L$, or $1+i\alpha_N L$ for the FGB

$p(z)$	$1+i\alpha z$ in the case of the lowest order Gaussian beam, $1+i\alpha_N z$ for the FGB
$\Pr(I \le I_T)$	Probability of fade falling below fade threshold I_T
r	Transverse distance from the beam axis
$\mathbf{r}$	Vector with length r transverse to the beam axis
$rect(x)$	Rectangle function
$R_N(L)$	$L\left(1+\frac{1}{\Lambda_{N0}^2}\right)$
$U_0(r,L)$	Free space beam field at the receiver (distance L from the transmitter), and at transverse distance r from the beam axis
$U_N(r,0)$	Field of the FGB at the transmitter.
$U_{N0}(r,L)$	Field of the FGB at a point along the free space propagation path
$U_N(r,L)$	Field of the FGB in atmospheric turbulence
W	Free space beam radius of lowest order Gaussian beam at the receiver
W_0	Beam radius (spot size) of the lowest order Gaussian beam at the transmitter
$W_N(0)$, W_{N0}	Spot size of the FGB of order N at the transmitter, equal to $\frac{W_0}{\sqrt{N+1}}$
$W_N(L)$	$W_N(0)\sqrt{1+\Lambda_{N0}^2}$
α	Propagation parameter equivalent to $2/kW_0^2 + i\,1/F_0$

α_N	Propagation parameter for the FGB, equivalent to $2/kW_{N0}^2$
$\Gamma(x)$	Gamma function
γ	Propagation path amplitude parameter equal to $\frac{p(z)}{p(L)}$
γ'	$\frac{p(z')}{p(z)} = \frac{1+i\alpha z'}{1+i\alpha z}$
δ	Kronecker delta function
∇^2	Laplacian operator
η	$\frac{1}{2}(z+z')$
Θ_0	Gaussian beam curvature parameter at the transmitter, equivalent to $1-\frac{z}{F_0}$
Θ	Gaussian beam curvature parameter at the receiver
$\bar{\Theta}_N$	Flattened Gaussian beam curvature parameter defined by $\frac{\Lambda_N^2}{1+\Lambda_N^2}$
λ	Wavelength
Λ	Fresnel ratio of the standard Gaussian beam at the receiver, equivalent to $2L/kW^2$
Λ_0	Fresnel ratio of a Gaussian beam at the transmitter, $2L/kW_0^2$
Λ_{N0}	Fresnel ratio of the FGB at the transmitter, $\frac{2L}{kW_N^2(0)}$

Λ_N	$\frac{2L}{kW_N^2}$
μ	$z - z'$
ξ	$1 - \frac{\eta}{L}$
σ_1^2	Rytov variance, equivalent to $1.23C_n^2 k^{7/6} L^{11/6}$
σ_s	Effective spot size of a FGB at the transmitter
σ_P^2	Phase variance for the standard Gaussian beam
$\sigma_{mn}(z)$	Spot size of a Laguerre-Gaussian beam of angular and radial modes *m* and *n* , respectively, at a distance *z* from the transmitter
σ_I^2	Scintillation index
ϕ_0	Beam phase
$\Phi_m(\mathbf{r}, L)$	Normalized Born approximation, defined by $\frac{U_m(\mathbf{r}, L)}{U_0(\mathbf{r}, L)}$ for the standard Gaussian beam and by $\frac{U_{Nm}(r, L)}{U_{N0}(r, L)}$ for the FGB
$\Phi_n(\mathbf{K})$	Three dimensional power spectrum at $\mathrm{K}_z = 0$.
$\Phi_N(L)$	$\tan^{-1} \Lambda_{N0}$
$\psi(\mathbf{r}, L)$	Rytov approximation of the complex phase perturbation due to turbulence

CHAPTER 1 INTRODUCTION

The atmosphere refers to the region surrounding the surface of the Earth to a distance of several hundred kilometers, and is composed of numerous elements, primarily nitrogen and oxygen, and compounds including water, carbon dioxide, carbon monoxide, nitrous oxide and ozone. All of these particles have an effect on the transmission of an optical wave through absorption, scattering, and refractive index fluctuations. Various layers of the atmosphere exhibit unique temperature, pressure, and density characteristics which play an important role in the refractive index.

One of the major functions of the atmosphere is to absorb radiation. This absorption is a function of wavelength, so that propagation of wavelengths below 0.2 μm is essentially eliminated, while propagation at visible wavelengths (between 0.4 and 0.7 μm) is almost unimpeded.

Electromagnetic radiation in the atmosphere is attenuated at visible and infrared ranges due to both absorption and scattering. If the particulates are small in comparison to the wavelength of the beam, the scattering which results is known as Rayleigh scattering. Scattering by particles which are comparable in size to the wavelength is referred to as Mie scattering while scattering by larger particles (such as raindrops) is described by geometric optics models. While Rayleigh scattering is multidirectional, the scattering produced by larger particles is concentrated in the direction of propagation.

Both absorption and scattering are deterministic effects which can be predicted, based on a variety of atmospheric conditions such as altitude, latitude, and meteorological range.

The most deleterious effects of the atmosphere on a propagating laser beam are generally caused by small random temperature fluctuations which are manifested as variations in the index of refraction. The cascade theory of turbulence, attributed to Kolmogorov, depicts turbulent air movement as a set of eddies of various sizes extending from large, L_0, called the outer scale, to small scale size, l_0, called the inner scale. In the layer of the surface up to about 100 meters, the outer scale is assumed to grow linearly with the height above the ground, while the inner scale is mere millimeters near the surface (although it can be as large as several centimeters in the upper regions of the atmosphere). As they are influenced by inertial forces, large eddies break up into smaller ones, forming a cascade of scale sizes between L_0 and l_0 known as the inertial range. Eddies smaller than l_0 are considered to be in the dissipation range. Although the cascade theory generally refers to changes in velocity, the turbulence induced by this wind speed causes a continuous mixing which results in the aforementioned index of refraction fluctuations. In the visible and near infrared regions of the spectrum, the index of refraction fluctuations are nearly exclusively caused by temperature variations resulting from this mixing.

The refractive index structure parameter, C_n^2, which is effectively constant in the case of horizontal propagation paths but which is a function of altitude in the case of vertical or slant paths, is considered to be the most critical parameter along the propagation path in characterizing the effects of atmospheric turbulence.[1] In the case of plane or spherical waves, which are limiting cases of the Gaussian beam, the Rytov

variance, $\sigma_1^2 = 1.23 C_n^2 k^{7/6} L^{11/6}$, which represents the irradiance fluctuations associated with an unbounded plane wave, determines what we consider to be weak ($\sigma_1^2 << 1$), moderate, or strong ($\sigma_1^2 > 1$) fluctuation conditions. Here $k = 2\pi/\lambda$ is the optical wave number, λ is the wavelength, L is the propagation distance, and C_n^2 is the structure constant of the index of refraction. However, in the case of the Gaussian beam wave and its variations, which we consider in this paper, this classification is not accurate. In this case, we define the weak fluctuation regime as being characterized by both $\sigma_1^2 < 1$ and $\sigma_1^2 \Lambda^{5/6} < 1$, with $\Lambda = \frac{2L}{kW^2}$ where W represents the beam radius at the receiver in the absence of turbulence. Moderate to strong conditions are marked by regimes where these parameters are both much greater than 1.

CHAPTER 2 PROPAGATION OF GAUSSIAN BEAMS

2.1 Free space Propagation

The lowest order Gaussian beam wave, TEM_{00} , propagating in free space, in the absence of atmospheric turbulence, from a transmitter located at the plane $z = 0$, is described by the equation

$$U_0(r,0) = a_0 \exp\left(-\frac{r^2}{W_0^2} - i\frac{kr^2}{2F_0}\right) \tag{2.1}$$

where a_0 represents the on-axis amplitude of the beam at the transmitter, W_0 represents the beam radius, F_0 represents the phase front radius of curvature, and $r = \sqrt{x^2 + y^2}$ gives the distance from the beam axis in the transverse direction. The beam in Equation (2.1) is often expressed in the form

$$U_0(r,0) = a_0 \exp\left(-\tfrac{1}{2}\alpha kr^2\right) \tag{2.2}$$

with

$$\alpha = \frac{2}{kW_0^2} + i\frac{1}{F_0}. \tag{2.3}$$

The phase front radius of curvature, F_0 , is infinite in the case of a collimated beam, a finite positive number in the case of a convergent beam, and a finite negative number if the beam is divergent.

From the form of the Gaussian beam wave in equation (2.1), we identify the amplitude as

$$A_0 = a_0 \exp\left(-r^2 \Big/ W_0^{\,2} \right) \tag{2.4}$$

and the phase as

$$\phi_0 = -\frac{kr^2}{2F_0} \tag{2.5}$$

Assuming that the beam originates at $z = 0$, propagates along the positive z axis, and that at any point along the propagation path the field is rotationally symmetric, then the wave equation can be expressed in terms of cylindrical coordinates as

$$\frac{1}{r}\frac{\partial}{\partial r}\left(r\frac{\partial U_0}{\partial r} \right) + \frac{\partial^2 U_0}{\partial z^2} + k^2 U_0 = 0 \tag{2.6}$$

Because the beam propagates along the *z*-axis, we can rewrite U_0 as $V(r,z)e^{ikz}$, and equation (2.6) thus becomes

$$\frac{1}{r}\frac{\partial}{\partial r}\left(r\frac{\partial V}{\partial r}\right)+\frac{\partial^2 V}{\partial z^2}+2ik\frac{\partial V}{\partial z}=0\,. \tag{2.7}$$

Since the propagation distance is much greater than the transverse spread of the wave, we can use the paraxial approximation to simplify our calculations.

Given two points in space, $\mathbf{R}=(\mathbf{r},L)$ and $\mathbf{S}=(\mathbf{s},z)$, with $\mathbf{r}$ and $\mathbf{s}$ transverse to the axis of propagation, then the distance between the points $|\mathbf{R}-\mathbf{S}|$ is

$$|\mathbf{R}-\mathbf{S}|=\left|(L-z)^2+(\mathbf{r}-\mathbf{s})^2\right|^{1/2}=|L-z|\left[1+\frac{(\mathbf{r}-\mathbf{s})^2}{(L-z)^2}\right]^{1/2}$$

(see Fig. 2.1). When the transverse distance $|\mathbf{r}-\mathbf{s}|$ is much smaller than the longitudinal separation |L-z|, the distance $|\mathbf{R}-\mathbf{S}|$ can be approximated by expanding the factor $\left[1+\frac{(\mathbf{r}-\mathbf{s})^2}{(L-z)^2}\right]^{1/2}$ in a binomial series and dropping all but the first two terms.

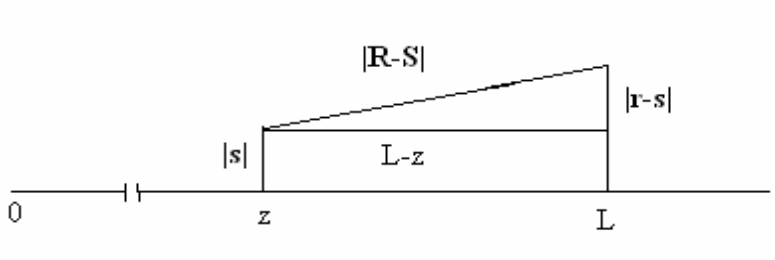

Figure 2.1 Geometry of the paraxial approximation

Hence, we have that

$$|\mathbf{R}-\mathbf{S}|\approx|L-z|+\frac{|\mathbf{r}-\mathbf{s}|^2}{2|L-z|},\quad |\mathbf{r}-\mathbf{s}|<<|L-z| \tag{2.8}$$

as a result of which we find that the second term in (2.7) is much smaller than either of the other two terms, and can thus be ignored. The result is the paraxial wave equation

$$\frac{1}{r}\frac{\partial}{\partial r}\left(r\frac{\partial V}{\partial r}\right)+2ik\frac{\partial V}{\partial z}=0\,. \tag{2.9}$$

2.2 The Huygens-Fresnel Integral

The complex amplitude of a wave at distance z from the transmitter can be represented using the Huygens-Fresnel integral:

$$U_0\left(r,z\right)=-2ik\int\int_{-\infty}^{\infty}G\left(\mathbf{s},\mathbf{r};z\right)U_0(s,0)d^2s \tag{2.10}$$

where $G\left(\mathbf{s},\mathbf{r};z\right)$ is a Green's function. For free space propagation, the Green's function is a spherical wave which can be expressed in the form

$$G\left(\mathbf{s},\mathbf{r};z\right)=\frac{1}{4\pi z}\exp\left[ikz+\frac{ik}{2z}\left|\mathbf{s}-\mathbf{r}\right|^2\right]. \tag{2.11}$$

Beginning with the equation for the Gaussian beam at $z=0$, (see equation (2.2)), we write

$$U_0(\mathbf{s},0)=a\exp\left(-\tfrac{1}{2}\alpha ks^2\right)=a\exp\left[\frac{ik}{2z}(i\alpha z)s^2\right]. \tag{2.12}$$

Substituting (2.12) into (2.10), and taking a =1 for simplicity, the complex amplitude

$$U_0(r,z) = -\frac{ik}{2\pi z}\exp\left(ikz + \frac{ik}{2z}r^2\right)\int\int_{-\infty}^{\infty}\exp\left(-\frac{ik}{z}\mathbf{r}\cdot\mathbf{s}\right)\exp\left(\frac{ik}{2z}(1+i\alpha z)s^2\right)d^2s \quad (2.13)$$

Converting to polar coordinates in the integrals, the field becomes

$$\begin{aligned} U_0(r,z) = &-\frac{ik}{2\pi z}\exp\left(ikz + \frac{ik}{2z}r^2\right) \\ &\times\int_0^{\infty}\int_0^{2\pi}\exp\left(-\frac{ik}{z}rs\cos\theta\right)\exp\left[\frac{ik}{2z}(i+i\alpha z)s^2\right]sd\theta ds \end{aligned} \quad (2.14)$$

From Appendix II in [1], using equation 9 followed by 10,

$$U_0(r,z) = \frac{1}{1+i\alpha z}\exp\left(ikz + \frac{ik}{2z}\left(\frac{i\alpha z}{1+i\alpha z}\right)r^2\right) \quad (2.15)$$

which is the complex amplitude of a Gaussian beam propagated a distance z from the transmitter through free space.

2.3 The Effect of Atmospheric Turbulence

In the presence of atmospheric turbulence, an electromagnetic wave experiences fluctuations caused by random changes in the index of refraction. Assuming sinusoidal time variations in the electric field, Maxwell's equations for the field of an electromagnetic wave hold that, for vector amplitude $\mathbf{E}(\mathbf{R})$:

$$\nabla^2\mathbf{E} + k^2 n^2(\mathbf{R})\mathbf{E} + 2\nabla[\mathbf{E}\cdot\nabla\log n(\mathbf{R})] = 0 \tag{2.16}$$

where $\mathbf{R} = (x, y, z)$ is a point in space, and $n(\mathbf{R})$ is the index of refraction. Since the beam is contained in a narrow cone in the direction of propagation, we can ignore the last term in the equation, simplifying (2.16) to

$$\nabla^2\mathbf{E} + k^2 n^2(\mathbf{R})\mathbf{E} = 0\,. \tag{2.17}$$

Decomposing the remaining terms into the 3 scalar equations composing **E**, and letting U(**R**) be one of the scalar equations transverse to the direction of propagation ,

$$\nabla^2 U + k^2 n^2(\mathbf{R})U = 0 \tag{2.18}$$

In order to solve this equation, which cannot be solved in closed form due to the random nature of $n(\mathbf{R})$, it is standard practice to introduce one of two perturbation theories.

2.4 Solution by the Born Approximation

For an optical wave propagating along the positive z-axis at a distance $z = L$ from the source, the optical field is represented by $U(\mathbf{R}) = U_0(\mathbf{R}) + U_1(\mathbf{R}) + U_2(\mathbf{R}) + \ldots$, where $U_0(\mathbf{R})$ is the unperturbed portion of the field (the field in the absence of turbulence), and $U_1(\mathbf{R})$ represents the first order perturbations , $U_2(\mathbf{R})$, the second order perturbations, and so forth, caused by random inhomogeneities in the atmosphere.

The index of refraction in equation (2.18), can be expressed as $n(\mathbf{R}) \approx 1 + n_1(\mathbf{R})$, where $\overline{n(\mathbf{R})} \approx 1$ and $n_1(\mathbf{R})$ is a small random variable with mean 0. Neglecting $n_1^2(\mathbf{R})$ as insignificant compared to $n_1(\mathbf{R})$, we can then approximate $n^2(\mathbf{R}) \approx 1 + 2n_1(\mathbf{R})$. Assuming weak fluctuations, where propagation lengths are generally less than a few hundred meters, we can substitute this into (2.18), yielding the following set of equations:

$$\nabla^2 U + k^2[1 + 2n_1(\mathbf{R})]U = 0$$

$$\nabla^2 U + k^2 U + 2k^2 n_1(\mathbf{R})U = 0$$

$$\nabla^2 \left(U_o + U_1 + U_2 + \ldots\right) + k^2 \left(U_o + U_1 + U_2 + \ldots\right) + 2k^2 n_1(\mathbf{R})\left(U_o + U_1 + U_2 + \ldots\right) = 0 \qquad (2.19)$$

$$\left(\nabla^2 U_o + \nabla^2 U_1 + \nabla^2 U_2 + \ldots\right) + \left(k^2 U_o + k^2 U_1 + k^2 U_2 + \ldots\right) + \left(2k^2 n_1(\mathbf{R})U_o + 2k^2 n_1(\mathbf{R})U_1 + 2k^2 n_1(\mathbf{R})U_2 + \ldots\right) = 0 .$$

Equating terms of the same order gives the following set of equations:

$$\nabla^2 U_o + k^2 U_o = 0$$

$$\nabla^2 U_1 + k^2 U_1 = -2k^2 n_1(\mathbf{R}) U_o \qquad (2.20)$$

$$\nabla^2 U_2 + k^2 U_2 = -2k^2 n_1(\mathbf{R}) U_1$$

The solution of the first of these equations is simply $U_0(\mathbf{R})$.

Solving the second equation using the method of Green's function,

$$U_1(\mathbf{R}) = \iiint_V G(\mathbf{S},\mathbf{R})[2k^2 n_1(\mathbf{S}) U_o(\mathbf{S})] d^3S$$

$$U_1(\mathbf{R}) = 2k^2 \iiint_V G(\mathbf{S},\mathbf{R})[n_1(\mathbf{S}) U_o(\mathbf{S})] d^3S\ , \qquad (2.21)$$

where $G(\mathbf{S},\mathbf{R}) = \dfrac{1}{4\pi|\mathbf{R}-\mathbf{S}|}\exp(ik|\mathbf{R}-\mathbf{S}|)$. Equation (2.21) thus describes $U_1(\mathbf{R})$ as a sum of spherical waves generated at various points **S** throughout the "scattering volume" V. Because the scattering angle is very small we can use the paraxial approximation (2.8) in the expression of the Green's function in (2.21), and

$$\begin{aligned} U_1(\mathbf{r},L) &= \frac{2k^2}{4\pi}\iiint_V \frac{1}{(L-z)}\exp\left[ik(L-z)+\frac{ik|\mathbf{r}-\mathbf{s}|^2}{2(L-z)}\right] n_1(\mathbf{s}) U_0(\mathbf{s}) d^3s \\ &= \frac{k^2}{2\pi}\int_0^L dz \int_{-\infty}^{\infty}\int d^2s \exp\left[ik(L-z)+\frac{ik|\mathbf{r}-\mathbf{s}|^2}{2(L-z)}\right]\frac{n_1(\mathbf{s},z)}{(L-z)} U_0(\mathbf{s},z). \end{aligned} \qquad (2.22)$$

$\langle U_1(\mathbf{r},L)\rangle$ will be equal to zero since $\langle n_1(\mathbf{s},z)\rangle = 0$ by definition.

Solving for $U_m(\mathbf{r},L)$, m = 2,3,4,…, will yield a similar result, with $U_0(\mathbf{s},z)$ replaced by $U_{m-1}(\mathbf{s},z)$. Generally, however, $\langle U_m(\mathbf{r},L)\rangle$ will not be zero for $m>1$.

2.5 The Rytov Approximation

Representing the field of the electromagnetic wave in terms of multiplicative rather than additive perturbations, we write $U(\mathbf{R}) = U(\mathbf{r},L) = U_0(\mathbf{r},L)\exp\left[\psi(\mathbf{r},L)\right]$, where ψ is the complex phase perturbation due to turbulence equal to $\psi(\mathbf{r},L) = \psi_1(\mathbf{r},L) + \psi_2(\mathbf{r},L) + \ldots$. We define ψ_1 as the first order complex phase perturbation, ψ_2 as the second order complex phase perturbation, and so forth. Relating these perturbations to the Born approximations just defined, we first let $\Phi_m(\mathbf{r},L) = \dfrac{U_m(\mathbf{r},L)}{U_0(\mathbf{r},L)}$ be the normalized Born approximation. Equating the first order terms for the Born and Rytov approximations, we have

$$U_0(\mathbf{r},L)\exp\left[\psi_1(\mathbf{r},L)\right] = U_0(\mathbf{r},L) + U_1(\mathbf{r},L). \tag{2.23}$$

Dividing by $U_o(\mathbf{r},L)$, this becomes $\exp\left[\psi_1(\mathbf{r},L)\right] = 1 + \dfrac{U_1(\mathbf{r},L)}{U_0(\mathbf{r},L)}$. Taking the natural logarithm, we find that in the first order the Rytov and Born approximations are equal:

$$\psi_1(\mathbf{r},L) = \ln\left[1+\Phi_1(\mathbf{r},L)\right] \approx \Phi_1(\mathbf{r},L) \text{ when } \left|\Phi_1(\mathbf{r},L)\right| << 1 \tag{2.24}$$

where $\Phi_1(\mathbf{r},L)$ is defined by

$$\Phi_1(\mathbf{r},L) = \frac{U_1(\mathbf{r},L)}{U_0(\mathbf{r},L)} = \frac{k^2}{2\pi}\int_0^L dz \int_{-\infty}^{\infty}\int d^2s \exp\left[ik\left(L-z\right) + \frac{ik\left|\mathbf{r}-\mathbf{s}\right|^2}{2\left(L-z\right)}\right]\frac{n_1\left(\mathbf{s},z\right)}{\left(L-z\right)}\frac{U_0\left(\mathbf{s},z\right)}{U_0(\mathbf{r},L)}. \tag{2.25}$$

$U_0(\mathbf{r},L)$ is the field at the receiver ($z = L$), and $U_0(\mathbf{s},z)$ is the field at some arbitrary point along the propagation path.

Equating the second order terms of the Born and Rytov approximations, we have

$$U_0\left(\mathbf{r},L\right)\exp\left[\psi_1\left(\mathbf{r},L\right)+\psi_2\left(\mathbf{r},L\right)\right] = U_0\left(\mathbf{r},L\right)\left[1+\Phi_1\left(\mathbf{r},L\right)+\Phi_2\left(\mathbf{r},L\right)\right] \tag{2.26}$$

and hence, $\psi_1\left(\mathbf{r},L\right)+\psi_2\left(\mathbf{r},L\right) = \ln\left[1+\Phi_1\left(\mathbf{r},L\right)+\Phi_2\left(\mathbf{r},L\right)\right]$. Using a Maclaurin series expansion for the function on the right hand side,

$$\left[\psi_1(\mathbf{r},L)+\psi_2(\mathbf{r},L)\right] \approx \Phi_1(\mathbf{r},L)+\Phi_2(\mathbf{r},L)-\tfrac{1}{2}\Phi_1^2(\mathbf{r},L), \quad \Phi_1(\mathbf{r},L) << 1, \Phi_2(\mathbf{r},L) << 1 \tag{2.27}$$

Since it was previously shown that $\psi_1\left(\mathbf{r},L\right) = \Phi_1\left(\mathbf{r},L\right)$, we can then approximate $\psi_2\left(\mathbf{r},L\right) = \Phi_2\left(\mathbf{r},L\right) - \tfrac{1}{2}\Phi_1^2\left(\mathbf{r},L\right)$. From the Born approximation for $U_m(\mathbf{r},L)$, we know that

$$U_2(\mathbf{r},L)=\frac{k^2}{2\pi}\int_0^L dz\int_{-\infty}^{\infty}\int d^2s\exp\left[ik(L-z)+\frac{ik\left|\mathbf{r}-\mathbf{s}\right|^2}{2(L-z)}\right]\frac{n_1(\mathbf{s},z)}{(L-z)}U_1(\mathbf{s},z) \tag{2.28}$$

$$\Phi_2(\mathbf{r},L)=\frac{k^2}{2\pi}\int_0^L dz\int_{-\infty}^{\infty}\int d^2s\exp\left[ik\left(L-z\right)+\frac{ik\left|\mathbf{r}-\mathbf{s}\right|^2}{2\left(L-z\right)}\right]\frac{n_1\left(\mathbf{s},z\right)}{\left(L-z\right)}\frac{U_1\left(\mathbf{s},z\right)}{U_0(\mathbf{r},L)} \tag{2.29}$$

and so,

$$\Phi_2(\mathbf{r},L)=\frac{k^2}{2\pi}\int_0^L dz\int_{-\infty}^{\infty}\int d^2s\exp\left[ik\left(L-z\right)+\frac{ik\left|\mathbf{r}-\mathbf{s}\right|^2}{2\left(L-z\right)}\right]\frac{n_1\left(\mathbf{s},z\right)}{\left(L-z\right)}\frac{U_0\left(\mathbf{s},z\right)\Phi_1\left(\mathbf{s},z\right)}{U_0(\mathbf{r},L)} \tag{2.30}$$

since $\dfrac{U_1\left(\mathbf{s},z\right)}{U_0\left(\mathbf{s},z\right)}=\Phi_1\left(\mathbf{s},z\right)$.

2.6 First Order Spectral Representations

In order to develop spectral representations of the Born and Rytov approximations, we first write the equation of the index of refraction in the form of a two dimensional Riemann-Stieltjes integral

$$n_1(\mathbf{s},z)=\int_{-\infty}^{\infty}\int\exp(i\mathbf{K}\cdot\mathbf{s})dv(\mathbf{K},z) \tag{2.31}$$

where $dv(\mathbf{K}, z)$ is the random amplitude of the refractive index flux and $\mathbf{K} = \left(\mathrm{K}_x, \mathrm{K}_y, 0\right)$ is the 3-D wave vector with $\mathrm{K}_z = 0$.

Equation (2.31) assumes the wave is homogeneous and isotropic in the plane transverse to the direction of propagation. To determine the first order spectral representation, the unperturbed field Gaussian beam $U_0\left(\mathbf{r}, L\right)$ at propagation distance L from the source, given in equation (2.15), is expressed as

$$U_0\left(\mathbf{r}, L\right) = \frac{1}{p(L)} \exp\left[ikL - \frac{\alpha k r^2}{2p(L)}\right] \tag{2.32}$$

where $p(L) = 1 + i\alpha L, \quad \alpha = \frac{2}{kW_0^2} + i\frac{1}{F_0}$, W_o is the beam radius and F_o is the phase front radius of curvature at $z = 0$. From this we can determine

$$\frac{U_0(\mathbf{s}, z)}{U_0(\mathbf{r}, L)} = \frac{p(L)}{p(z)} \exp[ik(z-L)] \exp\left(-\frac{\alpha k s^2}{2p(z)}\right) \exp\left(\frac{\alpha k r^2}{2p(L)}\right). \tag{2.33}$$

If we now substitute (2.33) and (2.31) into (2.25), we will have, after changing the order of the integration and combining the like exponential terms

$$\begin{aligned} \Phi_1(\mathbf{r}, L) = \frac{k^2}{2\pi} \int_0^L dz \int_{-\infty}^{\infty} \int \frac{dv(\mathbf{K}, z)}{(L-z)} \frac{p(L)}{p(z)} \exp\left(\frac{\alpha k r^2}{2p(L)}\right) \\ \times \int_{-\infty}^{\infty} \int \exp\left[\frac{ik\left|\mathbf{r} - \mathbf{s}\right|^2}{2(L-z)}\right] \exp\left(-\frac{\alpha k s^2}{2p(z)}\right) \exp\left(i\mathbf{K}\cdot\mathbf{s}\right) d^2 s \end{aligned} \tag{2.34}$$

Letting $\gamma = \dfrac{p(z)}{p(L)}$ and $\dfrac{ik\left|\mathbf{r}-\mathbf{s}\right|^2}{2(L-z)} = \dfrac{iks^2}{2(L-z)} + \dfrac{ikr^2}{2(L-z)} - \dfrac{2ik\mathbf{s}\cdot\mathbf{r}}{2(L-z)}$, we have

$$\begin{aligned}\Phi_1(\mathbf{r},L) = \frac{k^2}{2\pi}\int_0^L dz \int_{-\infty}^{\infty}\int \frac{dv(\mathbf{K},z)}{\gamma(L-z)}\exp\left(\frac{kr^2}{2}\frac{\alpha(L-z)+ip(L)}{(L-z)p(L)}\right) \\ \times \int_{-\infty}^{\infty}\int \exp(i\mathbf{K}\cdot\mathbf{s})\exp\left(\frac{ks^2}{2}\frac{-\alpha(L-z)+ip(z)}{(L-z)p(z)}\right)\exp\left[\frac{-ik\mathbf{r}\cdot\mathbf{s}}{L-z}\right]d^2s\end{aligned} \tag{2.35}$$

By replacing $p(z) = 1 + i\alpha z$ and $p(L) = 1 + i\alpha L$, (2.35) becomes

$$\begin{aligned}\Phi_1(\mathbf{r},L) = \frac{k^2}{2\pi}\int_0^L dz \int_{-\infty}^{\infty}\int \frac{dv(\mathbf{K},z)}{\gamma(L-z)}\exp\left(\frac{ikr^2}{2}\frac{\gamma}{(L-z)}\right) \\ \times \int_{-\infty}^{\infty}\int \exp(i\mathbf{K}\cdot\mathbf{s})\exp\left(\frac{iks^2}{2}\frac{1}{\gamma(L-z)}\right)\exp\left[\frac{-ik\mathbf{r}\cdot\mathbf{s}}{L-z}\right]d^2s.\end{aligned} \tag{2.36}$$

We then arrive at the following expression for $\Phi_1(\mathbf{r},L)$:

$$\begin{aligned}\Phi_1(\mathbf{r},L) = \frac{k^2}{2\pi}\int_0^L dz \int_{-\infty}^{\infty}\int \frac{dv(\mathbf{K},z)}{\gamma(L-z)}\exp\left(\frac{ikr^2\gamma}{2(L-z)}\right) \\ \times \int_{-\infty}^{\infty}\int \exp\left[i\left(\mathbf{K}-\frac{k\mathbf{r}}{L-z}\right)\cdot\mathbf{s}\right]\exp\left(\frac{iks^2}{2\gamma(L-z)}\right)d^2s.\end{aligned} \tag{2.37}$$

Evaluating the second integral in (2.37), and simplifying according to Appendix II in [1],

$$\int_{-\infty}^{\infty}\int \exp\left[i\left(\mathbf{K} - \frac{k\mathbf{r}}{L-z} \right)\cdot \mathbf{s} \right] \exp\left[\frac{iks^2}{2\gamma(L-z)} \right] d^2 s$$
$$= \frac{2\pi i\gamma\left(L-z\right)}{k} \exp\left\{ \frac{-i\gamma}{2}\left[\frac{\left(L-z\right)\mathrm{K}^2}{k} + \frac{kr^2}{(L-z)} - 2\mathbf{K}\cdot\mathbf{r} \right] \right\} \tag{2.38}$$

We can substitute (2.38) into (2.37) to obtain

$$\Phi_1\left(\mathbf{r},L\right) = ik\int_0^L dz \int_{-\infty}^{\infty}\int d\nu\left(\mathbf{K},z\right) \exp\left[\frac{-i\gamma\left(L-z\right)\mathrm{K}^2}{2k} \right] \exp\left(i\gamma\mathbf{K}\cdot\mathbf{r}\right). \tag{2.39}$$

2.7 Second Order Spectral Representations

From equation (2.30), we have

$\Phi_2(\mathbf{r},L) = \frac{k^2}{2\pi}\int_0^L dz \int_{-\infty}^{\infty}\int d^2 s \exp\left[ik\left(L-z\right) + \frac{ik\left|\mathbf{r}-\mathbf{s}\right|^2}{2\left(L-z\right)} \right] \frac{n_1\left(\mathbf{s},z\right)}{\left(L-z\right)} \frac{U_0\left(\mathbf{s},z\right)\Phi_1\left(\mathbf{s},z\right)}{U_0(\mathbf{r},L)}$, into

which we substitute equations (2.31), (2.33), and (2.39). This results in

$$\Phi_2(\mathbf{r},L) = \frac{k^2}{2\pi}\int_0^L dz \int_{-\infty}^{\infty}\int d^2 s \exp\left[ik\left(L-z\right) + \frac{iks^2}{2\left(L-z\right)} + \frac{ikr^2}{2\left(L-z\right)} - \frac{ik\mathbf{r}\cdot\mathbf{s}}{\left(L-z\right)} \right]$$
$$\times \frac{1}{\left(L-z\right)} \frac{p\left(L\right)}{p\left(z\right)} \exp\left[ik\left(z-L\right) \right] \exp\left[-\frac{\alpha ks^2}{2p\left(z\right)} \right] \exp\left[\frac{\alpha kr^2}{2p\left(L\right)} \right] \tag{2.40}$$
$$\times \int_{-\infty}^{\infty}\int \exp\left(i\mathbf{K}\cdot\mathbf{s}\right) d\nu\left(\mathbf{K},z\right) ik\int_0^z dz' \int_{-\infty}^{\infty}\int d\nu\left(\mathbf{K}',z'\right) \exp\left[\frac{-i\gamma\left(z-z'\right)\mathrm{K}^2}{2k} \right] \exp\left(i\gamma'\mathbf{K}'\cdot\mathbf{s}\right)$$

where $\gamma' = \dfrac{p(z')}{p(z)} = \dfrac{1+i\alpha z'}{1+i\alpha z}$.

Equation (2.40) simplifies to

$$\begin{aligned}\Phi_2(\mathbf{r},L) = {} & \frac{ik^3}{2\pi}\int_0^L dz \int_0^z dz' \int_{-\infty}^{\infty}\int\int_{-\infty}^{\infty}\int d\nu(\mathbf{K},z)\,d\nu(\mathbf{K}',z') \\ & \times \exp\left[\frac{-i\gamma(z-z')\mathrm{K}'^2}{2k}\right]\frac{1}{\gamma(L-z)}\exp\left[\frac{\alpha k r^2}{2p(L)}\right]\exp\left[\frac{ikr^2}{2(L-z)}\right] \\ & \times \int_{-\infty}^{\infty}\int d^2s \exp\left[\frac{iks^2}{2(L-z)}\right]\exp\left[-\frac{\alpha k s^2}{2p(z)}\right]\exp\left[-\frac{ik\mathbf{r}\cdot\mathbf{s}}{(L-z)}\right]\exp\left(i\gamma'\mathbf{K}'\cdot\mathbf{s}\right)\exp\left(i\mathbf{K}\cdot\mathbf{s}\right)\end{aligned} \tag{2.41}$$

We can combine the exponentials to obtain

$$\exp\left[\frac{\alpha k r^2}{2p(L)}\right]\exp\left[\frac{ikr^2}{2(L-z)}\right] = \exp\left[\frac{ir^2k\gamma}{2(L-z)}\right] \tag{2.42}$$

and similarly,

$$\exp\left[\frac{iks^2}{2(L-z)}\right]\exp\left[-\frac{\alpha k s^2}{2p(z)}\right] = \exp\left[\frac{iks^2}{2\gamma(L-z)}\right]. \tag{2.43}$$

Hence equation (2.41) becomes, upon substitution of (2.42) and(2.43)

$$\begin{aligned}\Phi_2(\mathbf{r},L) = {} & \frac{ik^3}{2\pi}\int_0^L dz \int_0^z dz' \int_{-\infty}^{\infty}\int\int_{-\infty}^{\infty}\int \frac{d\nu(\mathbf{K},z)\,d\nu(\mathbf{K}',z')}{\gamma(L-z)}\exp\left[\frac{ikr^2\gamma}{2(L-z)} - \frac{i\gamma'\mathrm{K}'^2}{2k}(z-z')\right] \\ & \times \int_{-\infty}^{\infty}\int d^2s \exp\left[\frac{iks^2}{2\gamma(L-z)}\right]\exp\left\{i\mathbf{s}\cdot\left[\mathbf{K}+\gamma'\mathbf{K}' - \frac{k\mathbf{r}}{(L-z)}\right]\right\}\end{aligned} \tag{2.44}$$

We can evaluate the innermost integral in equation (2.44) in the same way that we evaluated the second integral in (2.37), and thus rewrite

$$\int_{-\infty}^{\infty}\int d^2 s \exp\frac{iks^2}{2\gamma(L-z)}\exp\left\{i\mathbf{s}\cdot\left[\mathbf{K}+\gamma'\mathbf{K}'-\frac{k\mathbf{r}}{(L-z)}\right]\right\}$$
$$= 2\pi\frac{i\gamma(L-z)}{k}\exp\left\{-\frac{i\gamma(L-z)\left[\mathbf{K}+\gamma'\mathbf{K}'-\frac{k\mathbf{r}}{(L-z)}\right]^2}{2k}\right\} \tag{2.45}$$

Replacing (2.45) into (2.44) results in

$$\Phi_2(\mathbf{r},L) = -k^2\int_0^L dz\int_0^z dz'\int_{-\infty}^{\infty}\int\int_{-\infty}^{\infty}\int d\nu(\mathbf{K},z)d\nu(\mathbf{K}',z')$$
$$\times\exp\left[i\gamma\left(\mathbf{K}+\gamma'\mathbf{K}'\right)\cdot\mathbf{r}-\frac{i\gamma\left|\mathbf{K}+\gamma'\mathbf{K}'\right|^2}{2k}(L-z)-\frac{i\gamma'\kappa'^2}{2k}(z-z')\right]. \tag{2.46}$$

2.8 Statistical Moments of the Rytov Approximations

For any two points, $\mathbf{r}_1$ and $\mathbf{r}_2$, on the transverse plane at $z=L$, the three second order statistical moments are defined by:

$$E_1(\mathbf{r},\mathbf{r}) = \left\langle\Phi_2(\mathbf{r},L)\right\rangle = \left\langle\psi_2(\mathbf{r},L)\right\rangle + \tfrac{1}{2}\left\langle\psi_1^2(\mathbf{r},L)\right\rangle,$$
$$E_2(\mathbf{r}_1,\mathbf{r}_2) = \left\langle\Phi_1(\mathbf{r}_1,L)\Phi_1{}^*(\mathbf{r}_2,L)\right\rangle = \left\langle\psi_1(\mathbf{r}_1,L)\right\rangle\left\langle\psi_1{}^*(\mathbf{r}_2,L)\right\rangle, \tag{2.47}$$
$$E_3(\mathbf{r}_1,\mathbf{r}_2) = \left\langle\Phi_1(\mathbf{r}_1,L)\Phi_1(\mathbf{r}_2,L)\right\rangle = \left\langle\psi_1(\mathbf{r}_1,L)\right\rangle\left\langle\psi_1(\mathbf{r}_2,L)\right\rangle$$

These moments are used to calculate all the statistical quantities of interest. Working first with $E_2(\mathbf{r}_1,\mathbf{r}_2)$, we have, upon substitution of (2.39) into (2.47)

$$E_2\left(\mathbf{r}_1,\mathbf{r}_2\right)=k^2\int_0^L dz\int_0^L dz'\int_{-\infty}^{\infty}\int\int\int\left\langle d\nu(\mathbf{K},z)d\nu^*(\mathbf{K}',z')\right\rangle$$
$$\times\exp\left[i\gamma(z)\mathbf{K}\cdot\mathbf{r}_1-i\gamma^*(z')\mathbf{K}'\cdot\mathbf{r}_2-\frac{i\kappa^2\gamma(z)}{2k}\left(L-z\right)+\frac{i\kappa^2\gamma^*(z')}{2k}\left(L-z'\right)\right] \tag{2.48}$$

.

Now, we use the relationship

$$\left\langle d\nu\left(\mathbf{K},z\right)d\nu^*\left(\mathbf{K}',z'\right)\right\rangle=F_n\left(\mathbf{K},\left|z-z'\right|\right)\delta\left(\mathbf{K}-\mathbf{K}'\right)d^2\kappa d^2\kappa' \tag{2.49}$$

where δ represents the Kronecker delta function, and $F_n\left(\mathbf{K},\left|z-z'\right|\right)\equiv F_n\left(\kappa_x,\kappa_y,0,\left|z-z'\right|\right)$ is a two-dimensional spectral density of the index of refraction, which has an appreciable value only when $\left|z-z'\right|$ is close to zero.

The three dimensional power spectrum obeys the relation

$$F_n\left(\kappa_x,\kappa_y,0,\left|\mu\right|\right)=\int_{-\infty}^{\infty}\Phi_n\left(\kappa_x,\kappa_y,\kappa_z\right)\cos\left(\mu\kappa_z\right)d\kappa_z \tag{2.50}$$

Performing an inverse Fourier transform on (2.50), we have

$$\Phi_n\left(\kappa_x,\kappa_y,\kappa_z\right)=\frac{1}{2\pi}\int_{-\infty}^{\infty}F_n\left(\kappa_x,\kappa_y,0,\left|\mu\right|\right)\cos\left(\mu\kappa_z\right)d\mu \tag{2.51}$$

which gives

$$\int_{-\infty}^{\infty}F_n\left(\mathbf{K},\left|\mu\right|\right)d\mu=2\pi\Phi_n\left(\kappa_x,\kappa_y,0\right)=2\pi\Phi_n\left(\mathbf{K}\right) \tag{2.52}$$

for $\kappa_z=0$.

Letting $z-z'=\mu,$ and $\eta=\frac{1}{2}\left(z+z'\right)$ gives

$$\begin{aligned}&\int_0^L dz\int_0^L dz'F_n\left(\mathbf{K},\left|z-z'\right|\right)\exp\left\{-\frac{i\kappa^2}{2k}\left[\gamma(z)(L-z)-\gamma^*(z')(L-z')\right]\right\}\\&\quad=\int_0^L d\eta\int_{-\infty}^{\infty}d\mu\,F_n\left(\mathbf{K},\left|\mu\right|\right)\exp\left\{-\frac{i\kappa^2}{2k}\left[\left(\gamma-\gamma^*\right)(L-z')\right]\right\}\end{aligned} \tag{2.53}$$

where we have used the fact that, since $z-z'$ (and therefore μ) is of significant value only near zero, we can extend the limits of integration without appreciably changing the result. Further, we have used the approximations $z\approx z'\approx\eta$. Substituting (2.52) into (2.53), we can rewrite (2.53) as:

$$\begin{aligned}&\int_0^L d\eta\int_{-\infty}^{\infty}d\mu F_n\left(\mathbf{K},\left|\mu\right|\right)\exp\left[-\frac{i\kappa^2}{2k}\left(\gamma-\gamma^*\right)\left(L-\eta\right)\right]\\&\quad=2\pi\int_0^L d\eta\,\Phi_n\left(\mathbf{K}\right)\exp\left[-\frac{i\kappa^2}{2k}\left(\gamma-\gamma^*\right)\left(L-\eta\right)\right]\end{aligned} \tag{2.54}$$

Substituting (2.54) as well as the results of (2.49) and (2.52) into equation (2.48) gives

$$E_2(\mathbf{r}_1,\mathbf{r}_2)=2\pi k^2\int_0^L d\eta\int_{-\infty}^{\infty}\int d^2\kappa\,\Phi_n(\mathbf{K})\exp\left[i\mathbf{K}\cdot\left(\gamma\mathbf{r}_1-\gamma^*\mathbf{r}_2\right)-\frac{i\kappa^2}{2k}\left(\gamma-\gamma^*\right)\left(L-\eta\right)\right]. \quad (2.55)$$

In order to determine $E_3(\mathbf{r}_1,\mathbf{r}_2)$ from equation (2.47), we write

$$\begin{aligned}E_3\left(\mathbf{r}_1,\mathbf{r}_2\right)=&-k^2\int_0^L dz\int_0^L dz'\int_{-\infty}^{\infty}\int\int_{-\infty}^{\infty}\int\left\langle d\nu(\mathbf{K},z)d\nu\left(\mathbf{K}',z'\right)\right\rangle\\&\times\exp\left[i\gamma(z)\mathbf{K}\cdot\mathbf{r}_1-i\gamma(z')\mathbf{K}'\cdot\mathbf{r}_2-\frac{i\kappa^2\gamma(z)}{2k}\left(L-z\right)-\frac{i\kappa^2\gamma(z')}{2k}\left(L-z'\right)\right]\end{aligned} \quad (2.56)$$

and use the fact that n_1 is a real function to equate $d\nu\left(\mathbf{K}',z'\right)$ with $d\nu^*\left(-\mathbf{K}',z'\right)$ and thus, from the relationship in (2.49), determine that

$$\left\langle d\nu\left(\mathbf{K},z\right)d\nu\left(\mathbf{K}',z'\right)\right\rangle=F_n\left(\mathbf{K},\left|z-z'\right|\right)\delta\left(\mathbf{K}+\mathbf{K}'\right)d^2\kappa d^2\kappa' \quad (2.57)$$

Making the same variable changes to μ and η as in(2.54), we see that

$$E_3(\mathbf{r}_1,\mathbf{r}_2)=-2\pi k^2\int_0^L d\eta\int_{-\infty}^{\infty}\int d^2\kappa\,\Phi_n(\mathbf{K})\exp\left[i\gamma\mathbf{K}\cdot\left(\mathbf{r}_1-\mathbf{r}_2\right)-\frac{i\kappa^2\gamma}{2k}\left(L-\eta\right)\right] \quad (2.58)$$

Finally, the first statistical moment in (2.47) can be determined with the aid of (2.46), so that

$$E_1(\mathbf{r},\mathbf{r}) = \left\langle \Phi_2(\mathbf{r},L)\right\rangle = -k^2 \int_0^L dz \int_0^z dz' \int_{-\infty}^{\infty}\int\int\int \left\langle d\nu(\mathbf{K},z) d\nu(\mathbf{K}',z')\right\rangle$$
$$\times \exp\left[i\gamma\left(\mathbf{K}+\gamma'\mathbf{K}'\right)\cdot\mathbf{r} - \frac{i\gamma\left|\mathbf{K}+\gamma'\mathbf{K}'\right|^2}{2k}(L-z) - \frac{i\gamma'\kappa'^2}{2k}(z-z')\right] \tag{2.59}$$

Using the relationship found in (2.57), and estimating $\gamma' \approx 1$, we can reduce (2.59) to

$$E_1(\mathbf{r},\mathbf{r}) = -\pi k^2 \int_0^L d\eta \int_{-\infty}^{\infty}\int d^2\kappa \Phi_n(\mathbf{K}). \tag{2.60}$$

Because E_1 does not depend upon **r,** we also have that $E_1(\mathbf{r},\mathbf{r}) = E_1(0,0)$.

CHAPTER 3 OTHER BEAM SHAPES

A variety of techniques has been investigated in order to overcome the effects of atmospheric turbulence. Recently, the investigation into the effect of turbulence on the shape of the beam has been of increasing interest. A wide variety of beam shapes has been considered, including Gaussian [1], Hermite-Gaussian[3,5,6], off-axis Hermite-Gaussian[3], Hermite-cosh-Gaussian [3], cosh(sinh)-Gaussian [4], cosh(sinh), cosine(sine), Bessel, annular, Laguerre-Gaussian[6,8], Super Gaussian, and Flattened Gaussian beams.

3.1 Hermite-Sinusoidal-Gaussian Beams

The propagation of the general classification of Hermite-Sinusoidal-Gaussian beams in free space, in the absence of atmospheric turbulence, as well as some special cases of these beams under the effect of turbulence, has been examined by Baykal [3,4], who developed log-amplitude and phase correlation and structure functions to evaluate whether these beams, under specific parameters, could be helpful in mitigating the effects of turbulence.

Baykal begins with an off-axis Hermite-Gaussian beam, whose field at the transmitter is defined by

$$U_{n,m}^{OA}\left(s_x, s_y, 0\right) = A_{n,m} H_n\left(a_x s_x + b_x\right) H_m\left(a_y s_y + b_y\right) \times \exp\left[-\tfrac{1}{2} k\left(a_x {s_x}^2 + a_y {s_y}^2\right)\right] \exp\left[-i\left(V_x s_x + V_y s_y\right)\right] \exp\left(-i\varphi\right) \tag{3.1}$$

in which $A_{n,m}$ is the amplitude of the field at the origin of the source plane, H_m and H_n are Hermite polynomials of orders *m* and *n* determining the field distribution in the s_x and s_y directions, a_j is a complex parameter characterizing the width of the Hermite polynomials in the s_j direction, with $j = x$ or y, b_j is a complex parameter characterizing the displacement of the Hermite polynomials in the s_j direction, and $\alpha_j = \frac{1}{k\alpha_{sj}^2} + \frac{i}{F_j}$, with α_{sj} and F_j indicating the source size and the focal length in the s_j direction. Using the Huygens Fresnel integral, Baykal develops the field equation at $\left(p_x, p_y, z\right)$ in the absence of turbulence, and the correlation functions of the log-amplitude fluctuations and of the phase fluctuations at the receiver plane $(z = L)$ in a turbulent atmosphere. He then determines the log amplitude and phase structure functions of the beam in turbulence. Extending the field at the source plane to include the more general Hermite-sinusoidal-Gaussian beam by representing it as the superposition of two off-axis Hermite-Gaussian beams, he generalizes his result to introduce any form of hyperbolic cosine, hyperbolic sine, cosine, or sine dependence into the Hermite-Gaussian beam.

Although no conclusion as to the usefulness of these functions in lasercom situations has been drawn, because the effect on the intensity or power scintillation noise or on the angle of arrival fluctuations have not yet been developed, the behavior in atmospheric turbulence of the Hermite-cosh-Gaussian beam is of particular interest

because, through its cosh dependence, it is possible to concentrate the energy of the beam into the outer lobes, yielding what is, in effect, two separate propagating beams.

3.2 Hermite-Gaussian Beams

Higher order solutions of the paraxial wave equation can be used to generate higher order Gaussian beam modes in rectangular coordinates. The higher order Hermite-Gaussian beams are defined at the transmitter $(z = 0)$ plane to be

$$U_{mn}(x, y, 0) = H_m\left(\frac{\sqrt{2}x}{W_0}\right) H_n\left(\frac{\sqrt{2}y}{W_0}\right) \exp\left(-\frac{x^2 + y^2}{W_0^2}\right) \tag{3.2}$$

where $H_m(x)$ is a Hermite polynomial of order *m*, and the assumption is made that the spot size W_0 at the transmitter is the same in both the *x*- and *y*- directions. Upon propagation, the free space field at the receiver will be

$$\begin{aligned} V_{mn}(x, y, z) = & \frac{1}{\sqrt{p_x(z)\, p_y(z)}} H_m\left(\frac{\sqrt{2}x}{W_x}\right) H_n\left(\frac{\sqrt{2}y}{W_y}\right) \\ & \times \exp\left(-\frac{x^2}{W_x^2} - \frac{y^2}{W_y^2} - i\frac{kx^2}{2F_x} - i\frac{ky^2}{2F_y}\right) \exp\left[i\varphi_m(z) + i\varphi_n(z)\right], \end{aligned} \tag{3.3}$$

where $p_x(z)$ and $p_y(z)$ are the same as the parameter $p(z) = 1 + i\alpha z$ introduced for the lowest order Gaussian beam, oriented in the x and y transverse directions, respectively, W_x and W_y are parameters related to the spot size at the transmitter in the same manner

as $W(z)$ is related to W_0 for the standard Gaussian beam, F_x and F_y represent the radius of curvature in the transverse x and y directions at the receiver, and $\varphi_m(z)$ and $\varphi_n(z)$ are phase factors. The "spot size" for a Hermite-Gaussian beam is not defined in the usual manner, since higher order modes form a pattern of spots, rather than a single spot.(see Figure 3.1) In free-space the "effective" spot size was defined by Carter [5] to be

$$\sigma_{s,p}(z) = \sqrt{\frac{4\int\int_{-\infty}^{\infty} s^2 I_{mn}(x,y,z)dxdy}{\int\int_{-\infty}^{\infty} I_{mn}(x,y,z)dxdy}} \tag{3.4}$$

where *s* represents either *x* or *y* and *p* represents either *m* or *n*.

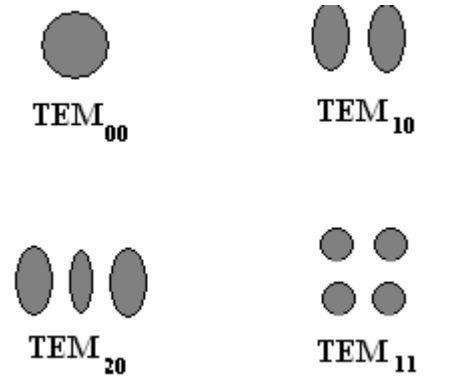

Figure 3.1 Light patterns for higher mode Hermite-Gaussian beams

The irradiance can be deduced from (3.2) to be

$$I_{mn}(x,y,z)=\frac{W_{x,0}W_{y,0}}{W_xW_y}H_m{}^2\left(\frac{\sqrt{2}x}{W_x}\right)H_n{}^2\left(\frac{\sqrt{2}y}{W_y}\right)\exp\left(-\frac{x^2}{W_x{}^2}-\frac{y^2}{W_y{}^2}\right) \tag{3.5}$$

and, by substitution of (3.5) into (3.4), the "effective spot size" of the Hermite-Gaussian beam at the transmitter is found to be the rectangular domain $\sigma_{x,m}(z)\times\sigma_{y,n}(z)$ given by

$$\sigma_{x,m}(z)=\sqrt{2m+1}\,W_x(z),\quad \sigma_{y,n}(z)=\sqrt{2n+1}\,W_y(z)$$

Young et al. [7] extended this to determine the mean intensity of the Hermite-Gaussian TEM_{10} beam at the receiver (x,y,L) in atmospheric turbulence to be

$$\begin{aligned}\left\langle I(x,y,L)\right\rangle_{10}=&\left[\frac{8x^2W_0^2}{W^4\left(1+1.78\sigma_1^2\Lambda\right)^3}+\frac{3.56\sigma_1^2\Lambda\left(1+\sigma_1^2\Lambda\right)}{\left(1+1.78\sigma_1^2\Lambda\right)^3}\right]\\&\times\exp\left[-\frac{2\left(x^2+y^2\right)}{W^2\left(1+1.78\sigma_1^2\Lambda\right)}\right]\end{aligned} \tag{3.6}$$

where Λ is given by $\frac{2L}{kW^2}$. A comparison of the mean intensity of this beam as it propagates through turbulence with its free space intensity reveals that, as turbulence increases, the beam becomes more Gaussian. Further, a ratio of the spot size at the receiver of the TEM_{10} Hermite-Gaussian beam in turbulence to the same beam in free space demonstrates, in the presence of turbulence, less additional broadening beyond normal diffraction.

3.3 Laguerre-Gaussian Beams

Higher order solutions to the paraxial wave equation when circular symmetry is assumed allow cylindrical coordinates to be used to describe the beam, resulting in the field at the transmitter $(z = 0)$ plane being

$$U_{mn}(r,\theta,0) = \left(\frac{\sqrt{2}\,r}{W_0}\right)^m (-i)^m \exp(im\theta)\exp\left(-\frac{r^2}{W_0^2}\right) L_n^{(m)}\left(\frac{2r^2}{W_0^2}\right) \tag{3.7}$$

where **r** represents a directional distance from the radial axis at an angle θ, W_0 is the radius of the lowest order Gaussian beam mode, and $L_n^{(m)}(x)$ is an associated Laguerre polynomial of angular and radial modes *m* and *n*, respectively. This field defines a Laguerre-Gaussian beam, whose field after propagation a distance z in free space has been shown to be [1]:

$$\begin{aligned} U_{mn}(r,\theta,z) = C_{mn}\frac{W_0}{W}\left[\frac{\sqrt{2}r}{W(z)}\right]^m L_n^{(m)}\left[\frac{2r^2}{W^2(z)}\right]\exp\left[-i(2n+m+1)\varphi(z)\right] \\ \times\exp\left[ikz + im\theta - \frac{r^2}{W^2} - i\frac{kr^2}{2F}\right] \end{aligned} \tag{3.8}$$

where C_{mn} is a phase constant, and W and F represent the spot size and phase front radius of curvature for a TEM_{00} beam.

The irradiance of the field at distance z from the transmitter is, therefore,

$$I(r,\theta,z) = \left|U_{mn}(r,\theta,z)\right|^2$$
$$= \frac{W_0^2}{W^2}\left[\frac{2r^2}{W^2}\right]^m \left[L_n^{(m)}\left(\frac{2r^2}{W^2}\right)\right]^2 \exp\left(-\frac{2r^2}{W^2}\right) \tag{3.9}$$

Again, the spot size at the transmitter must be redefined to accommodate a field whose spot pattern is a set of concentric rings. Following Carter's definition for the spot size of the Hermite-Gaussian beam (equation (3.4)), Andrews and Phillips [8] have defined the spot size for a Laguerre-Gaussian beam to be

$$\sigma_{mn}(z) = \sqrt{\frac{2\int_0^{2\pi}\int_0^{\infty} r^2 I_{mn}(r,\theta,z)\,r\,dr\,d\theta}{\int_0^{2\pi}\int_0^{\infty} I_{mn}(r,\theta,z)\,r\,dr\,d\theta}} \tag{3.10}$$

Therefore the spot size at the receiver after propagation in free space is given by

$$\sigma_{mn}(z) = \sqrt{2n+m+1}\,W\,. \tag{3.11}$$

The spot size as a result of optical turbulence has been computed at the receiver for the TEM_{01} beam and, as in the case of the higher order Hermite beam, results predict less additional broadening due to turbulence than for the TEM_{00} Gaussian beam. Since the higher order modes have a distribution of energy which is farther from the radial axis than is the case for the Gaussian beam, it makes sense that the additional broadening due to turbulence is less . These results appear to confirm the hypothesis that changing the

shape of the beam might mitigate certain deleterious effects of atmospheric turbulence on the propagated beam.

3.4 Super-Gaussian Beams

There are many applications where laser beams which present a flat topped intensity profile are encountered or desirable, among them laser processing and manufacturing. The question as to whether such a beam might be desirable in the field of free space laser communications where atmospheric turbulence is present has yet to be determined.

One of the models for describing flat topped profiles is the Super Gaussian function, which has been defined in prior works [9,10] as

$$SG(x, w_{SG}; \tau) = A \exp\left[-\left(\frac{|x|}{w_{SG}} \right)^{\tau} \right] \tag{3.12}$$

where A is the maximum value of the function, x is the beam radius, w_{SG} is a scale factor, and τ is the Super-Gaussian power. The value of τ affects the rapidity with which the function goes from its maximum value to zero. The function reduces to the standard Gaussian for τ =2, while for higher values of τ the profile tends to be more and more flat. As τ approaches infinity, the cross-section of the function tends to the rectangle function $rect(x/2w_{SG})$.

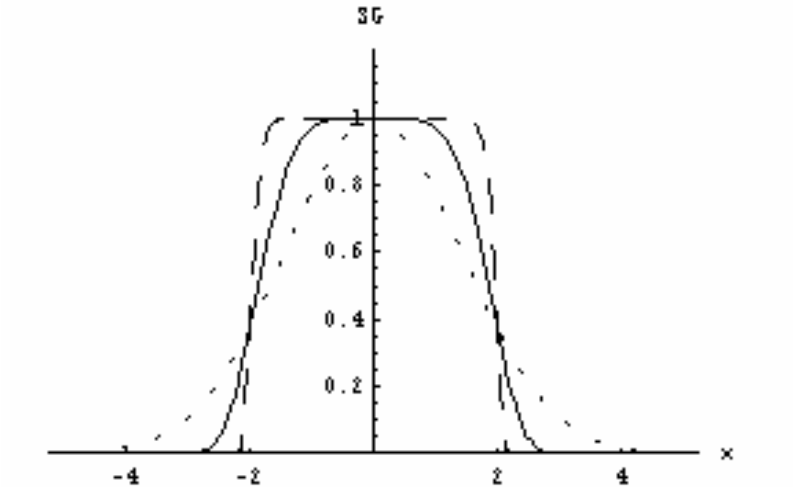

Figure 3.2 Super-Gaussian Profiles for w_{SG}=2, τ = 2(dotted), 5(solid), and 20(dashed).

Although the super Gaussian function is a relatively simple expression, in analytical situations such as the propagation of flat-topped beams it has, to date, been dealt with only by using numerical methods. Consequently, other models have been sought which resemble the super Gaussian beam in profile, but whose propagation equations are somewhat more tractable. Several models of these "top-hat" beams have been proposed and are considered in the following chapter.

CHAPTER 4 MODELING THE FLATTENED GAUSSIAN BEAM

If a beam is axially symmetric and its radial profile is flattened Gaussian across a plane $z = 0$ then it is commonly referred to as a Flattened Gaussian beam (FGB). The extent of the zone where the profile is flat is controlled by an integer index N such that for increasing N the flattened Gaussian profiles become closer and closer to the rectangle function. First introduced by Gori in 1994 [10], these beams have been intensely studied of late from several perspectives using a variety of models.

4.1 Flattened-Gaussian profiles of Gori

In seeking a model of the FGB which allows us to attain a flattened Gaussian profile without increasing the power of the exponential, we follow the lead of Gori who begins with the circularly symmetric Gaussian function e^{-r^2} which is then multiplied by the correction factor e^{r^2} in order to flatten the beam to the constant 1. Expressing this factor as a power series gives

$$F(r) = e^{-r^2} \sum_{n=0}^{\infty} \frac{r^{2n}}{n!} = 1 \tag{4.1}$$

Truncating this series at N terms gives an approximation,

$$F_N(r) = e^{-r^2} \sum_{n=0}^{N} \frac{r^{2n}}{n!}, \quad N = 0,1,2,... \tag{4.2}$$

which approaches zero as $r \to \infty$. For $N = 0$, this is the standard Gaussian beam, while for larger N we have the flattened beam pictured in figure 4.1.

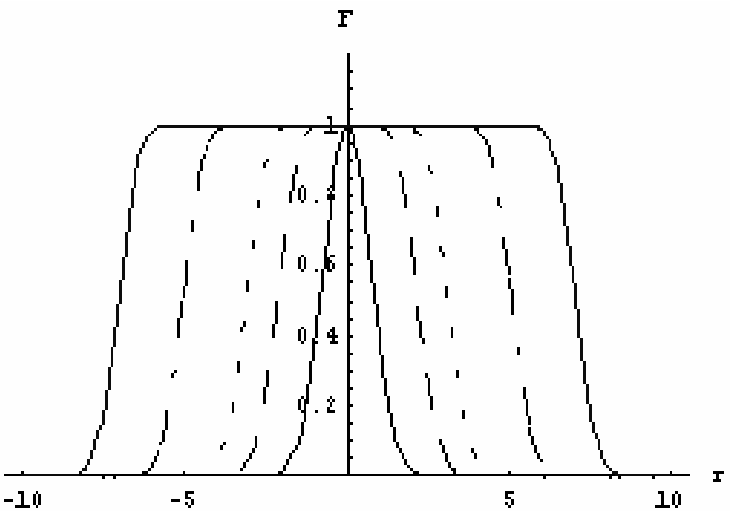

Figure 4.1: **Flattened Gaussian Profiles $F_N(r)$ for (innermost to outermost) N=0,4,9,25,49**

In order to rescale F_N to approximate the flat-top beam, or rectangle function, we estimate the width of the function (at $1/e$) for various values of N. The maximum value of $F = e^{-r^2} r^{2n}$ can be found by setting $F' = 0$.

$$F' = -2re^{-r^2} r^{2n} + e^{-r^2} 2nr^{2n-1} = 2e^{-r^2} r^{2n-1} \left(n - r^2\right) = 0 \tag{4.3}$$

Hence, the maximum value of F is reached when $r = \sqrt{n}$. Since the outermost contribution to the sum F_N comes from the Nth term, the width of $F_N \approx \sqrt{N}$. Rescaling gives a new function

$$G_N(r) = \exp\left(-Nr^2\right)\sum_{n=0}^{N}\frac{N^n r^{2n}}{n!}, \quad N = 1, 2, \ldots \tag{4.4}$$

In order to write the field distributions in a form compatible with ordinary Gaussian beams, a spot size W_0 at the transmitter is introduced, and the field distribution of FGBs at z = 0 is written in the form

$$V_N(r,0) = A\exp\left(\frac{-r^2}{W_0^2}\right)\sum_{m=0}^{N}\frac{1}{m!}\left(\frac{r}{W_0}\right)^{2m}. \tag{4.5}$$

where A is the magnitude of the wave.

To allow for the changing width of the beam as N increases, the function is rescaled according to the form of equation (4.4), arriving at

$$U_N(r,0) = A\exp\left(-\frac{Nr^2}{W_0^2}\right)\sum_{m=0}^{N}\frac{1}{m!}\left(\frac{Nr^2}{W_o^2}\right)^{m} \quad N = 1, 2, \ldots \tag{4.6}$$

Since this form excludes the case where N=0 gives the strictly Gaussian curve, the function is scaled by the factor $N+1$ instead of N, and we arrive at the form given by Bagini et al.[12]:

$$U_{N0}(r,0) = A_0 \exp\left[\frac{-(N+1)r^2}{W_0^2}\right]\sum_{m=0}^{N}\frac{1}{m!}\left(\frac{\sqrt{N+1}\,r}{W_0}\right)^{2m} \qquad N = 0,1,2,\ldots \tag{4.7}$$

When N=0, this now reduces to the strictly Gaussian beam. When $N \to \infty$, the equation tends to $A_0 \operatorname{circ}\left(r/W_0\right)$.

Gori's model has been the subject of much study in the past decade. Santarsiero, Aiello, Borghi and Vicalvi have studied the focusing characteristics of the beam [13]. Baida Lu and Shirong Luo have analyzed its propagated intensity distribution and its pointing stability[15,16].

In comparing Gori's flattened Gaussian beam to the super- Gaussian profile, Santasario and Borghi [9] noted that, although the two were identical only in the limiting cases, the differences between them in all other cases were so small as to be indistinguishable in experimental situations. Baida Lu, Shirong Luo and Xiaoling Ji [10] also noted that, given the same propagation factor and waist width, the SGB and the FGB would demonstrate nearly identical characteristics as they propagated through a paraxial ABCD system. This flattened Gaussian beam model is therefore preferable to the super-Gaussian model, since it has the advantage of analytical solutions in propagation scenarios.

4.2 Multi-Gaussian beams

In 2001, Anthony Tovar introduced an alternate model for producing a flattened profile[14]. By writing the profile as a sum of finite-width Gaussian functions side by side, his model produces a class of beams which, like Gori's model, has the shape of the super-Gaussian beams while having propagation characteristics which can be analytically determined. Each of the Gaussian beams in the sum has an identical spot size, *w*, but is offset by a specified amount from the axis:

$$G(r) = \frac{\sum_{m=-N}^{N} \exp\left[-\left(\frac{r-mw}{w}\right)^2\right]}{\sum_{m=-N}^{N} \exp\left(-m^2\right)} \tag{4.8}$$

Figure 4.2 shows the individual beams which make up the multi-Gaussian beam of order *N*=4.

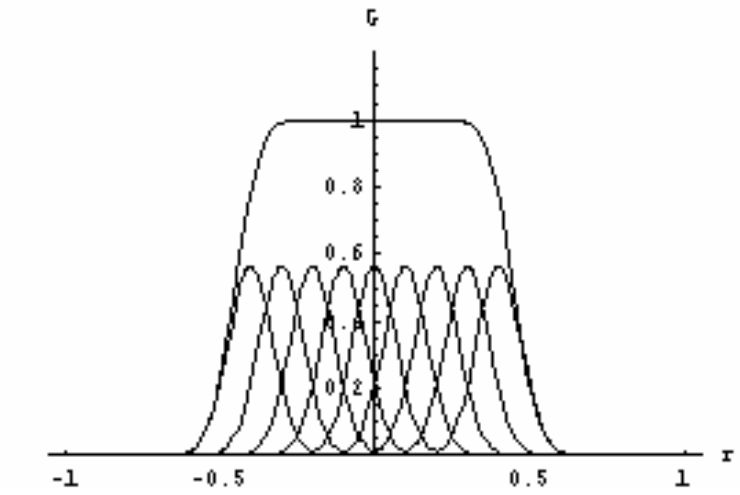

Figure 4.2: A 4th order multi-Gaussian beam profile with its component Gaussian functions at w=1 cm.

The number of Gaussian functions which compose the multi-Gaussian shape is $2N+1$, with $N=0$ corresponding to the fundamental Gaussian beam mode. As the order N of the beam approaches infinity, the shape of the beam approaches the circ function. The denominator in equation (4.8) is a normalization function which causes $G(r)$ to reach its maximum at unity (See Fig.4.3).

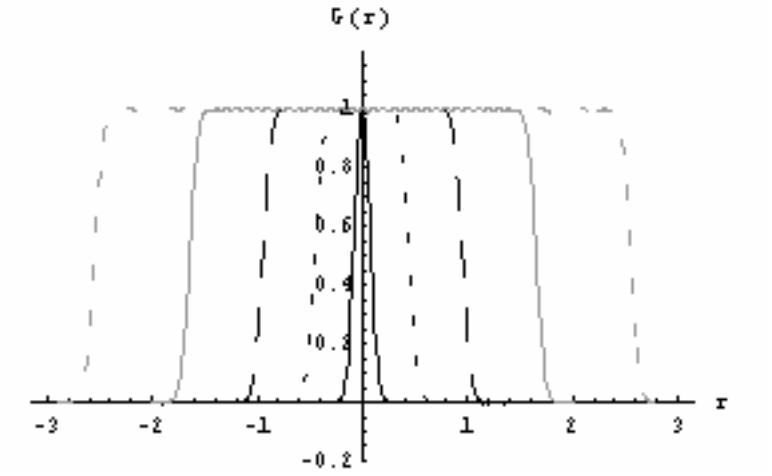

Figure 4.3: Multi-Gaussian beam of spot size 10 centimeters with (innermost to outermost) N=0,4,9,16,25

The width of the beam at the waist plane, W, is related to the width of each of the identical component beams, w, by the relation

$$w = \frac{W}{N + \left\{1 - \ln\left[\sum_{m=-N}^{N} \exp\left(-m^2\right)\right]\right\}^{1/2}}. \tag{4.9}$$

The value of the sum in (4.9) is typically about 1.77 for $N \geq 2$, hence the denominator has a value of $N + 0.654$. The width of the component beams, w, is the "rise distance" of the beam (analogous to the rise time of a pulse).

Tovar's analysis of the propagation characteristics of this model included both ABCD optical systems and free space. In free space propagation, the multi-Gaussian beam becomes Gaussian in the far field as the Gaussian beams overlap increasingly while the phase curvature of the individual beams becomes flat. However, if the rise distance of the beam is smaller than a wavelength, the beam cannot be modeled as multi-Gaussian, and the beam does not become Gaussian in the far field.

This model compares favorably to the super-Gaussian function in its values, while retaining the benefit of analytic solutions in beam propagation situations.

4.3 Baykal's Model

In an examination of the effects of propagation through atmospheric turbulence on the flattened Gaussian beam, Baykal and Eyyuboglu [17,18] model the beam as a superposition of Gaussian beams where the field equation is

$$U(\mathbf{r},0)=\sum_{n=1}^{N}\frac{(-1)^{n-1}}{N}\binom{N}{n}\exp\left(-\frac{n\mathbf{r}^2}{W_o^2}\right). \tag{4.10}$$

In (4.10), the amplitude of the field at the transmitter is taken to be unity, and the phase factor of the field is set to zero. The result is a beam which, as it flattens with increasing order *N*, also decreases in amplitude, as shown in figure 4.4.

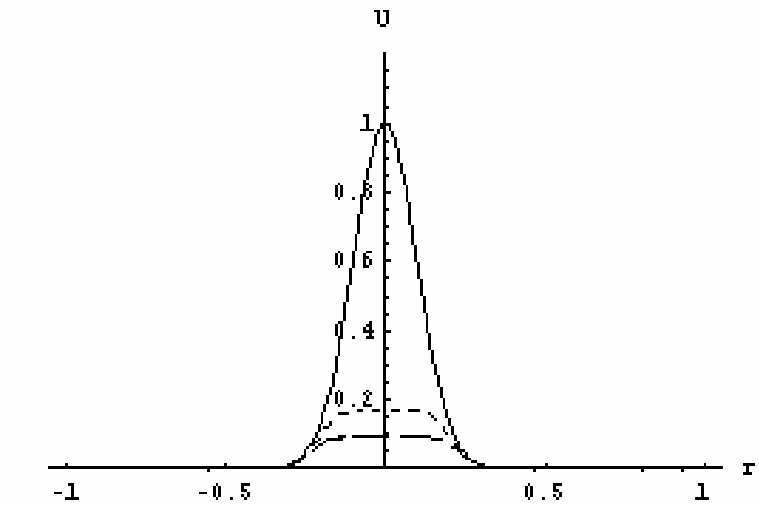

Figure 4.4 Baykal's flattened Gaussian beam model with N=1 (solid), N=6 (dotted), and N=11 (dashed) for a beam with $W_0 = 10$ cm.

In figure 4.4, the order N=1 is that of the standard Gaussian beam.

This model has recently been the focus of study of atmospheric effects on propagated intensity and on scintillation [17, 18, 19]. Although Cai was able to develop an analytical formula for the average intensity of the beam in a turbulent atmosphere, the deduced scintillation index, beam size during propagation, and kurtosis parameter determined by Baykal, Eyyuboglu, and Arpali are complex expressions which, while allowing insight into the characteristics of the propagated beam, cannot be analytically determined and must be treated numerically.

CHAPTER 5 FREE SPACE PROPAGATION OF FLATTENED GAUSSIAN BEAMS

In this study of the propagation of the flattened Gaussian beam, we have elected to work with the model proposed by Gori, as presented in section 4.1 and represented by the field equation given by equation (4.7).

5.1 Paraxial Propagation

The propagation of flattened Gaussian beams can be established by expressing the field of the beam at the transmitter in terms of equation (4.7), and using the relation [16]

$$x^n = n!\sum_{m=0}^{n}\binom{n}{m}(-1)^m L_m(x) \tag{5.1}$$

which gives

$$U_{N0}(r,0) = A_0 \exp\left[\frac{-(N+1)r^2}{W_0^2}\right]\sum_{n=0}^{N}\sum_{m=0}^{n}\binom{n}{m}\frac{(-1)^m}{2^n}L_m\left[\frac{2(N+1)r^2}{W_0^{\,2}}\right]. \tag{5.2}$$

Using the Huygens-Fresnel integral for free space (see Equation (2.10)), we can determine the equation of the beam a distance L from the transmitter. Beginning with

$$U_{N0}(r,L) = -\frac{ik}{2\pi L}\exp(ikL)\int\int_{-\infty}^{\infty} U_N(s,0)\exp\left(\frac{ik}{2L}|\mathbf{s}-\mathbf{r}|^2\right)d^2s\,, \tag{5.3}$$

and substituting equation (5.2), we obtain

$$\begin{aligned} U_{N0}(r,L) = -\frac{ik}{2\pi L}\exp(ikL)\int\int_{-\infty}^{\infty} A_0\exp\left[-\frac{(N+1)s^2}{W_0^2}\right]\sum_{n=0}^{N}\sum_{m=0}^{n}\binom{n}{m}\frac{(-1)^m}{2^n} \\ \times L_m\left[\frac{2(N+1)s^2}{W_0^2}\right]\exp\left(\frac{ik}{2L}|\mathbf{s}-\mathbf{r}|^2\right)d^2s \end{aligned} \tag{5.4}$$

Reversing the order of summation and integration, and rewriting the absolute value, (5.4) becomes

$$\begin{aligned} U_{N0}(r,L) = -\frac{A_0}{2\pi}\frac{ik}{L}\exp\left(ikL+\frac{ik}{2L}r^2\right)\sum_{n=0}^{N}\sum_{m=0}^{n}\binom{n}{m}\frac{(-1)^m}{2^n} \\ \times\int_{-\infty}^{\infty}\exp\left[-\frac{(N+1)s^2}{W_0^2}+\frac{ik}{2L}s^2\right]L_m\left[\frac{2(N+1)s^2}{W_0^2}\right]\int_0^{2\pi}\exp\left(-\frac{ik}{L}sr\cos\theta\right)d\theta sds. \end{aligned} \tag{5.5}$$

Solving the innermost integral in (5.5) yields

$$\begin{aligned} U_{N0}(r,L) = -A_0\frac{ik}{L}\exp\left(ikL+\frac{ik}{2L}r^2\right)\sum_{n=0}^{N}\sum_{m=0}^{n}\binom{n}{m}\frac{(-1)^m}{2^n} \\ \times\int_{-\infty}^{\infty} s\exp\left\{\left[-\frac{(N+1)}{W_0^2}+\frac{ik}{2L}\right]s^2\right\}L_m\left[\frac{2(N+1)s^2}{W_0^2}\right]J_0\left(\frac{kr}{L}s\right)ds \end{aligned} \tag{5.6}$$

where $J_0(x)$ is a Bessel function of order 0. It can be shown, using identity 7.421.4 in [23], that (5.6) is equivalent to

$$U_{N0}(r,L) = A_0 \frac{W_N(0)}{W_N(L)} \exp\left[ikL - i\Phi_N(L) - \frac{r^2}{W_N^2(L)} + \frac{ikr^2}{2R_N(L)}\right] \times \sum_{n=0}^{N}\sum_{m=0}^{n} \binom{n}{m} \frac{(-1)^m}{2^n} L_m\left[\frac{2r^2}{W_N^2(L)}\right] \exp\left[-2im\Phi_N(L)\right] \tag{5.7}$$

where $k = \frac{2\pi}{\lambda}$, $W_N(L) = W_N(0)\sqrt{1+\left(\frac{2L}{kW_N{}^2(0)}\right)^2}$, $R_N(L) = L\left[1+\left(\frac{kW_N{}^2(0)}{2L}\right)^2\right]$,

$\Phi_N(L) = \tan^{-1}\frac{2L}{kW_N^2(0)}$ and $W_N(0) = \frac{W_0}{\sqrt{N+1}}$.

This is the field of the flattened Gaussian beam after propagation in free space only, and is not accurate in the presence of atmospheric turbulence.

5.2 On-Axis Intensity

The on-axis intensity of the propagated FGB can be determined as follows. We begin with the field at a point along the z axis:

$$U_{N0}(0;z) = A_0 \frac{W_N(0)}{W_N(L)} \exp\left\{i\left[kz - \Phi_N(z)\right]\right\} \sum_{n=0}^{N}\sum_{m=0}^{n} \binom{n}{m} \frac{(-1)^m}{2^n} \exp\left[-2im\Phi_N(z)\right]. \tag{5.8}$$

From this, using Newton's binomial expansion,

$$U_{N0}(0;z) = A_0 \frac{W_N(0)}{W_N(L)} \exp\left\{i\left[kz - \Phi_N(z)\right]\right\} \sum_{n=0}^{N} \left\{\frac{1-\exp\left[-2i\Phi_N(z)\right]}{2}\right\}^n . \tag{5.9}$$

The summation in the above equation can be rewritten as

$$\sum_{n=0}^{N} \left\{\frac{1-\exp\left[-2i\Phi_N(z)\right]}{2}\right\}^n = \sum_{n=1}^{N+1} \left\{\frac{1-\exp\left[-2i\Phi_N(z)\right]}{2}\right\}^{n-1} . \tag{5.10}$$

From the law of geometric progression, which states that $\sum_{k=1}^{n} a(q)^{k-1} = \frac{a(q^n-1)}{q-1}$ $, q \neq 1,$

we obtain $\sum_{n=1}^{N+1} \left\{\frac{1-\exp\left[-2i\Phi_N(z)\right]}{2}\right\}^{n-1} = \frac{\left\{\frac{1-\exp\left[-2i\Phi_N(z)\right]}{2}\right\}^{N+1} - 1}{\frac{1-\exp\left[-2i\Phi_N(z)\right]}{2} - 1}$. Multiplying by

$\frac{2^{N+1}}{2^{N+1}}$, this becomes $\frac{\left(1-\exp\left[-2i\Phi_N(z)\right]\right)^{N+1} - 2^{N+1}}{2^N\left\{1-\exp\left[-2i\Phi_N(z)\right]\right\} - 2^{N+1}} = \frac{\left(1-\exp\left[-2i\Phi_N(z)\right]\right)^{N+1} - 2^{N+1}}{2^N\left\{1-\exp\left[-2i\Phi_N(z)\right] - 2\right\}}$.

The summation in (5.9) is, therefore, $\frac{\left\{1-\cos\left[2\Phi_N(z)\right] + i\sin\left[2\Phi_N(z)\right]\right\}^{N+1} - 2^{N+1}}{-2^N\left\{1+\cos\left[2\Phi_N(z)\right] - i\sin\left[2\Phi_N(z)\right]\right\}}$.

Using double angle formulas, we find that

$$\sum_{n=0}^{N} \left\{\frac{1-\exp\left[-2i\Phi_N(z)\right]}{2}\right\}^n = \frac{1-\sin^{N+1}\left[\Phi_N(z)\right]\exp\left\{-i(N+1)\left[\Phi_N(z) - \pi/2\right]\right\}}{\cos\left[\Phi_N(z)\right]\exp\left[-i\Phi_N(z)\right]} \tag{5.11}$$

Hence, using (5.11) in (5.9) together with some trigonometric identities, the on-axis intensity becomes

$$I_{N0}(0,z)=\left\langle U_N(0,z)U_N^*(0,z)\right\rangle=\left|A_0^2\right|\frac{W_N^2(0)}{W_N^2(z)} \times\frac{1+\sin^{2N+2}\left[\Phi_N(z)\right]-2\sin^{N+1}\left[\Phi_N(z)\right]\cos\left\{(N+1)\left[\Phi_N(z)-\pi/2\right]\right\}}{\cos^2\left[\Phi_N(z)\right]}. \tag{5.12}$$

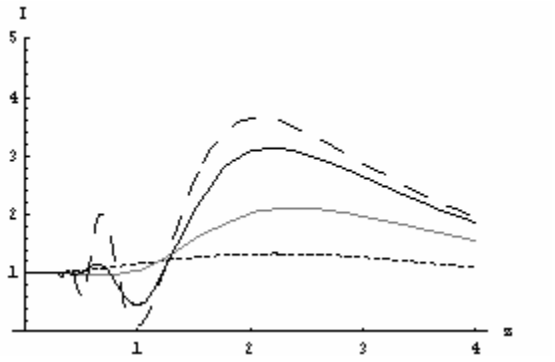

Figure 5.1 On-axis intensity of the FGB as a function of propagation distance *z* km for N=1 (dotted),4(solid gray),16(solid black), and 49(dashed).
Here, $A_0=1; W_0=1\text{ mm}; \lambda=0.5\mu\text{m}$**.**

Plots of the intensity as a function of z (see figure 5.1) for different values of N reveal that:

- As the order of the beam approaches infinity, the intensity curves tend to $I_\infty(0;z)=4\left|A_0\right|^2\sin^2\left(\frac{kW_0^2}{4z}\right)$, which is the on-axis intensity for a circular aperture.
- The curves of propagated intensity of FGBs are similar to the curves of propagated intensity for super-Gaussian beams[12].

5.3 Spot size

It has been shown in several studies of the intensity distribution profile of the FGB as it propagates both in free space and also in turbulence that the initial flattened beam shape transforms into a circular ring which gradually reverts to a circular Gaussian profile in the far field. [12, 15, 19]. Just as the changing beam shape of the higher order Gaussian beams (section 3.2) required a new definition of beam spot size, we examine the spot size of the propagated FGB using the format suggested by Andrews and Phillips in [8]:

$$\sigma_s^2 = \frac{2\int_0^\infty \left|U_N(r)\right|^2 r^3 dr}{\int_0^\infty \left|U_N(r)\right|^2 r dr}. \tag{5.13}$$

Using the equation for the field given in (4.7), we can rewrite (5.13) as

$$\sigma_s^2 = \frac{2\int_0^\infty r^2 \exp\left[-\frac{2(N+1)r^2}{W_0^2}\right]\left[\sum_{m=0}^{N}\frac{1}{m!}\left(\frac{\sqrt{N+1}\,r}{W_0}\right)^{2m}\right]^2 r dr}{\int_0^\infty \exp\left[-\frac{2(N+1)r^2}{W_0^2}\right]\left[\sum_{m=0}^{N}\frac{1}{m!}\left(\frac{\sqrt{N+1}\,r}{W_0}\right)^{2m}\right]^2 r dr}. \tag{5.14}$$

Letting $u = \frac{(N+1)r^2}{W_0^2}$, and interchanging summation and integration in both the numerator and denominator, we now have

$$\sigma_s^2 = \frac{2W_0^2}{N+1} \frac{\sum_{m=0}^{N} \frac{1}{m!} \sum_{p=0}^{N} \frac{1}{p!} \int_0^{\infty} u^{m+p+1} e^{-2u} du}{\sum_{m=0}^{N} \frac{1}{m!} \sum_{p=0}^{N} \frac{1}{p!} \int_0^{\infty} u^{m+p} e^{-2u} du}. \tag{5.15}$$

The integrals in (5.15) are gamma functions, and the effective spot size, σ_s, can be determined from the resulting equation

$$\sigma_s^2 = \frac{W_0^2}{N+1} \frac{\sum_{m=0}^{N} \frac{1}{m!2^m} \sum_{p=0}^{N} \frac{1}{p!2^p} \Gamma(m+p+2)}{\sum_{m=0}^{N} \frac{1}{m!2^m} \sum_{p=0}^{N} \frac{1}{p!2^p} \Gamma(m+p+1)}. \tag{5.16}$$

The spot size given by (5.16) appears cumbersome. However, it is simply a double finite sum and, given any order FGB, will yield a multiple of the spot size, W_0, of the standard Gaussian beam at the transmitter. For a beam of order N=0, equation (5.16) predictably determines $\sigma_s = W_0$. Given the beams of order 5 and 10, with which we will work most frequently in this paper, we will have $\sigma_s = 0.9356\, W_0$ and $\sigma_s = 0.9427\, W_0$, respectively. In general, $\sigma_s \approx W_0$ for all N.

Although not specifically addressing the spot size of the beam in their work, Bagini et al[12], determined the numerator and denominator of (5.13) to have the following values

$$\int_0^\infty \left|U_N(r)\right|^2 r^3 dr = \left|A_0\right|^2 \frac{{W_0}^4}{8(N+1)^2} \sum_{n=0}^{N}\sum_{m=0}^{N} \frac{n+m+1}{2^{n+m}} \binom{n+m}{n} \tag{5.17}$$

and

$$\int_0^\infty \left|U_N(r)\right|^2 r dr = \left|A_0\right|^2 \frac{{W_0}^2}{4(N+1)} \sum_{n=0}^{N} \left[\sum_{m=n}^{N} \frac{1}{2^m} \binom{m}{n}\right]^2. \tag{5.18}$$

The effective spot size of the beam can therefore be expressed as

$$\sigma_s^2 = \frac{W_0^2}{N+1} \frac{\sum_{n=0}^{N}\sum_{m=0}^{N} \frac{n+m+1}{2^{n+m}} \binom{n+m}{n}}{\sum_{n=0}^{N}\left[\sum_{m=n}^{N} \frac{1}{2^m} \binom{m}{n}\right]^2} \tag{5.19}$$

The values of the spot size determined from (5.19) are precisely those determined using (5.16).

CHAPTER 6 PROPAGATION IN THE PRESENCE OF ATMOSPHERIC TURBULENCE

6.1 The First Order Spectral Representation

In order to consider the effects of the atmosphere upon the propagated flattened Gaussian beam, we use the Huygens-Fresnel integral in a manner parallel to that considered in Chapter 2.

Beginning with the equation for a flattened Gaussian beam at the transmitter,

$$U_{N0}(r,0) = A_0 \exp\left[-\frac{(N+1)r^2}{W_0^2}\right]\sum_{n=0}^{N}\frac{1}{n!}\left(\frac{\sqrt{N+1}r}{W_0}\right)^{2n} \tag{6.1}$$

and using the substitution $W_{N0}{}^2 = \frac{W_0{}^2}{N+1}$, we have

$$U_{N0}(r,0) = A_0 \exp\left[-\frac{r^2}{W_{N0}^2}\right]\sum_{n=0}^{N}\frac{1}{n!}\left(\frac{r^2}{W_{N0}^2}\right)^{n}. \tag{6.2}$$

The free-space field of an optical wave at a receiver which is distance L from the source can be obtained using the Huygens-Fresnel integral:

$$U_{N0}(\mathbf{r},L) = -\frac{ik}{2\pi L}\exp(ikL)\int\int U_{N0}(\mathbf{s},0)\exp\left(\frac{ik}{2L}|\mathbf{s}-\mathbf{r}|^2\right)d^2s \tag{6.3}$$

Upon substitution of equation (6.2) into this equation and simplifying the result, we have:

$$\begin{aligned} U_{N0}(r,L) = -A_0\frac{ik}{L}\exp\left(ikL+\frac{ik}{2L}r^2\right)\sum_{n=0}^{N}\frac{1}{n!W_{N0}^{2n}} \\ \times\int_{-\infty}^{\infty} s^{2n+1}\exp\left[\frac{ik}{2L}\left(1-\frac{2L}{ikW_{N0}^2}\right)s^2\right]J_0\left(\frac{kr}{L}s\right)ds \end{aligned} \tag{6.4}$$

where J_0 refers to the Bessel function of the first kind. Selecting, for convenience, A_0=1 and setting $\alpha_N = \frac{2}{kW_{N0}{}^2}$, this now becomes:

$$\begin{aligned} U_{N0}(r,L) = -\frac{ik}{L}\exp\left(ikL+\frac{ik}{2L}r^2\right)\sum_{n=0}^{N}\frac{1}{n!W_{N0}^{2n}} \\ \times\int_{-\infty}^{\infty} s^{2n+1}\exp\left[\frac{ik}{2L}(1+i\alpha_N L)s^2\right]J_0\left(\frac{kr}{L}s\right)ds. \end{aligned} \tag{6.5}$$

The integral in the above equation can be solved using Equation 14 in Appendix II, [1], resulting in

$$U_{N0}(r,L) = -\frac{ik}{2L}\exp\left(ikL + ik\frac{r^2}{2L}\right)\sum_{n=0}^{N}\frac{1}{{W_{N0}}^{2n}}\frac{1}{\left[\left(\frac{k}{i2L}\right)\left(1+i\alpha_N L\right)\right]^{n+1}} \times {}_1F_1\left[n+1;1;\frac{ikr^2}{2L\left(1+i\alpha_N L\right)}\right] \tag{6.6}$$

in which ${}_1F_1$ is the confluent hypergeometric function. Making use of Kummer's transformation [22], this equation becomes

$$U_{N0}\left(r,L\right) = \frac{1}{\left(1+i\alpha_N L\right)}\exp\left(ikL - \frac{k\alpha_N r^2}{2\left(1+i\alpha_N L\right)}\right)\sum_{n=0}^{N}\frac{1}{{W_{N0}}^{2n}}\left(\frac{2iL}{k\left(1+i\alpha_N L\right)}\right)^n \times {}_1F_1\left[-n;1;\frac{ikr^2}{2L\left(1+i\alpha_N L\right)}\right] \tag{6.7}$$

With $U_{N0}\left(r,L\right)$ defined, we shall now use this free space (and, therefore, unperturbed) field at a distance L from the transmitter to determine the value of the first order Born approximation, which is equivalent to the first order Rytov approximation.

As in the case of the Gaussian field, when given the unperturbed field $U_{N0}\left(\mathbf{R}\right)$, we can determine the first order perturbations $U_{N1}\left(\mathbf{R}\right)$ through the relation

$$U_{N1}\left(\mathbf{R}\right) = \iiint_V G(\mathbf{S},\mathbf{R})\left[2k^2 n_1\left(\mathbf{S}\right)U_{N0}\left(\mathbf{S}\right)\right]d^3S\,, \tag{6.8}$$

with $G(\mathbf{S},\mathbf{R})$ being the Green's function $G(\mathbf{S},\mathbf{R}) = \frac{1}{4\pi|\mathbf{R}-\mathbf{S}|}\exp(ik|\mathbf{R}-\mathbf{S}|)$. Using cylindrical coordinates and employing the paraxial approximation, the first order perturbation becomes

$$U_{N1}(\mathbf{r},L) = \frac{k^2}{2\pi}\int_0^L dz \int\int_{-\infty}^{\infty} d^2s \exp\left[ik(L-z) + \frac{ik}{2(L-z)}|\mathbf{s}-\mathbf{r}|^2\right] U_{N0}(\mathbf{s},z)\frac{n_1(\mathbf{s},z)}{(L-z)}. \quad (6.9)$$

where we have used the notation $U_{N0}(r,L)$ to indicate the unperturbed field for the FGB of order N, $U_{N1}(r,L)$ to represent the first order perturbations, $U_{N2}(r,L)$ the second order perturbations, and so forth. Hence, we have, from (6.7)

$$\begin{aligned} U_{N0}(r,L) = {} & \frac{1}{(1+i\alpha_N L)}\exp\left(ikL - \frac{k\alpha_N r^2}{2(1+i\alpha_N L)}\right)\sum_{n=0}^{N}\frac{1}{W_{N0}{}^{2n}}\left(\frac{2iL}{k(1+i\alpha_N L)}\right)^n \\ & \times {}_1F_1\left[-n;1;\frac{ikr^2}{2L(1+i\alpha_N L)}\right] \end{aligned} \quad (6.10)$$

and, applying this to (6.9), therefore

$$\begin{aligned} U_{N1}(r,L) = {} & \frac{k^2}{2\pi}\int_0^L dz \int\int_{-\infty}^{\infty} d^2s \exp\left[ik(L-z) + \frac{ik}{2(L-z)}|\mathbf{s}-\mathbf{r}|^2\right] \\ & \times \frac{1}{(1+i\alpha_N z)}\exp\left(ikz - \frac{k\alpha_N s^2}{2(1+i\alpha_N z)}\right)\sum_{n=0}^{N}\frac{1}{W_{N0}{}^{2n}}\left(\frac{2iz}{k(1+i\alpha_N z)}\right)^n \\ & \times {}_1F_1\left[-n;1;\frac{iks^2}{2z(1+i\alpha_N z)}\right]\frac{n_1(\mathbf{s},z)}{(L-z)}. \end{aligned} \quad (6.11)$$

The normalized first order approximation, Φ_1, is equal to $\dfrac{U_{N1}(r,L)}{U_{N0}(r,L)}$, or

$$\Phi_1 = \frac{k^2}{2\pi}\int_0^L dz \int\int_{-\infty}^{\infty} d^2 s \exp\left[ik(L-z) + \frac{ik\left|\mathbf{s}-\mathbf{r}\right|^2}{2(L-z)}\right]\frac{n_1(\mathbf{s},z)}{L-z}$$
$$\times \frac{\dfrac{1}{1+i\alpha_N z}\exp\left[ikz - \dfrac{k\alpha_N s^2}{2\left(1+i\alpha_N z\right)}\right]\displaystyle\sum_{n=0}^{N}\left\{\left[\frac{2iz}{k\left(1+i\alpha_N z\right)}\right]^n \frac{1}{W_{N0}^{2n}}\,{}_1F_1\left[-n;1;\frac{iks^2}{2z\left(1+i\alpha_N z\right)}\right]\right\}}{\dfrac{1}{1+i\alpha_N L}\exp\left[ikL - \dfrac{k\alpha_N r^2}{2\left(1+i\alpha_N L\right)}\right]\displaystyle\sum_{n=0}^{N}\left\{\left[\frac{2iL}{k\left(1+i\alpha_N L\right)}\right]^n \frac{1}{W_{N0}^{2n}}\,{}_1F_1\left[-n;1;\frac{ikr^2}{2L\left(1+i\alpha_N L\right)}\right]\right\}} \quad (6.12)$$

By combining the exponentials, simplifying, and changing the order of summation and integration this can be written

$$\Phi_1 = \frac{k^2}{2\pi\displaystyle\sum_{n=0}^{N}\left\{\left[\frac{2iL}{k\left(1+i\alpha_N L\right)}\right]^n \frac{1}{W_{N0}^{2n}}\,{}_1F_1\left[-n;1;\frac{ikr^2}{2L\left(1+i\alpha_N L\right)}\right]\right\}}$$
$$\times \int_0^L dz \sum_{m=0}^{N}\left\{\left[\frac{2iz}{k\left(1+i\alpha_N z\right)}\right]^m \frac{1}{W_{N0}^{2m}}\right\}\int\int_{-\infty}^{\infty} d^2 s\,{}_1F_1\left[-m;1;\frac{iks^2}{2z\left(1+i\alpha_N z\right)}\right] \quad (6.13)$$
$$\times \exp\left[\frac{ik\left|\mathbf{s}-\mathbf{r}\right|^2}{2(L-z)} - \frac{k\alpha_N s^2}{2\left(1+i\alpha_N z\right)} + \frac{k\alpha_N r^2}{2\left(1+i\alpha_N L\right)}\right]\frac{1+i\alpha_N L}{1+i\alpha_N z}\frac{n_1(\mathbf{s},z)}{L-z}.$$

To determine the first order spectral representation of this approximation, we again use

$$n_1(\mathbf{s},z) = \int\int_{-\infty}^{\infty}\exp\left(i\mathbf{K}\cdot\mathbf{s}\right)d\nu\left(\mathbf{K},z\right). \quad (6.14)$$

Substituting this into (6.13), and reversing the order of integration, we find

$$\Phi_1 = \frac{k^2}{2\pi\sum_{n=0}^{N}\left\{\left[\frac{2iL}{k\left(1+i\alpha_N L\right)}\right]^n \frac{1}{W_{N0}^{2n}}\,{}_1F_1\left[-n;1;\frac{ikr^2}{2L\left(1+i\alpha_N L\right)}\right]\right\}} \int_0^L dz \int\int_{-\infty}^{\infty} d\nu\left(\mathbf{K},z\right)$$
$$\times\frac{1+i\alpha_N L}{1+i\alpha_N z}\frac{1}{L-z}\sum_{m=0}^{N}\left[\frac{2iz}{k\left(1+i\alpha_N z\right)}\right]^m \frac{1}{W_{N0}^{2m}}\int\int_{-\infty}^{\infty} d^2s\,{}_1F_1\left[-m;1;\frac{iks^2}{2z\left(1+i\alpha_N z\right)}\right] \quad (6.15)$$
$$\times\exp\left[\frac{ik\left|\mathbf{s}-\mathbf{r}\right|^2}{2(L-z)}-\frac{k\alpha_N s^2}{2\left(1+i\alpha_N z\right)}+\frac{k\alpha_N r^2}{2\left(1+i\alpha_N L\right)}+i\mathbf{K}\cdot\mathbf{s}\right].$$

Working with the innermost integral which we shall call *I*, we arrive at

$$I = \int\int_{-\infty}^{\infty} d^2s\,{}_1F_1\left[-m;1;\frac{iks^2}{2z\left(1+i\alpha_N z\right)}\right]\exp\left[\frac{iks^2-k\alpha_N s^2 z-k\alpha_N s^2 L+k\alpha_N s^2 z}{2(L-z)\left(1+i\alpha_N z\right)}\right]$$
$$\times\exp\left[\frac{ikr^2-k\alpha_N r^2 L+k\alpha_N r^2 L-kz\alpha_N r^2}{2(L-z)\left(1+i\alpha_N L\right)}\right]\exp\left[i\left(\frac{-k\mathbf{r}}{(L-z)}+\mathbf{K}\right)\cdot\mathbf{s}\right] \quad (6.16)$$

which further reduces to

$$I = 2\pi\int_{-\infty}^{\infty} sds\;{}_1F_1\left[-m;1;\frac{iks^2}{2z\left(1+i\alpha_N z\right)}\right]\exp\left[\frac{iks^2\left(1+i\alpha_N L\right)}{2(L-z)\left(1+i\alpha_N z\right)}\right]$$
$$\times\exp\left[\frac{ikr^2\left(1+i\alpha_N z\right)}{2(L-z)\left(1+i\alpha_N L\right)}\right]J_0\left[\left(\frac{-k\mathbf{r}}{(L-z)}+\mathbf{K}\right)s\right] \quad (6.17)$$

Noting that the hypergeometric function given can be written in the form of a Laguerre polynomial, we now have

$$\Phi_1 = \frac{k^2}{\sum_{n=0}^{N}\left\{\left[\frac{2iL}{k\left(1+i\alpha_N L\right)}\right]^n \frac{1}{W_{N0}^{2n}} L_n\left[\frac{ikr^2}{2L\left(1+i\alpha_N L\right)}\right]\right\}}$$
$$\times \int_0^L dz \int\int_{-\infty}^{\infty} d\nu\left(\mathbf{K},z\right)\frac{1+i\alpha_N L}{1+i\alpha_N z}\frac{1}{L-z}\exp\left[\frac{ikr^2\left(1+i\alpha_N z\right)}{2(L-z)\left(1+i\alpha_N L\right)}\right]\sum_{m=0}^{N}\left[\frac{2iz}{k\left(1+i\alpha_N z\right)}\right]^m \quad (6.18)$$
$$\times \frac{1}{W_{N0}^{2m}}\int_{-\infty}^{\infty} sds\, L_m\left[\frac{iks^2}{2z\left(1+i\alpha_N z\right)}\right]\exp\left[\frac{iks^2\left(1+i\alpha_N L\right)}{2(L-z)\left(1+i\alpha_N z\right)}\right]J_0\left[\left(\frac{-k\mathbf{r}}{(L-z)}+\mathbf{K}\right)s\right].$$

We can use equation 7.421-4 in [17] to evaluate the innermost integral in (6.18), resulting in

$$\Phi_1 = \frac{k^2}{\sum_{n=0}^{N}\left\{\left[\frac{2iL}{k\left(1+i\alpha_N L\right)}\right]^n \frac{1}{W_{N0}^{2n}} L_n\left[\frac{ikr^2}{2L\left(1+i\alpha_N L\right)}\right]\right\}}$$
$$\times \int_0^L dz \int\int_{-\infty}^{\infty} d\nu\left(\mathbf{K},z\right)\frac{1}{\gamma\left(L-z\right)}\exp\left[\frac{ikr^2\gamma}{2(L-z)}\right]\sum_{m=0}^{N}\left[\frac{2iz}{k\left(1+i\alpha_N z\right)}\right]^m \frac{1}{W_{N0}^{2m}}$$
$$\times \frac{1}{2}\left(\frac{-ik}{2\gamma(L-z)}\right)^{-m-1}\left(\frac{-ik}{2\gamma(L-z)}-\frac{ik}{2z\left(1+i\alpha_N z\right)}\right)^m \exp\left(\frac{-\left(\mathbf{K}-\frac{k\mathbf{r}}{L-z}\right)^2}{\frac{-2ik}{\gamma(L-z)}}\right) \quad (6.19)$$
$$\times L_m\left[\frac{ik}{2z\left(1+i\alpha_N z\right)}\left(\mathbf{K}-\frac{k\mathbf{r}}{L-z}\right)^2 \frac{1}{\frac{-2ik}{\gamma(L-z)}\left(\frac{ik}{2z\left(1+i\alpha_N z\right)}+\frac{ik}{2\gamma(L-z)}\right)}\right]$$

where γ has been used to represent the complex path weighting parameter defined by

$$\gamma = \frac{1 + i\alpha_N z}{1 + i\alpha_N L}. \tag{6.20}$$

The second Laguerre polynomial in (6.19) reduces to

$$\begin{aligned} & L_m\left[\frac{ik}{2z\left(1+i\alpha_N z\right)}\left(\mathbf{K}-\frac{k\mathbf{r}}{L-z}\right)^2 \frac{1}{\frac{-2ik}{\gamma(L-z)}\left(\frac{ik}{2z\left(1+i\alpha_N z\right)}+\frac{ik}{2\gamma(L-z)}\right)}\right] \\ & = L_m\left[\frac{i\left(\mathbf{K}\left(L-z\right)-k\mathbf{r}\right)^2}{2kL\left(1+i\alpha_N L\right)}\right] \end{aligned} \tag{6.21}$$

Simplifying some of the factors in (6.19), we have

$$\left(\frac{-ik}{2\gamma(L-z)}\right)^{-m-1}\left(\frac{-ik}{2\gamma(L-z)}-\frac{ik}{2z\left(1+i\alpha_N z\right)}\right)^m = \left(\frac{2i\gamma(L-z)}{k}\right)\left(\frac{L\gamma}{z}\right)^m \tag{6.22}$$

and

$$\exp\left(\frac{-\left(\mathbf{K}-\frac{k\mathbf{r}}{L-z}\right)^2}{\frac{-2ik}{\gamma(L-z)}}\right)\exp\left[\frac{ikr^2\gamma}{2(L-z)}\right] = \exp\left(\frac{\gamma\kappa^2(L-z)}{2ik}+i\gamma\mathbf{K}\cdot\mathbf{r}\right) \tag{6.23}$$

As a result of these simplifications, we can now write

$$\Phi_1 = \frac{ik}{A_n(r)} \int_0^L dz \int\int_{-\infty}^{\infty} d\nu(\mathbf{K}, z) \exp\left(\frac{\gamma\kappa^2 (L-z)}{2ik} + i\gamma \mathbf{K}\cdot\mathbf{r} \right) \times \sum_{m=0}^{N} \left[\frac{2iL}{k\left(1+i\alpha_N L\right)} \right]^m \frac{1}{W_{N0}^{2m}} L_m \left[\frac{i\left[\mathbf{K}(L-z) - k\mathbf{r}\right]^2}{2kL\left(1+i\alpha_N L\right)} \right]. \tag{6.24}$$

where $A_n(r) = \sum_{n=0}^{N} \left\{ \left[\frac{2iL}{k\left(1+i\alpha_N L\right)} \right]^n \frac{1}{W_{N0}^{2n}} L_n \left[\frac{ikr^2}{2L\left(1+i\alpha_N L\right)} \right] \right\}$. Equation (6.24) is the first order spectral representation for the flattened Gaussian beam.

6.2 Statistical Moments of the Rytov Approximations

6.2.1 Computation of $E_2(\mathbf{r}_1,\mathbf{r}_2)$

As with the Gaussian beam, we begin with the computation of E_2 defined by

$$E_2(r_1, r_2) = \left\langle \Phi_1(r_1) \Phi_1^*(r_2) \right\rangle \tag{6.25}$$

where $\langle\ \rangle$ represents the ensemble average of the two quantities.

Then

$$\left\langle \Phi_1(r_1)\Phi_1^{*}(r_2)\right\rangle = \frac{k^2}{A_n(r_1)A_n^{*}(r_2)}\sum_{m=0}^{N} B_m \sum_{p=0}^{N} B_p^{*}$$
$$\times \int_0^L dz \int_0^L dz' \int_{-\infty}^{\infty}\int_{-\infty}^{\infty}\int_{-\infty}^{\infty}\left\langle d\nu(\mathbf{K},z)d\nu^{*}(\mathbf{K}',z')\right\rangle \exp\left(\frac{\gamma\kappa^2(L-z)}{2ik} - \frac{\gamma^{*}\kappa'^2(L-z')}{2ik}\right) \quad (6.26)$$
$$\times \exp\left(i\gamma\mathbf{K}\cdot\mathbf{r}_1 - i\gamma^{*}\mathbf{K}'\cdot\mathbf{r}_2\right) L_m\left[\frac{i\left|\mathbf{K}(L-z)-k\mathbf{r}_1\right|^2}{2kL\left(1+i\alpha_N L\right)}\right] L_p\left[\frac{-i\left|\mathbf{K}'(L-z')-k\mathbf{r}_2\right|^2}{2kL\left(1-i\alpha_N L\right)}\right]$$

where $B_m = \left[\frac{2iL}{k\left(1+i\alpha_N L\right)}\right]^m \frac{1}{W_{N0}{}^{2m}}$. Treating $\left\langle d\nu(\mathbf{K},z)d\nu^{*}(\mathbf{K}',z')\right\rangle$ in the same manner as in §2.8, and using the substitutions $\eta = \frac{1}{2}\left(z+z'\right)$ and $z - z' = \mu,$ and the fact that $z \approx z' \approx \eta$, we can write

$$E_2\left(r_1,r_2\right) = \frac{k^2}{A_n(r_1)A_n^{*}(r_2)}\sum_{m=0}^{N} B_m \sum_{p=0}^{N} B_p^{*}$$
$$\times \int_0^L d\eta \int_{\xi_1}^{\xi_2} d\mu \int_{-\infty}^{\infty}\int d^2\kappa \int_{-\infty}^{\infty}\int d^2\kappa' F_n\left(\mathbf{K},|\mu|\right)\delta\left(\mathbf{K}-\mathbf{K}'\right)\exp\left(\frac{\gamma\kappa^2 - \gamma^{*}\kappa'^2}{2ik}(L-\eta)\right) \quad (6.27)$$
$$\times \exp\left(i\gamma\mathbf{K}\cdot\mathbf{r}_1 - i\gamma^{*}\mathbf{K}'\cdot\mathbf{r}_2\right) L_m\left[\frac{i\left|\mathbf{K}(L-\eta)-k\mathbf{r}_1\right|^2}{2kL\left(1+i\alpha_N L\right)}\right] L_p\left[\frac{-i\left|\mathbf{K}'(L-\eta)-k\mathbf{r}_2\right|^2}{2kL\left(1-i\alpha_N L\right)}\right]$$

which, as a result of the delta function, becomes

$$E_2(r_1,r_2)=\frac{k^2}{A_n(r_1)A_n^*(r_2)}\sum_{m=0}^{N}B_m\sum_{p=0}^{N}B_p^*$$
$$\times\int_0^L d\eta\int_{\xi_1}^{\xi_2}d\mu\int\int_{-\infty}^{\infty}d^2\kappa F_n(\mathbf{K},|\mu|)\exp\left(\frac{\kappa^2(L-\eta)}{2ik}\left(\gamma-\gamma^*\right)\right) \tag{6.28}$$
$$\times\exp\left(i\mathbf{K}\cdot\left(\gamma\mathbf{r}_1-\gamma^*\mathbf{r}_2\right)\right)L_m\left[\frac{i\left|\mathbf{K}(L-\eta)-k\mathbf{r}_1\right|^2}{2kL\left(1+i\alpha_N L\right)}\right]L_p\left[\frac{-i\left|\mathbf{K}(L-\eta)-k\mathbf{r}_2\right|^2}{2kL\left(1-i\alpha_N L\right)}\right]$$

Without loss of generality, we can now extend the limits of integration on μ and change the order of integration to give us

$$E_2(r_1,r_2)=\frac{k^2}{A_n(r_1)A_n^*(r_2)}\sum_{m=0}^{N}B_m\sum_{p=0}^{N}B_p^*$$
$$\times\int_0^L d\eta\int\int_{-\infty}^{\infty}d^2\kappa\exp\left[\frac{\kappa^2(L-\eta)}{2ik}\left(\gamma-\gamma^*\right)\right]\exp\left[i\mathbf{K}\cdot\left(\gamma\mathbf{r}_1-\gamma^*\mathbf{r}_2\right)\right] \tag{6.29}$$
$$\times L_m\left[\frac{i\left|\mathbf{K}(L-\eta)-k\mathbf{r}_1\right|^2}{2kL\left(1+i\alpha_N L\right)}\right]L_p\left[\frac{-i\left|\mathbf{K}(L-\eta)-k\mathbf{r}_2\right|^2}{2kL\left(1-i\alpha_N L\right)}\right]\int_{-\infty}^{\infty}d\mu F_n(\mathbf{K},|\mu|).$$

We have determined the solution to the innermost integration of (6.29) in equation (2.52), resulting in

$$E_2(\mathbf{r}_1,\mathbf{r}_2)=\frac{2\pi k^2}{A_n(r_1)A_n^*(r_2)}\sum_{m=0}^{N}B_m\sum_{p=0}^{N}B_p^*$$
$$\times\int_0^L d\eta\int\int_{-\infty}^{\infty}\Phi_n(\mathbf{K})d^2\kappa\exp\left(\frac{\kappa^2(L-\eta)}{2ik}\left(\gamma-\gamma^*\right)\right)\exp\left(i\mathbf{K}\cdot\left(\gamma\mathbf{r}_1-\gamma^*\mathbf{r}_2\right)\right) \tag{6.30}$$
$$\times L_m\left[\frac{i\left|\mathbf{K}(L-\eta)-k\mathbf{r}_1\right|^2}{2kL\left(1+i\alpha_N L\right)}\right]L_p\left[\frac{-i\left|\mathbf{K}(L-\eta)-k\mathbf{r}_2\right|^2}{2kL\left(1-i\alpha_N L\right)}\right]$$

Further simplification of (6.30) will depend upon the choice of the power spectrum $\Phi_n(\mathbf{K})$.

6.2.2 Computation of $E_3(\mathbf{r}_1,\mathbf{r}_2)$

Recalling, from §2.8, the definition of E_3, we write

$$\begin{aligned}
&E_3(r_1,r_2)=\left\langle \Phi_1(r_1)\Phi_1(r_2)\right\rangle \\
&=\frac{k^2}{A_n(r_1)A_n(r_2)}\sum_{m=0}^{N}B_m\sum_{p=0}^{N}B_p \\
&\times\int_0^L dz\int_0^L dz'\int\int_{-\infty}^{\infty}\int\int_{-\infty}^{\infty}\left\langle d\nu(\mathbf{K},z)d\nu(\mathbf{K}',z')\right\rangle\exp\left(\frac{\gamma\kappa^2(L-z)}{2ik}+\frac{\gamma\kappa'^2(L-z')}{2ik}\right) \\
&\times\exp\left(i\gamma\mathbf{K}\cdot\mathbf{r}_1+i\gamma\mathbf{K}'\cdot\mathbf{r}_2\right)L_m\left[\frac{i\left|\mathbf{K}(L-z)-k\mathbf{r}_1\right|^2}{2kL\left(1+i\alpha_N L\right)}\right]L_p\left[\frac{i\left|\mathbf{K}'(L-z')-k\mathbf{r}_2\right|^2}{2kL\left(1+i\alpha_N L\right)}\right]
\end{aligned} \tag{6.31}$$

Using the fact that n_1 is real, and hence that $\left\langle d\nu(\mathbf{K},z)d\nu(\mathbf{K}',z')\right\rangle=\left\langle d\nu(\mathbf{K},z)d\nu^*(-\mathbf{K}',z')\right\rangle$, along with the same substitutions shown in the computation of E_2, this simplifies to

$$\begin{aligned}
&E_3(r_1,r_2)=\left\langle \Phi_1(r_1)\Phi_1(r_2)\right\rangle=\frac{-k^2}{A_n(r_1)A_n(r_2)}\sum_{m=0}^{N}B_m\sum_{p=0}^{N}B_p \\
&\times\int_0^L d\eta\int_{\xi_1}^{\xi_2}d\mu\int\int_{-\infty}^{\infty}d^2K\int\int_{-\infty}^{\infty}d^2K'F_n\left(\mathbf{K},|\mu|\right)\delta(\mathbf{K}+\mathbf{K}')\exp\left(\frac{\gamma\kappa^2(L-\eta)}{2ik}+\frac{\gamma\kappa'^2(L-\eta)}{2ik}\right) \\
&\times\exp\left(i\gamma\mathbf{K}\cdot\mathbf{r}_1+i\gamma\mathbf{K}'\cdot\mathbf{r}_2\right)L_m\left[\frac{i\left|\mathbf{K}(L-\eta)-k\mathbf{r}_1\right|^2}{2kL\left(1+i\alpha_N L\right)}\right]L_p\left[\frac{i\left|\mathbf{K}'(L-\eta)-k\mathbf{r}_2\right|^2}{2kL\left(1+i\alpha_N L\right)}\right]
\end{aligned} \tag{6.32}$$

and thence to

$$E_3\left(r_1,r_2\right)=\frac{-2\pi k^2}{A_n(r_1)A_n(r_2)}\sum_{m=0}^{N}B_m\sum_{p=0}^{N}B_p$$
$$\times\int_0^L d\eta\int\int_{-\infty}^{\infty}d^2K\,\Phi_n\left(\mathbf{K}\right)\exp\left(\frac{\gamma\kappa^2(L-\eta)}{ik}\right) \tag{6.33}$$
$$\times\exp\left(i\gamma\mathbf{K}\cdot\left(\mathbf{r}_1-\mathbf{r}_2\right)\right)L_m\left[\frac{i\left|\mathbf{K}(L-\eta)-k\mathbf{r}_1\right|^2}{2kL\left(1+i\alpha_N L\right)}\right]L_p\left[\frac{i\left|\mathbf{K}(L-\eta)+k\mathbf{r}_2\right|^2}{2kL\left(1+i\alpha_N L\right)}\right]$$

6.2.3 **On axis values of E_2 and E_3**

We will consider the case where $\mathbf{r}_1=\mathbf{r}_2=0$. The resulting value of E_2 is

$$E_2(0,0)=\frac{2\pi k^2}{\sum_{n=0}^{N}B_n\sum_{q=0}^{N}B_q^*}\sum_{m=0}^{N}B_m\sum_{p=0}^{N}B_p^*\int_0^L d\eta\int\int_{-\infty}^{\infty}d^2\kappa\,\Phi_n\left(\mathbf{K}\right)$$
$$\times\exp\left(\frac{\kappa^2(L-\eta)}{2ik}\left(\gamma-\gamma^*\right)\right)L_m\left[\frac{i\left|\mathbf{K}(L-\eta)\right|^2}{2kL\left(1+i\alpha_N L\right)}\right]L_p\left[\frac{-i\left|\mathbf{K}(L-\eta)\right|^2}{2kL\left(1-i\alpha_N L\right)}\right] \tag{6.34}$$

and the resulting expression for E_3 is

$$E_3(0,0)=\frac{-2\pi k^2}{\sum_{n=0}^{N}B_n\sum_{q=0}^{N}B_q}\sum_{m=0}^{N}B_m\sum_{p=0}^{N}B_p\int_0^L d\eta\int\int_{-\infty}^{\infty}d^2K\,\Phi_n\left(\mathbf{K}\right)$$
$$\times\exp\left[\frac{\gamma\kappa^2(L-\eta)}{ik}\right]L_m\left[\frac{i\left|\mathbf{K}(L-\eta)\right|^2}{2kL\left(1+i\alpha_N L\right)}\right]L_p\left[\frac{i\left|\mathbf{K}(L-\eta)\right|^2}{2kL\left(1+i\alpha_N L\right)}\right] \tag{6.35}$$

Replacing $\Phi_n(\mathbf{K})$ with $\Phi_n(\kappa)$, i.e., assuming the atmosphere is statistically homogeneous and isotropic in each transverse plane where $\eta = \text{constant}$, we can replace all instances of $\mathbf{K}$ with its scalar magnitude κ, and $d^2\kappa = \kappa d\kappa d\theta$. Also, letting $\xi = 1 - \frac{\eta}{L}$, and thus $\gamma = 1 - \left(\bar{\Theta}_N - i\Lambda_N\right)\xi$, where $\Lambda_{N0} = \frac{2L}{kW_{N0}^2}$, $\bar{\Theta}_N = \frac{\Lambda_{N0}^2}{1+\Lambda_{N0}^2}$ and $\Lambda_N = \frac{\Lambda_{N0}}{1+\Lambda_{N0}^2}$, so that $\gamma - \gamma^* = -2i\Lambda_N\xi$, we have

$$E_2(0,0) = \frac{2\pi k^2}{\sum_{n=0}^{N} B_n \sum_{q=0}^{N} B_q^*} \sum_{m=0}^{N} B_m \sum_{p=0}^{N} B_p^* \int_0^1 L d\xi \int_0^{2\pi} d\theta \int_0^{\infty} \kappa d\kappa \, \Phi_n(\kappa) \times \exp\left(\frac{-\kappa^2 L\xi}{k}\left(\Lambda_N \xi\right)\right) L_m\left[\frac{i\left|\kappa L\xi\right|^2}{2kL\left(1+i\alpha_N L\right)}\right] L_p\left[\frac{-i\left|\kappa L\xi\right|^2}{2kL\left(1-i\alpha_N L\right)}\right] \tag{6.36}$$

Performing the integration over θ, the result is

$$E_2(0,0) = \frac{4\pi^2 k^2}{\sum_{n=0}^{N} B_n \sum_{q=0}^{N} B_q^*} \sum_{m=0}^{N} B_m \sum_{p=0}^{N} B_p^* \int_0^1 L d\xi \int_0^{\infty} \kappa d\kappa \, \Phi_n(\kappa) \times \exp\left(\frac{-\kappa^2 L\xi}{k}\left(\Lambda_N \xi\right)\right) L_m\left[\frac{i\left|\kappa L\xi\right|^2}{2kL\left(1+i\alpha_N L\right)}\right] L_p\left[\frac{-i\left|\kappa L\xi\right|^2}{2kL\left(1-i\alpha_N L\right)}\right] \tag{6.37}$$

If we use the Kolmogorov spectrum, $\Phi_n(\kappa) = 0.033 C_n^2 \kappa^{-11/3}$, this simplifies to

$$E_2(0,0) = (0.033)C_n^2 \frac{4\pi^2 k^2}{\sum_{n=0}^{N} B_n \sum_{q=0}^{N} B_q^*} \sum_{m=0}^{N} B_m \sum_{p=0}^{N} B_p^* \int_0^1 L d\xi \int_0^\infty \kappa^{-8/3} d\kappa$$
$$\times \exp\left(\frac{-\kappa^2 L\xi}{k} (\Lambda_N \xi) \right) L_m \left[\frac{i|\kappa L\xi|^2}{2kL(1+i\alpha_N L)} \right] L_p \left[\frac{-i|\kappa L\xi|^2}{2kL(1-i\alpha_N L)} \right] \tag{6.38}$$

A similar treatment of $E_3(0,0)$ results in

$$E_3(0,0) = \frac{-2\pi k^2}{\sum_{n=0}^{N} B_n \sum_{q=0}^{N} B_q} \sum_{m=0}^{N} B_m \sum_{p=0}^{N} B_p \int_0^1 L d\xi \int_{-\infty}^{\infty} \int d^2K \, \Phi_n(\mathbf{K})$$
$$\times \exp\left(\frac{\kappa^2 L\xi \left(1 - (\bar{\Theta}_N + i\Lambda_N)\xi\right)}{ik} \right) L_m \left[\frac{i|\mathbf{K}L\xi|^2}{2kL(1+i\alpha_N L)} \right] L_p \left[\frac{i|\mathbf{K}L\xi|^2}{2kL(1+i\alpha_N L)} \right] \tag{6.39}$$

which can be further simplified to

$$E_3(0,0) = \frac{-4\pi^2 (0.033) k^2 C_n^2}{\sum_{n=0}^{N} B_n \sum_{q=0}^{N} B_q} \sum_{m=0}^{N} B_m \sum_{p=0}^{N} B_p \int_0^1 L d\xi \int_0^\infty \kappa^{-8/3} d\kappa$$
$$\times \exp\left(\frac{\kappa^2 L\xi \left(1 - (\bar{\Theta}_N + i\Lambda_N)\xi\right)}{ik} \right) L_m \left[\frac{i|\kappa^2 L\xi^2|}{2k(1+i\alpha_N L)} \right] L_p \left[\frac{i|\kappa^2 L\xi^2|}{2k(1+i\alpha_N L)} \right]. \tag{6.40}$$

6.2.4 **Computation of $E_1(0,0)$**

To compute E_1, we shall use the phase variance. It has been shown in Chapter 8 of [1] that, for the general Gaussian beam wave, the phase variance is defined by

$$\sigma_p^2 = \frac{1}{2}\mathrm{Re}[E_2(\mathbf{r},\mathbf{r}) - E_3(\mathbf{r},\mathbf{r})] = 2\pi^2 k^2 L \int_0^1 \int_0^\infty \kappa \Phi_n(\kappa) \exp\left(-\frac{\Lambda L \kappa^2 \xi^2}{k}\right) \times \left\{ I_0\left(2\Lambda r \kappa \xi\right) + \cos\left[\frac{L\kappa^2}{k}\xi\left(1-\bar{\Theta}\xi\right)\right]\right\} d\kappa d\xi. \tag{6.41}$$

where I_0 is a modified Bessel function of the first kind and $\bar{\Theta} = 1 - \Theta$. In the limiting case of the plane wave ($\Lambda = 0, \quad \Theta = 1$), this reduces to

$$\sigma_p^2 = 2\pi^2 k^2 L \int_0^1 \int_0^\infty \kappa \Phi_n(\kappa) \left(1 + \cos\left(\frac{L\kappa^2 \xi}{k}\right)\right) d\kappa d\xi. \tag{6.42}$$

The use of the geometric optics approximation $\left(\frac{L\kappa^2}{k} << 1\right)$ allows us to further simplify this to

$$\sigma_p^2 \approx 4\pi^2 k^2 L \int_0^\infty \kappa \Phi_n(\kappa)\, d\kappa \tag{6.43}$$

which is simply $-2E_1(0,0)$. We shall assume the same relationships exist in order to determine a value for $E_1(0,0)$ for the flattened Gaussian beam.

From our computations in §6.2.3, we determined expressions for $E_2(0,0)$ and $E_3(0,0)$ for a flattened Gaussian beam. The value for $E_2(0,0) - E_3(0,0)$ is therefore

$$
\begin{aligned}
E_2(0,0)-E_3(0,0) &= \frac{4\pi^2k^2}{\sum_{n=0}^{N}B_n\sum_{q=0}^{N}B_q^*}\sum_{m=0}^{N}B_m\sum_{p=0}^{N}B_p^*\int_0^1 Ld\xi\int_0^\infty \kappa\Phi_n(\kappa)\,d\kappa \\
&\times\exp\left(\frac{-\kappa^2L\xi}{k}\left(\Lambda_N\xi\right)\right)L_m\left[\frac{i\left|\kappa L\xi\right|^2}{2kL\left(1+i\alpha_NL\right)}\right]L_p\left[\frac{-i\left|\kappa L\xi\right|^2}{2kL\left(1-i\alpha_NL\right)}\right] \\
&+\frac{4\pi^2k^2}{\sum_{n=0}^{N}B_n\sum_{q=0}^{N}B_q}\sum_{m=0}^{N}B_m\sum_{p=0}^{N}B_p\int_0^1 Ld\xi\int_0^\infty \kappa\Phi_n(\kappa)\,d\kappa \\
&\times\exp\left(\frac{\kappa^2L\xi\left(1-(\bar{\Theta}_N+i\Lambda_N)\xi\right)}{ik}\right)L_m\left[\frac{i\left|\kappa^2L\xi^2\right|}{2k\left(1+i\alpha_NL\right)}\right]L_p\left[\frac{i\left|\kappa^2L\xi^2\right|}{2k\left(1+i\alpha_NL\right)}\right]
\end{aligned}
\tag{6.44}
$$

Using the geometric optics approximation, noting that

ξ, $\Lambda_N=\dfrac{\Lambda_{N0}}{1+\Lambda_{N0}^2}$ where $\Lambda_{N0}=\dfrac{2L}{kW_{N0}^2}=\alpha_NL$ and $\bar{\Theta}_N=\dfrac{\Lambda_{N0}^2}{1+\Lambda_{N0}^2}$ are each less than 1, the

integral in each term of the sum simplifies to

$$
\int_0^1 Ld\xi\int_0^\infty \kappa\Phi_n(\kappa)\,d\kappa = L\int_0^\infty \kappa\Phi_n(\kappa)\,d\kappa\,. \tag{6.45}
$$

So we find that

$$
E_2(0,0)-E_3(0,0)=\frac{4\pi^2k^2L}{\sum_{n=0}^{N}B_n}\sum_{m=0}^{N}B_m\int_0^\infty \kappa\Phi_n(\kappa)\,d\kappa\left[\frac{\sum_{p=0}^{N}B_p^*}{\sum_{q=0}^{N}B_q^*}+\frac{\sum_{p=0}^{N}B_p}{\sum_{q=0}^{N}B_q}\right] \tag{6.46}
$$

and hence

$$E_2(0,0) - E_3(0,0) = 8\pi^2 k^2 L \int_0^\infty \kappa \Phi_n(\kappa)\, d\kappa \tag{6.47}$$

If we then assume that, as in the case of the lowest order Gaussian beam,

$\frac{1}{2}\mathrm{Re}\left[E_2(0,0) - E_3(0,0)\right] = -2E_1(0,0)$, we have

$$-4E_1(0,0) \approx 8\pi^2 k^2 L \int_0^\infty \kappa \Phi_n(\kappa)\, d\kappa \tag{6.48}$$

and so

$$E_1(0,0) \approx -2\pi^2 k^2 L \int_0^\infty \kappa \Phi_n(\kappa)\, d\kappa\,. \tag{6.49}$$

6.3 The Scintillation Index

The scintillation index, $\sigma_I^2(L)$, is given as

$$\sigma_I^2(L) = 2\,\mathrm{Re}\left[E_2(0,0) + E_3(0,0)\right] \tag{6.50}$$

where $E_2(0,0)$ and $E_3(0,0)$ are the second order statistical moments given in (6.38) and (6.40), respectively. Substitution of (6.38) and (6.40) into (6.50) results in

$$\sigma_I^2(L) = 2\,\mathrm{Re}\frac{4\pi^2k^2L}{\sum_{n=0}^{N}B_n\sum_{q=0}^{N}B_q^*}\sum_{m=0}^{N}B_m\sum_{p=0}^{N}B_p^*\int_0^1 d\xi\int_0^\infty d\kappa\kappa\Phi_n(\kappa)$$
$$\times\exp\left(\frac{-\kappa^2L\xi}{k}\left(\Lambda_N\xi\right)\right)L_m\left[\frac{i\left|\kappa^2L\xi^2\right|}{2k\left(1+i\alpha_NL\right)}\right]L_p\left[\frac{-i\left|\kappa^2L\xi^2\right|}{2k\left(1-i\alpha_NL\right)}\right]$$
$$-\frac{4\pi^2k^2L}{\sum_{n=0}^{N}B_n\sum_{q=0}^{N}B_q}\sum_{m=0}^{N}B_m\sum_{p=0}^{N}B_p\int_0^1 d\xi\int_0^\infty d\kappa\kappa\Phi_n(\kappa) \tag{6.51}$$
$$\times\exp\left(\frac{\kappa^2L\xi\left(1-(\bar{\Theta}_N+i\Lambda_N)\xi\right)}{ik}\right)L_m\left[\frac{i\left|\kappa^2L\xi^2\right|}{2k\left(1+i\alpha_NL\right)}\right]L_p\left[\frac{i\left|\kappa^2L\xi^2\right|}{2k\left(1+i\alpha_NL\right)}\right].$$

Upon evaluation, for which details are provided in the Appendix, and using the Kolmogorov spectrum, (6.51) simplifies to

$$\sigma_I^2 = 0.4885C_n^2k^{\frac{7}{6}}L^{\frac{11}{6}}\,\mathrm{Re}\left[\frac{\Lambda_N^{\frac{5}{6}}}{\sum_{n=0}^{N}B_n\sum_{q=0}^{N}B_q^*}\sum_{m=0}^{N}\sum_{b=0}^{m}B_m\frac{(-1)^b\,m!\left(\frac{i}{2\Lambda_N\left(1+i\Lambda_{N0}\right)}\right)^b}{(b!)^2(m-b)!}\right.$$
$$\times\sum_{p=0}^{N}\sum_{j=0}^{p}B_p^*\frac{p!\left(\frac{i}{2\Lambda_N\left(1-i\Lambda_{N0}\right)}\right)^j}{(j!)^2(p-j)!}\Gamma\left(-\frac{5}{6}+j+b\right)$$
$$-\frac{(i)^{\frac{5}{6}}}{\sum_{n=0}^{N}B_n\sum_{q=0}^{N}B_q}\sum_{m=0}^{N}\sum_{b=0}^{m}B_m\frac{m!\left(\frac{-1}{2\left(1+i\Lambda_{N0}\right)}\right)^b}{(b!)^2(m-b)!}\sum_{p=0}^{N}\sum_{j=0}^{p}B_p\frac{p!\left(\frac{-1}{2\left(1+i\Lambda_{N0}\right)}\right)^j}{(j!)^2(p-j)!} \tag{6.52}$$
$$\left.\times\Gamma\left(-\frac{5}{6}+j+b\right)\frac{16}{6b+6j+11}\,{}_2F_1\left(-\frac{5}{6}+j+b,\frac{11}{6}+j+b;\frac{17}{6}+j+b;\bar{\Theta}_N+i\Lambda_N\right)\right]$$

in which ${}_2F_1$ is the hypergeometric function. Using the Rytov variance, $\sigma_1^2 = 1.23 C_n^2 k^{7/6} L^{11/6}$, the coefficient is equivalent to $0.397\sigma_1^2$. The case N=0 correctly reduces equation (6.52) to the on-axis scintillation index for the standard Gaussian beam:

$$\sigma_I^2 = 3.86\sigma_1^2 \,\mathrm{Re}\left[i^{5/6} {}_2F_1\left(-\frac{5}{6}, \frac{11}{6}, \frac{17}{6}, \overline{\Theta} + i\Lambda \right) - \frac{11}{16}\Lambda^{5/6} \right]. \tag{6.53}$$

A comparison of the scintillation index with that of the lowest order TEM_{00} Gaussian beam (see Figures 6.1 through 6.4) reveals a "bump" in the index of the flattened Gaussian beam (FGB) which occurs with greater magnitude for successively larger values of N. The scintillation index for the FGB then falls below that of the standard Gaussian beam, gradually increasing in magnitude until it again surpasses it. For a beam radius of small size, the initial bump is quite small and it, as well as the propagation distance for which the scintillation index for the FGB is less than that of the Gaussian beam, occurs close enough to the transmitter (at a distance of 50 meters) that for propagation distances of any significance in free space optical systems there is virtually no difference between the scintillation index of the FGB and the standard Gaussian beam, as seen in Figure 6.1.

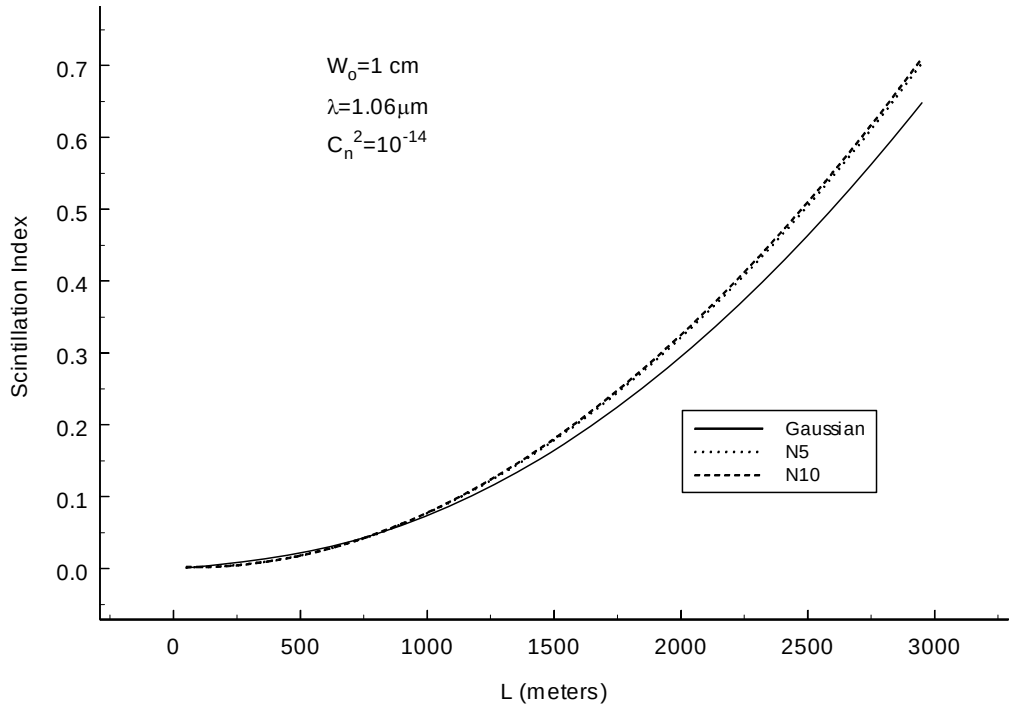

Figure 6.1 The scintillation index of FGBs of order N=5 and N=10 is compared to that of a standard Gaussian beam in the case where $W_0 = 1$ cm.

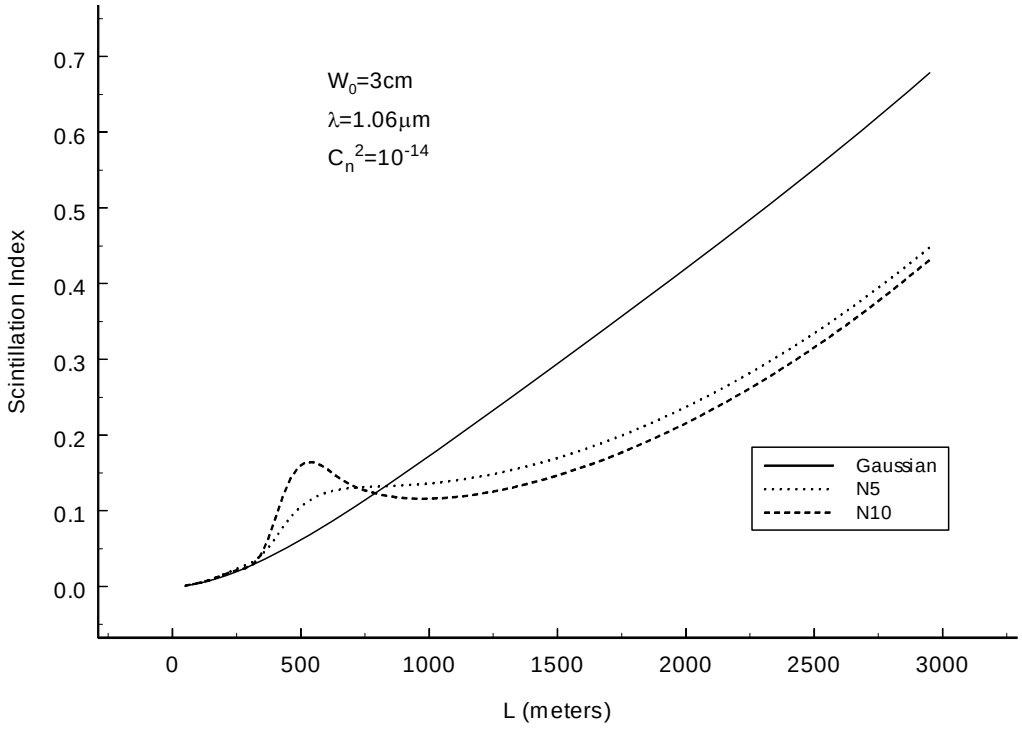

Figure 6.2 The scintillation index of FGBs of order N=5 and N=10 is compared to that of a standard Gaussian beam in the case where $W_0 = 3$ cm.

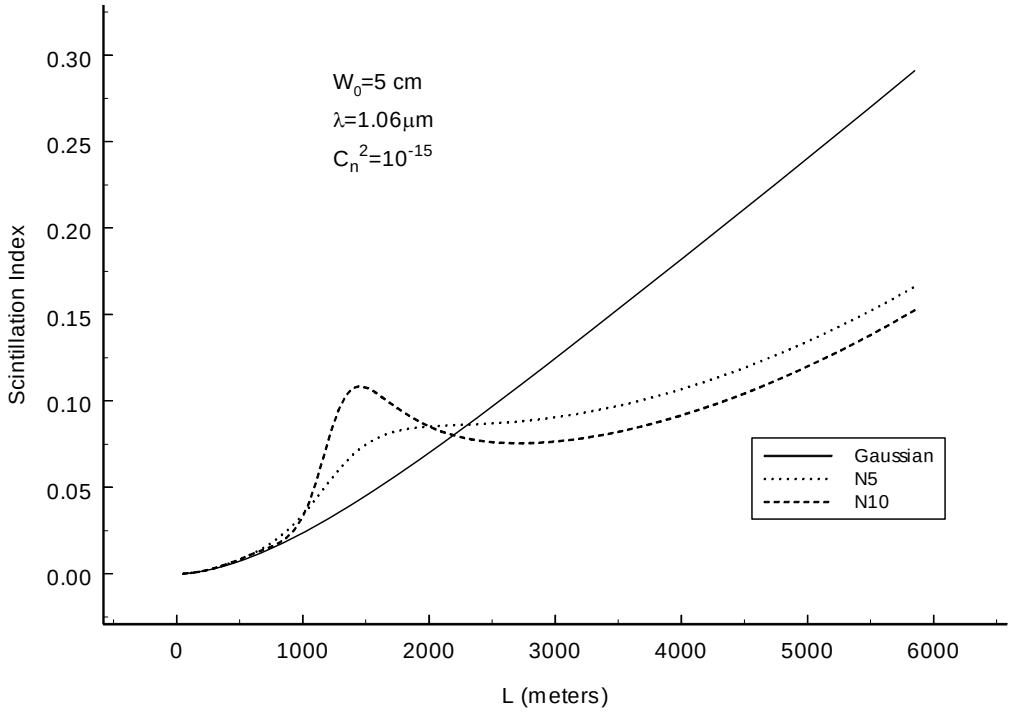

Figure 6.3 The scintillation index of FGBs of order N=5 and N=10 is compared to that of a standard Gaussian beam in the case where $W_0 = 5$ cm.

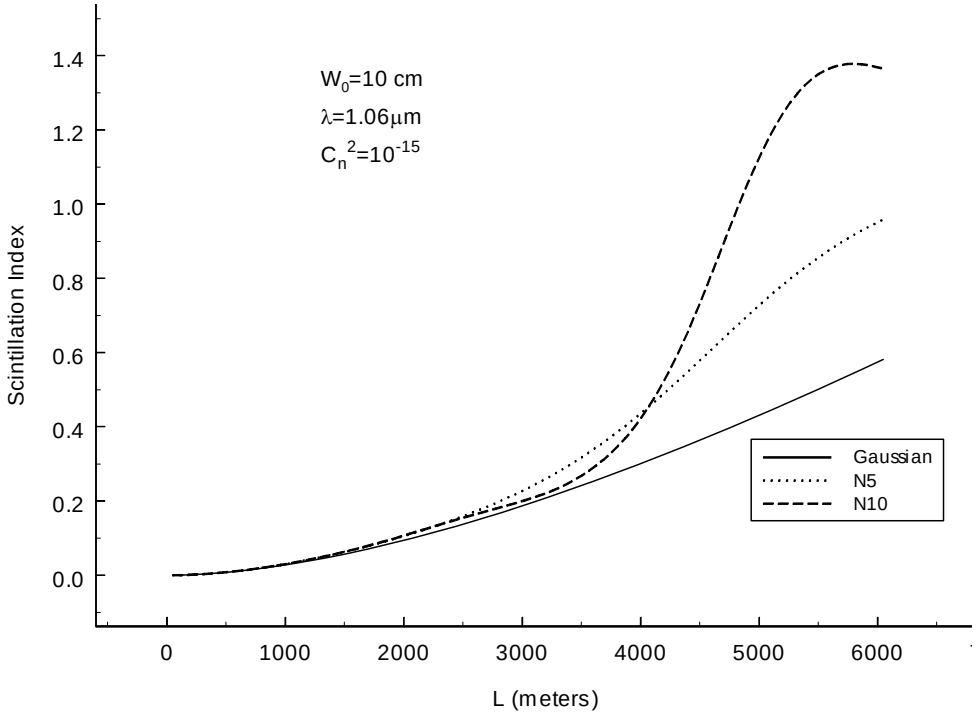

Figure 6.4 The scintillation index of FGBs of order N=5 and N=10 is compared to that of a standard Gaussian beam in the case where $W_0 = 10$ cm.

The distance L at which the "bump" in the scintillation index occurs is increasingly far from the transmitter as the spot size W_o increases. For spot size at the transmitter of 10 cm or larger (see Fig. 6.4), the bump is of considerable size, and we pass the boundary of weak vs. strong fluctuations (which occurs for this beam at approximately 6 kilometers) before the scintillation index for the FGB drops below that of the standard Gaussian beam.

To determine the cause of this initial "bump" in the scintillation index, we noted the occurrence of intensity fluctuations, shown in Figure 5.1, which varied with the order of the FGB. As an example, we show in Figure 6.5 that the distance from the transmitter at which the scintillation index jumps corresponds to a minimum value of the free space intensity of the beam.

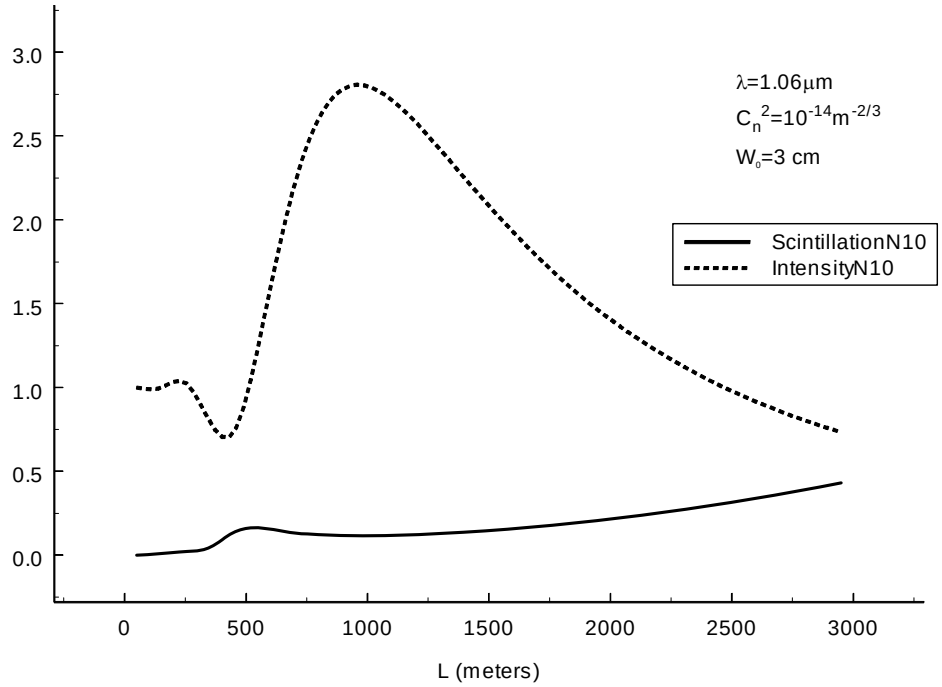

Figure 6.5 Scintillation index compared with free space intensity for a 3 centimeter FGB of order N=10. The correspondence of the local minimum intensity (dotted) with an increase in the scintillation index (solid) is seen.

As the spot size increases and thus the distance from the transmitter at which the increase in scintillation occurs, this intensity reduction tracks the scintillation index increase closely, although it does not correspond precisely. This result is attributable to the graphical comparison of scintillation with free space intensity rather than with beam intensity in the presence of atmospheric turbulence.

We compared the results of the scintillation theory derived above with a numerical simulation of FGBs propagated through the atmosphere. The simulation[24] employed a wave-optics code based on the split-step technique, in which the light waves are propagated in the transformed domain and the effect of atmospheric turbulence along the propagation path is simulated by a series of uncorrelated random phase screens.

The results, plotted in Figures 6.6 through 6.8, demonstrate that the theoretical scintillation index tracked that obtained from the simulated data quite well. The best agreement was in the case of the 5 cm beam (Fig. 6.7). Excellent agreement was also achieved in the case of the 10 cm beam for the first 5 km. (see Fig. 6.8), at which point the realm of strong turbulence was reached when the scintillation index attained a value of unity.

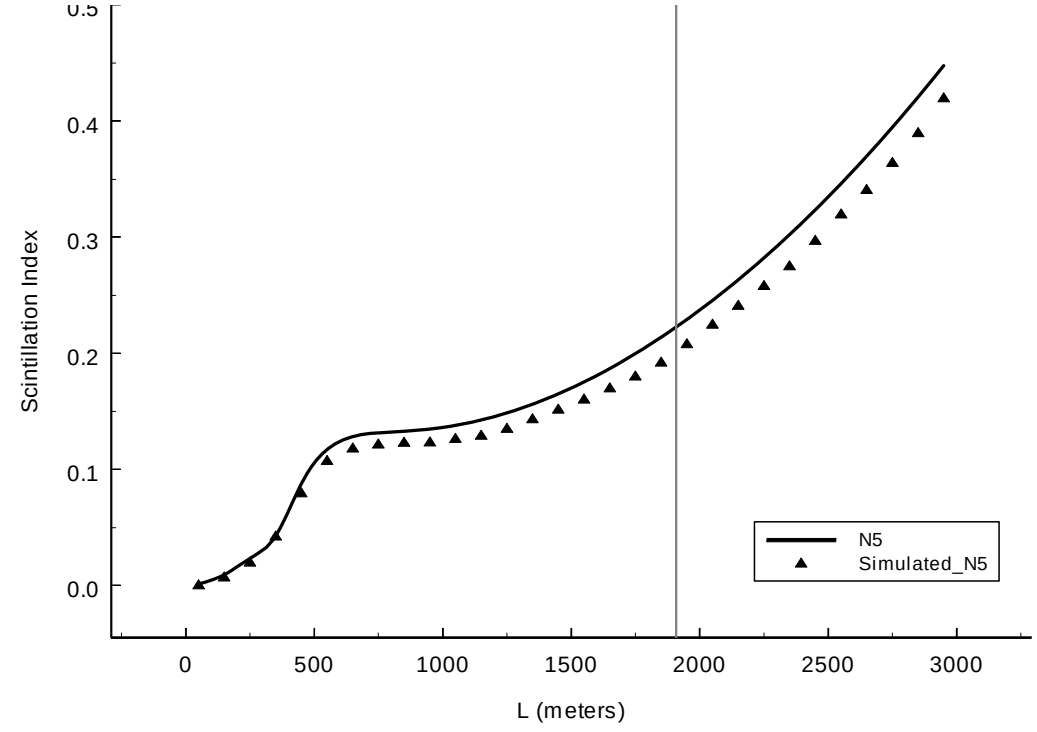

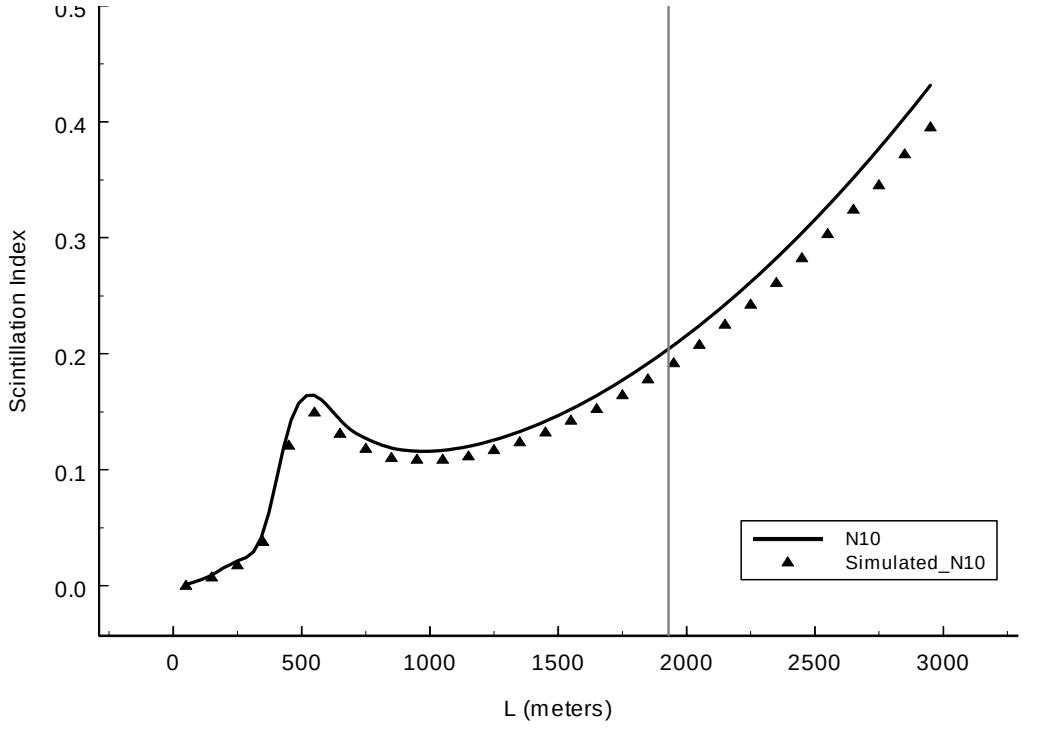

Figure 6.6 A comparison of theoretical and simulated data for the FGBs of order N=5 and N=10 with W_0=3 cm, λ=1.06μm, and $C_n^2=10^{-14}m^{-2/3}$. The vertical line indicates the propagation distance at which the Rytov variance is unity.

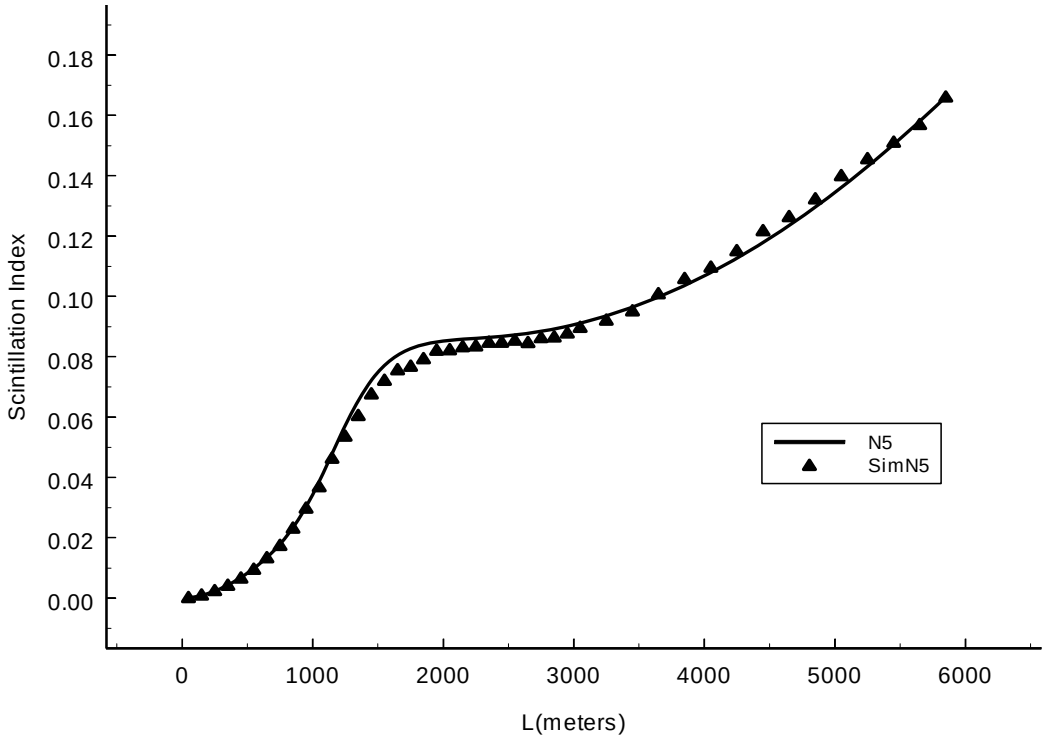

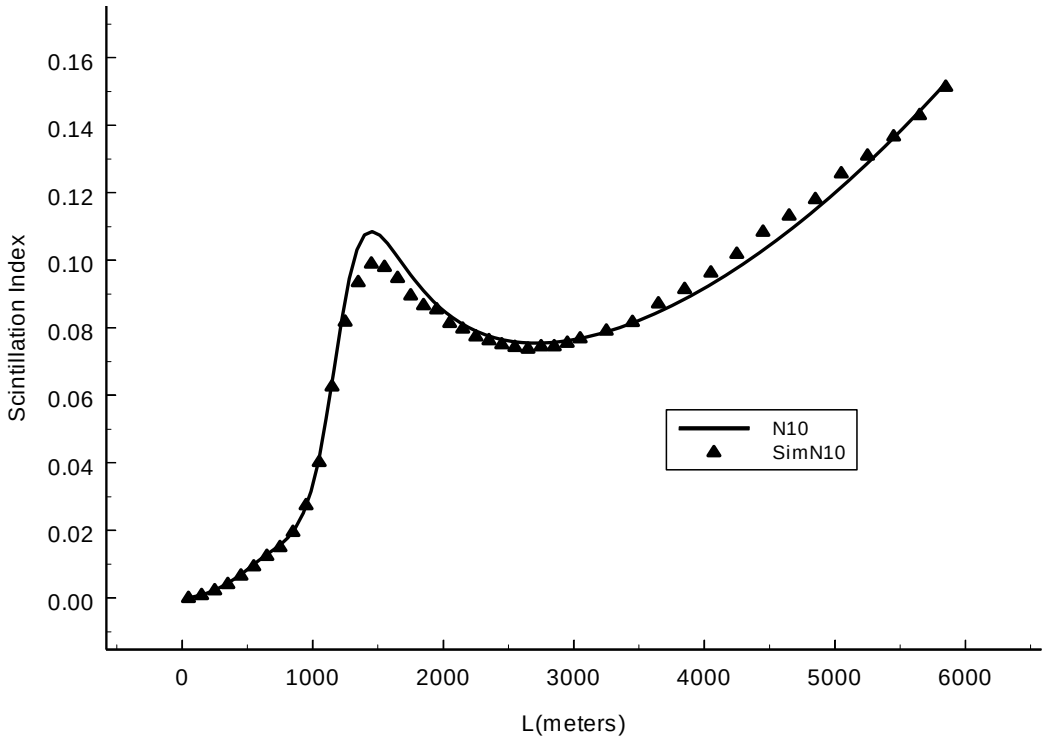

Figure 6.7 A comparison of theoretical and simulated data for the FGBs of order N=5 and N=10 with W_0=5 cm, λ=1.06μm, and $C_n^2=10^{-15}m^{-2/3}$.

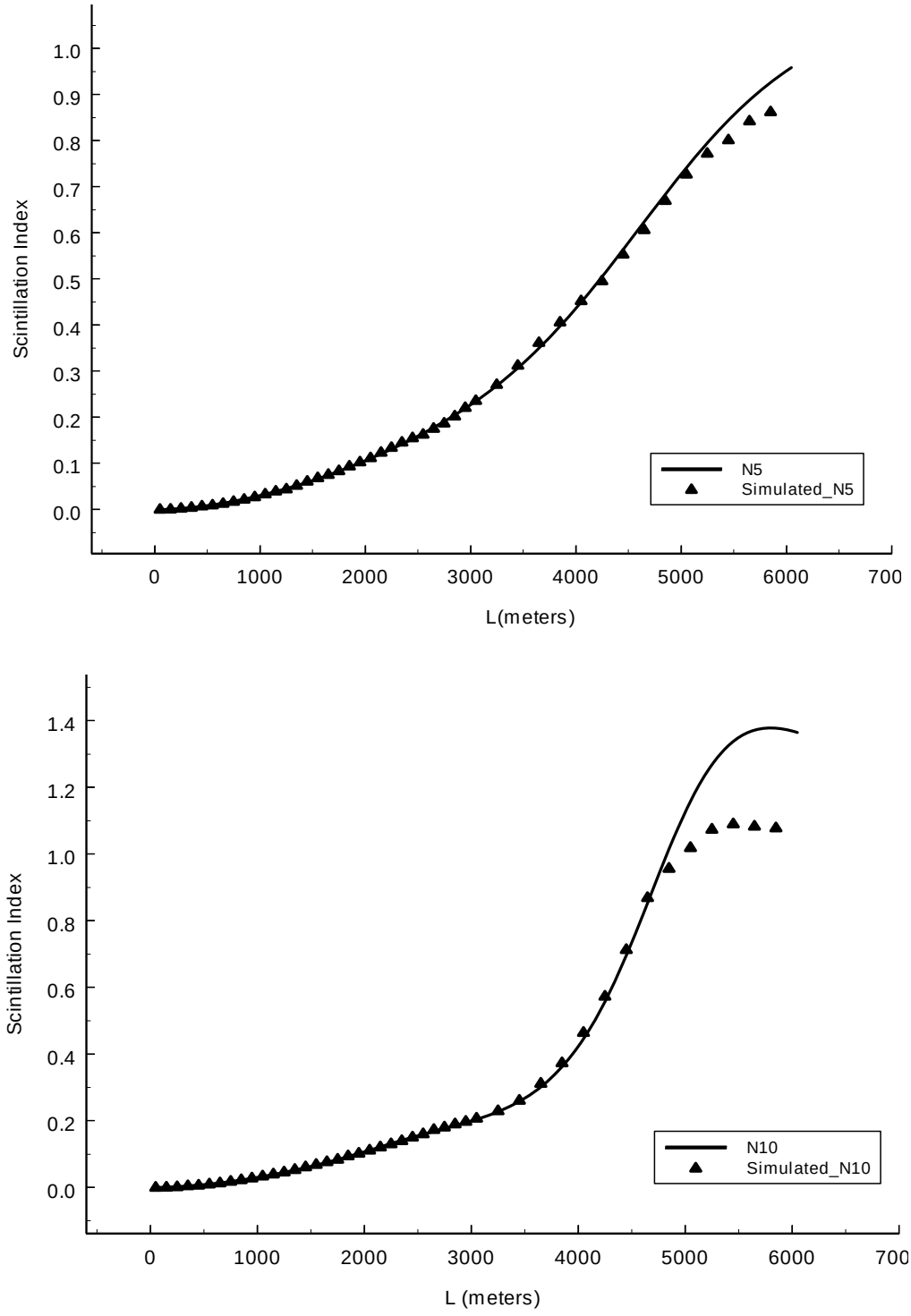

Figure 6.8 A comparison of theoretical and simulated data for the FGBs of order N=5 and N=10 with W_0=10 cm, λ=1.06μm, and $C_n^2=10^{-15}m^{-2/3}$.

It is interesting to compare the results shown here with those published by Baykal and Eyyuboglu [17]. Although the actual numerical results differ in the two studies due to the choice of beam model, both reveal the same "bump" in scintillation index, increasing in magnitude and distance from the transmitter with beam order.

6.4 Fade Statistics

6.4.1 Probability of Fade

Application of a free space optical system (FSO) is contingent upon the ability of the receiver to detect a signal, which can be severely hampered by scintillation. In particular, we are interested in determining the probability that the power at the receiver can be lost as a result of its falling below a specified threshold, known as the fade threshold. We can determine this probability mathematically by use of a probability density function (PDF) of the irradiance defined by

$$\Pr(I \le I_T) = \int_0^{I_T} p_I(I)dI \tag{6.54}$$

Since the work in this paper is restricted to weak scintillation conditions, we use the traditionally accepted lognormal model of the PDF [1]. For this model, the probability of fade becomes

$$\Pr(I \le I_T) = \frac{1}{2}\left\{1 + \operatorname{erf}\left[\frac{\frac{1}{2}\sigma_1^2(0,L) - 0.23F_T}{\sqrt{2}\sigma_1(0,L)}\right]\right\} \tag{6.55}$$

in which $\sigma_1^2(r,L)$ is the scintillation index of the beam, erf refers to the error function, and F_T is the fade threshold parameter defined by

$$F_T = 10\ \log_{10}\left[\frac{\langle I(0,L)\rangle}{I_T}\right]. \tag{6.56}$$

The fade threshold parameter is measured in decibels, and represents the dB level below the on-axis mean irradiance at which the threshold, I_T, is set.

In examining the effects of the order *N* on the probability of fade for a flattened Gaussian beam, we recall from section 6.3 that, for a small beam (1 cm), the scintillation index for a flattened Gaussian beam was nearly the same as for that of the standard Gaussian beam, except for the short range (from 50 meters until approximately 700 meters) when it peaks briefly above the Gaussian, then falls below the Gaussian curve at 100 meters, and lies slightly below it until it becomes and remains nearly Gaussian after 700 meters. This difference is small enough as to be nearly invisible on the long range curves with which we are concerned for FSO systems, and hence we would not expect to see a significant difference between the probability of fade for a Gaussian beam and a flattened Gaussian beam given a 1 centimeter spot size at the transmitter. In fact, as seen in figure 6.9, there is no fade benefit in a flattened beam of this size at the longer range.

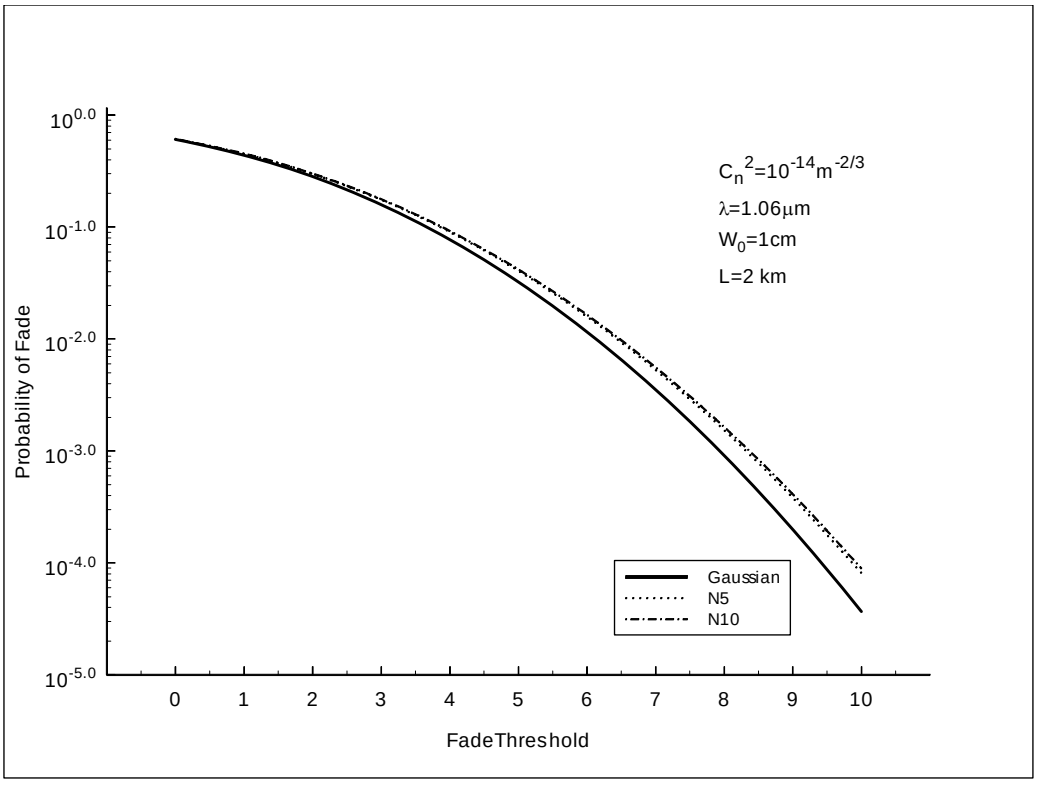

Figure 6.9 Probability of fade as a function of F_T for a 1 cm. beam.

For a 3 centimeter beam, we saw that the scintillation index of the flattened beam initially jumped slightly above that of the standard Gaussian beam, then quickly fell below it, and remained lower until we reached the weak/strong fluctuation boundary, which was at slightly over 2 kilometers for this beam. After this boundary has been exceeded, the weak fluctuation statistics may no longer accurately predict the effect of scintillation on the beam. In figure 6.10, we see the probability of fade for a 3 centimeter Gaussian beam compared with FGBs of order 5 and 10, showing a lowered fade probability for both flattened beams. In this case there is significant improvement.

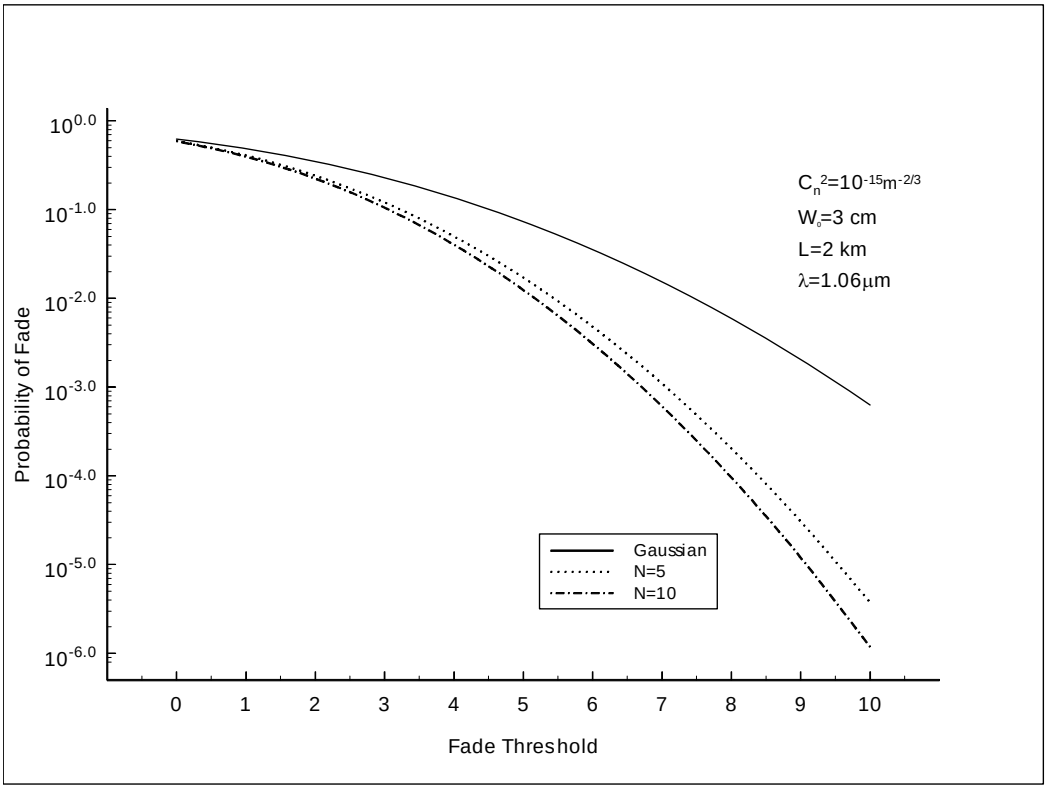

Figure 6.10 The probability of fade as a function of F_T for a 3 cm beam.

In the case of a 5 centimeter beam, we saw a scintillation index with similar properties to that of the 3 centimeter beam, although the distance from the transmitter at which the initial peak occurred was greater for the larger beam. For the 5 centimeter beam, the boundary between weak and strong fluctuations is also farther from the transmitter (>6 km), and so we would expect to see the same fade advantages of the flattened beam over the Gaussian at distances even farther from the transmitter. In figure 6.11, we compare the probability of fade for the 5 centimeter flattened beam at 5 kilometers from the transmitter to that of the same size standard Gaussian beam. As in the case of the 3 centimeter beam, there is significant improvement in the fade probability for the flattened Gaussian beam over the fundamental mode.

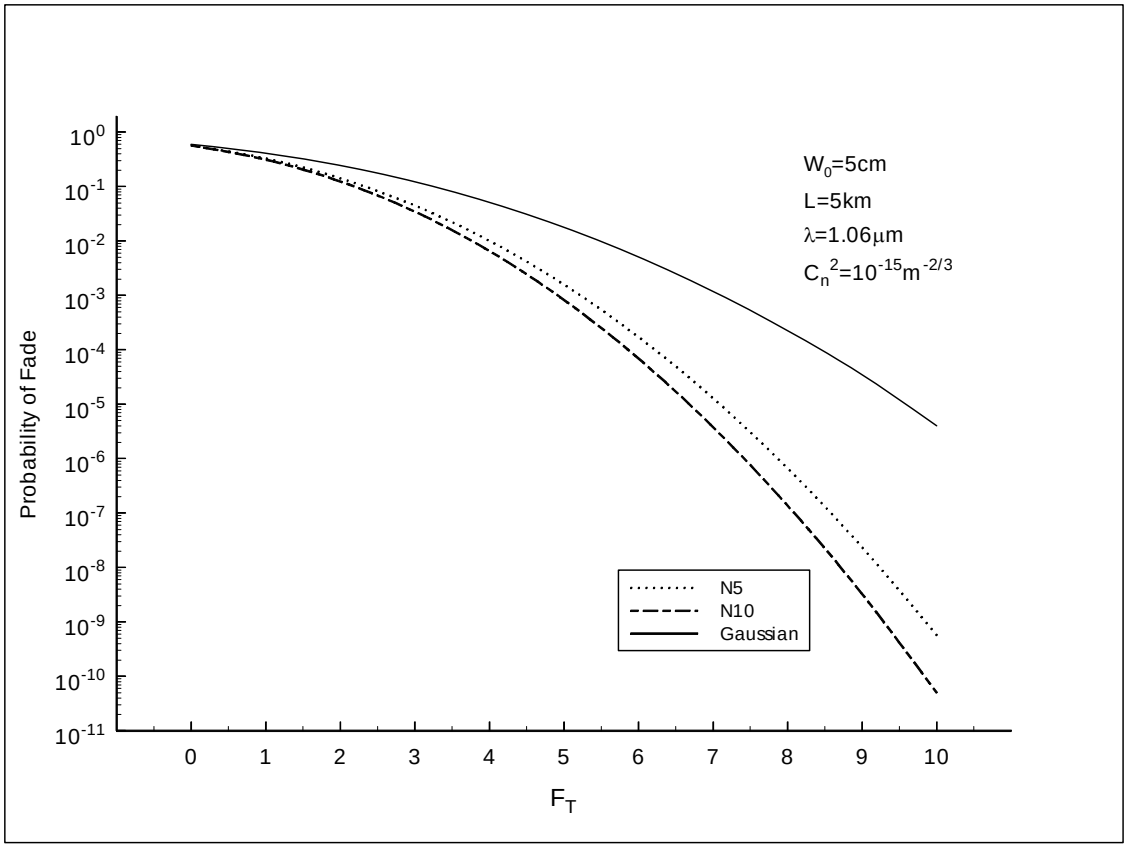

Figure 6.11 The probability of fade as a function of F_T for a 5 cm beam.

For a 10 centimeter FGB, the initial jump in the scintillation index was comparatively large and occurred far enough from the transmitter that we did not see it drop below that of the Gaussian beam before the weak/strong fluctuation boundary was reached. Consequently, we expect no advantage in fade probability under weak fluctuation conditions for a beam of this size.

6.4.2 **Mean Duration of Fade**

To determine the length of time which a signal is "down" in the event of a fade, we first determine the expected number of fades per unit time, $\langle n(I_T)\rangle$. Under weak fluctuation conditions and the lognormal PDF model, this value is given by [1]

$$\langle n(I_T)\rangle = \nu_0 \exp\left[-\frac{\left(\tfrac{1}{2}\sigma_1^2(0,L) - 0.23F_T\right)^2}{2\sigma_1^2(0,L)}\right] \tag{6.57}$$

where ν_0 is the quasi-frequency in Hertz. We shall set ν_0 equal to a constant value of 550 Hz in this model to enable comparisons to be made between the FGBs of various orders.

Once we have determined the probability of fade and the expected number of fades per unit time, the mean duration of fade can be ascertained using the ratio

$$\langle t(I_T)\rangle = \frac{\Pr(I \le I_T)}{\langle n(I_T)\rangle}. \tag{6.58}$$

Figure 6.12 compares the expected number of fades per second for a 3 centimeter Gaussian beam with that of flattened beams of orders 5 and 10 when the beam is propagated a distance of 2 kilometers. Figure 6.13 makes the same comparison for a 5 centimeter beam propagated a distance of 5 kilometers. Figure 6.14 compares the mean

duration of fade for the 3 centimeter FGB with the fade time of the standard Gaussian beam, while figure 6.15 does the same for the 5 centimeter beams.

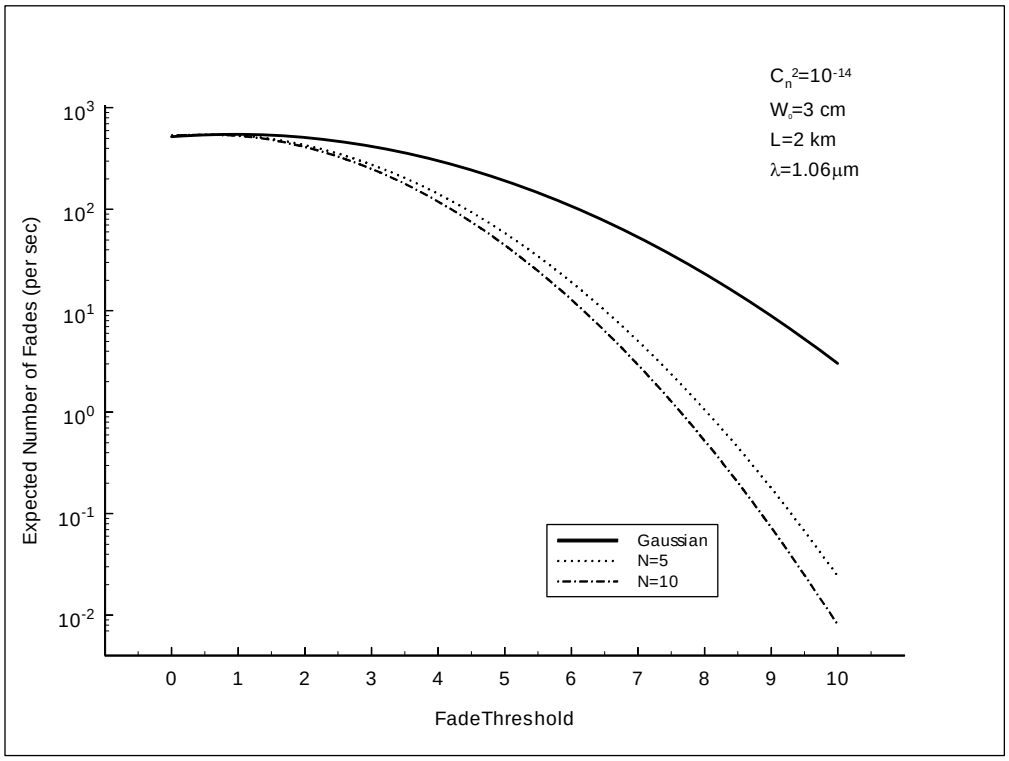

Figure 6.12 The expected number of fades per second for a Gaussian beam with W_0= 3 cm is compared with that of FGBs of order N=5 and N=10.

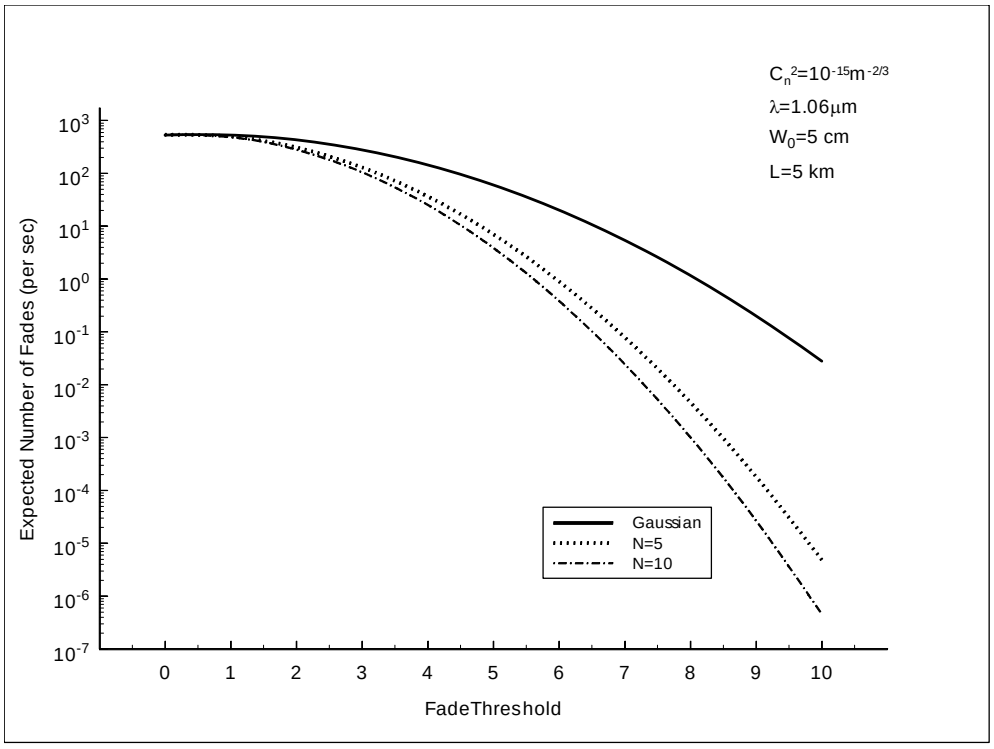

Figure 6.13 The expected number of fades per second for a Gaussian beam with W_0= 5 cm is compared with that of FGBs of order N=5 and N=10.

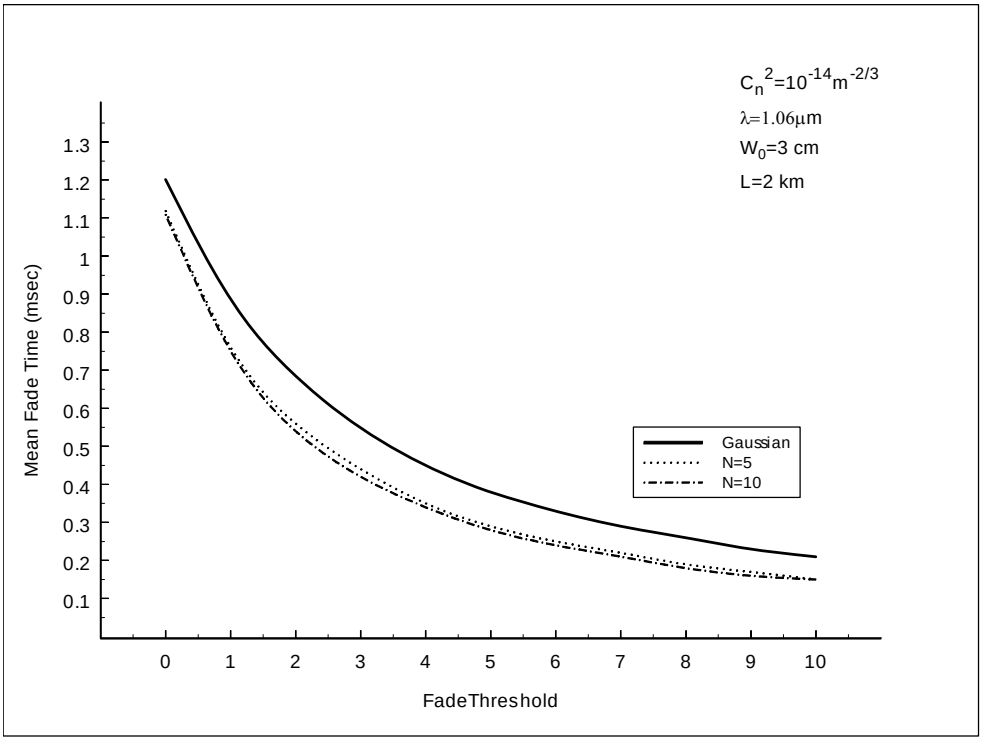

Figure 6.14 Mean duration of fade for the 3 cm. flattened Gaussian beams compared to that of the standard Gaussian beam. Propagation distance is 2 km.

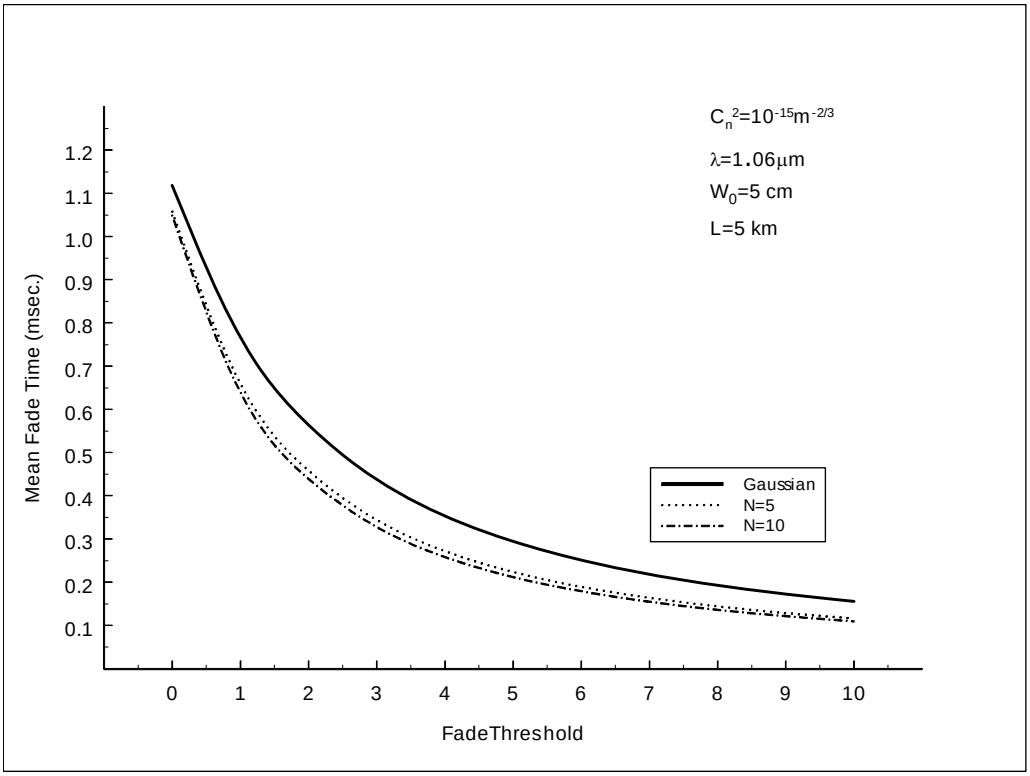

Figure 6.15 Mean duration of fade for the 5 cm. flattened Gaussian beams compared to that of the standard Gaussian beam. Propagation distance is 5 km.

The data shown in figures 6.12 and 6.13 reveal that the number of fades expected per unit time for the flattened Gaussian beam is significantly smaller than that of the standard Gaussian beam. When we examine the mean duration of fade, we find that the flattened beams offer only a slight decrease in duration of fade with each successive order of the beam, and that the beam radius does not significantly affect this fade time. These results are illustrated in figures 6.14 and 6.15.

6.5 Beam Wander

In the presence of atmospheric turbulence, an optical beam will experience random deflections as it propagates through large-scale inhomogeneities. The deflections cause the beam profile to move off the boresight, resulting in a random displacement of the beam "hot spot" (point of maximum irradiance) in the receiver plane. This phenomenon is known as beam wander. It has been determined [1] that beam wander is caused mostly by large-scale turbulence near the transmitter, and for this reason we use the geometric optics approximation, where diffraction effects are neglected, in its computation.

Following the analysis of the free space spot size for the lowest order Gaussian beam [1], the long term spot size of the Flattened Gaussian Beam of order N is $W_{LT}^2 \approx W_N{}^2 + W_N{}^2 T_{SS} + W_N{}^2 T_{LS}$, where the first term is the long term spot size due solely to diffraction, the second term is that due to small-scale spread, and the last term is that due to large-scale beam wander. Hence, we define the beam wander as

$$\left\langle r_c^2 \right\rangle = W_N{}^2 T_{LS} \tag{6.59}$$

where W_N represents the free space beam radius of the FGB of order N at distance L from the transmitter, which is approximately the same as W for the lowest order beam (see Section 5.3) and T_{LS} is the large scale contribution to T, defined as

$$T = -2E_1(0,0) - E_2(0,0)\,. \tag{6.60}$$

From (6.49) and (6.38), we obtain the expressions for $E_1(0,0)$ and $E_2(0,0)$, respectively. Therefore,

$$T = -2E_1(0,0) - E_2(0,0) \approx 4\pi^2 k^2 L \int_0^1 d\xi \int_0^\infty \kappa \Phi_n(\kappa)\, d\kappa$$
$$\times \left[1 - \frac{1}{\sum_{n=0}^{N} B_n \sum_{q=0}^{N} B_q^*} \sum_{m=0}^{N} B_m \sum_{p=0}^{N} B_p^* \right. \tag{6.61}$$
$$\left. \times \exp\left(\frac{-\kappa^2 L\xi}{k}\left(\Lambda_N \xi\right)\right) L_m\left[\frac{i\left|\kappa L\xi\right|^2}{2kL\left(1+i\alpha_N L\right)}\right] L_p\left[\frac{-i\left|\kappa L\xi\right|^2}{2kL\left(1-i\alpha_N L\right)}\right]\right]$$

To determine T_{LS}, we introduce the Large-Scale filter function $\exp\left[-\kappa^2 W_0^2\right]$ to eliminate the effects of small scale contributions, where W_0 is the radius of the standard Gaussian beam at the transmitter. Because it has been determined, in the case of the lowest order Gaussian beam, that beam wander effects occur when the beam is closest to the transmitter, the only beam size necessary to determine beam wander was the initial beam size at the transmitter. Following this reasoning, we have chosen to include only the beam size at the transmitter in our filter function. Further, having established that the spot size of the FGB is very close to that of the lowest order beam, we take $W_{N0} \approx W_0$ and $W_N \approx W$.

This action leads to

$$T_{LS} = 4\pi^2 k^2 L \int_0^1 d\xi \int_0^\infty \kappa \Phi_n(\kappa) \exp[-\kappa^2 W^2(z)]$$
$$\times \{1 - \frac{1}{\sum_{n=0}^{N} B_n \sum_{q=0}^{N} B_q^*} \sum_{m=0}^{N} B_m \sum_{p=0}^{N} B_p^* \tag{6.62}$$
$$\times \exp\left(\frac{-\kappa^2 L\xi}{k}\left(\Lambda_N \xi\right)\right) L_m\left[\frac{i\left|\kappa L\xi\right|^2}{2kL\left(1+i\alpha_N L\right)}\right] L_p\left[\frac{-i\left|\kappa L\xi\right|^2}{2kL\left(1-i\alpha_N L\right)}\right]\Bigg\} d\kappa$$

Therefore, the equation for beam wander is given as

$$\left\langle r_c^2 \right\rangle = 4\pi^2 k^2 L W_N^2 \int_0^1 d\xi \int_0^\infty \kappa \Phi_n(\kappa) \exp[-\kappa^2 W_0^2(z)]$$
$$\times \{1 - \frac{1}{\sum_{n=0}^{N} B_n \sum_{q=0}^{N} B_q^*} \sum_{m=0}^{N} B_m \sum_{p=0}^{N} B_p^* \exp\left(\frac{-\kappa^2 L\xi}{k}\left(\Lambda_N \xi\right)\right) \tag{6.63}$$
$$\times L_m\left[\frac{i\left|\kappa L\xi\right|^2}{2kL\left(1+i\alpha_N L\right)}\right] L_p\left[\frac{-i\left|\kappa L\xi\right|^2}{2kL\left(1-i\alpha_N L\right)}\right]\Bigg\} d\kappa$$

Using $W_N(z) = W_N(0)\sqrt{1+\left[\frac{\lambda z}{\pi W_N^2(0)}\right]^2} = W_N(0)\sqrt{1+\left[\frac{2z}{kW_N^2(0)}\right]^2}$, where $W_N(0)$=W_{N0} and

$W_{N0} = \frac{W_o}{\sqrt{N+1}}$, we have

$$\left\langle r_c^2 \right\rangle = 4\pi^2 k^2 L W_{N0}^2 \left(1 + \left[\frac{2L}{k W_{N0}^2} \right]^2 \right) \int_0^1 d\xi \int_0^\infty \kappa \Phi_n(\kappa) \exp[-\kappa^2 W_0^2]$$
$$\times \{1 - \frac{1}{\sum_{n=0}^{N} B_n \sum_{q=0}^{N} B_q^*} \sum_{m=0}^{N} B_m \sum_{p=0}^{N} B_p^* \exp\left(\frac{-\kappa^2 L \xi}{k} (\Lambda_N \xi) \right) \tag{6.64}$$
$$\times L_m \left[\frac{i|\kappa L \xi|^2}{2kL(1 + i\alpha_N L)} \right] L_p \left[\frac{-i|\kappa L \xi|^2}{2kL(1 - i\alpha_N L)} \right] \Big\} d\kappa$$

Solving the innermost integral in the case of the Kolmogorov spectrum, we again use the geometric optics approximation, which is valid when $\frac{L\kappa^2}{k} << 1$, and deduce that $\exp\left(\frac{-\kappa^2 L \Lambda_N \xi^2}{k} \right) = 1 - \frac{\kappa^2 L \Lambda_N \xi^2}{k}$. Also, each of the Laguerre polynomials can thus be approximated by unity. This last integral can then be rewritten as

$$0.033 C_n^2 \left[\int_0^\infty \kappa^{-8/3} \frac{\kappa^2 L \Lambda_N \xi^2}{k} \exp\left(-\kappa^2 W_0^2 \right) d\kappa \right]$$
$$= 0.033 C_n^2 \left[\frac{L \Lambda_N \xi^2}{2k} \left(W_0^2 \right)^{-1/6} \Gamma\left(1/6 \right) \right] \tag{6.65}$$

We now have

$$\left\langle r_c^2 \right\rangle = 0.132\, \pi^2 k^2 L C_n^2 W_{N0}^2 \left(1 + \left[\frac{2L}{k W_{N0}^2} \right]^2 \right)$$
$$\times \left[\frac{1}{3} \frac{L \Lambda_N}{2k} \left(W_0^2 \right)^{-1/6} \Gamma\left(1/6 \right) \right]. \tag{6.66}$$

If we substitute $\Lambda_N = \frac{\Lambda_{N0}}{1+\Lambda_{N0}^{\ 2}}$ and $\Lambda_{N0} = \frac{2L}{kW_{N0}^2}$ into (6.66), we can reduce (6.66) to

$$\left\langle r_c^2 \right\rangle = .044\pi^2\Gamma\left(\frac{1}{6}\right)L^3C_n^2W_0^{\ -1/3} \approx 2.42L^3C_n^2W_0^{\ -1/3} \tag{6.67}$$

which is essentially independent of the order N of the flattened beam.

A computer simulation study of beam wander for the flattened Gaussian beam reveals the same phenomenon [25]. In the simulation case, beam wander was measured as the root-mean-square beam centroid displacement, while calculated measurements developed in this paper are of the hot spot wander variance. The relation between the two has been established by Andrews [26] for the standard Gaussian beam to be

$$\left\langle \beta_c^2 \right\rangle = 0.56\left\langle r_c^2 \right\rangle, \tag{6.68}$$

in which the root-mean-square beam centroid displacement is represented by $\left\langle \beta_c^2 \right\rangle$. Since the results of these calculations are essentially independent of the beam order, we shall use the same relation for the FGB. A comparison of the simulation results with the theoretical results for a 3 centimeter beam is shown in figure 6.16. Similar results are seen for beams of other sizes.

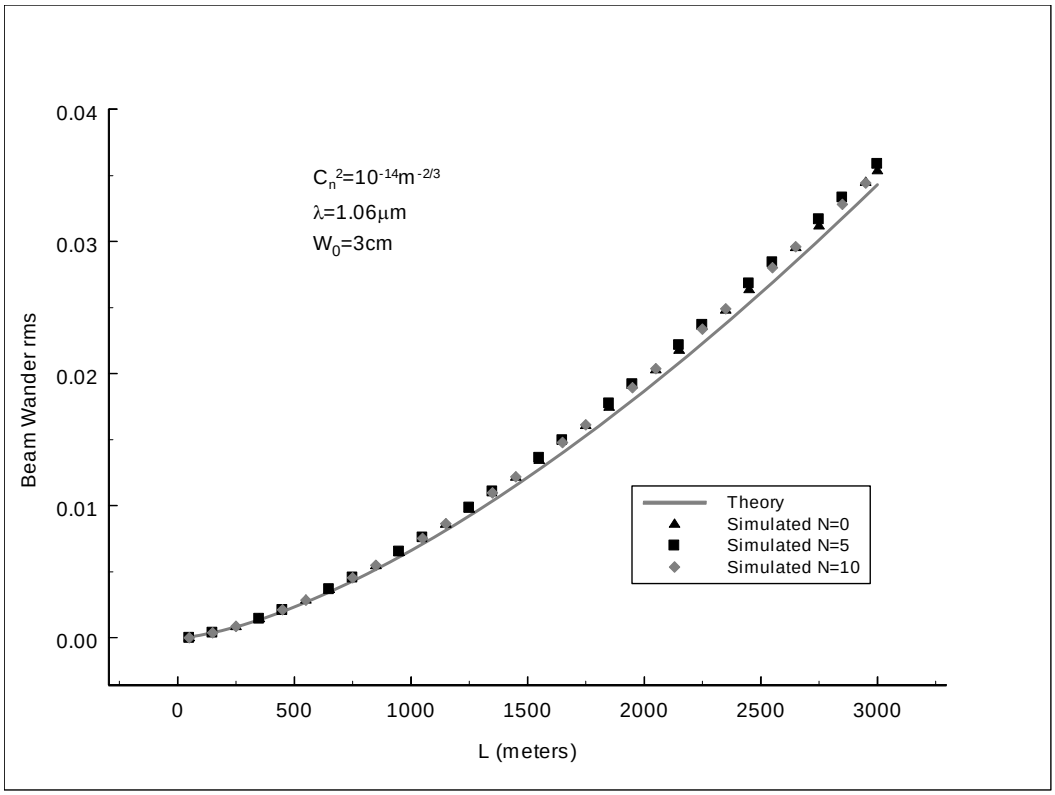

Figure 6.16 A comparison of computer simulated beam wander statistics to those developed for theory.

CHAPTER 7 CONCLUSIONS

7.1 Summary of Contributions

In this dissertation, the effect of atmospheric turbulence on the propagation of a flattened Gaussian beam in conditions of weak fluctuations is examined. In order to do so, we examined the effective spot size of the flattened beam at the transmitter, and developed the first and second order moments of the Rytov approximation. These led us to an analytical expression for the scintillation index, which was then confirmed by comparison to computer simulated data.

This research reveals a lowered scintillation index over that of a standard Gaussian beam for 3 centimeter beams propagated over a distance of 2 kilometers after an initial short-term rise in the scintillation index over that of the fundamental mode. Propagation of a 5 centimeter beam over a distance of 5 kilometers gives similar results. On the other hand, flattened beams of 1 centimeter or less show minimal change in the scintillation of the beam over that of the TEM_{00} mode, while a 10 centimeter flattened beam reveals such a large and protracted initial rise in scintillation over that of the standard Gaussian beam as to be more susceptible to scintillation in the weak regime. Further, it is noted that the index, N, of the flattened beam is critical in determining the magnitude of the difference between the scintillation of the standard Gaussian beam and that of the flattened beam.

We then considered the effect of the scintillation on fade statistics, with the following results:

- No improvement in the probability of fade for a 1 centimeter FGB over that of the standard Gaussian beam was noted. Significant improvement was evident for the 3 centimeter and 5 centimeter beams. There was no improvement in the case of the 10 centimeter flattened beam due to the larger scintillation index of that beam.
- A higher index, N, resulted in a lower probability of fade in the flattened beam. However, as the index increases, the differences between fade probabilities become smaller.
- The expected number of fades was lower for both the 3 and 5 centimeter flattened Gaussian beams than for the fundamental mode, with larger indices further reducing the number of fades.
- In the cases of the 3 and 5 centimeter beams, the mean fade time was lower for a flattened Gaussian beam than it had been for the standard Gaussian beam. The index of the beam did not significantly affect the result.

The beam wander, as determined by the large scale contributions to the long term spot size of the beam, was independent of the index of the beam and therefore identical to that of the fundamental mode in all cases studied. This result was supported by a computer simulation model.

7.2 Future Work

The results shown here have been under weak turbulent conditions, which can be useful in determining the benefits of the flattened beam when operating a free space optical system in, as an example, a mountaintop-to-mountaintop or aircraft-to-aircraft regime over distances of up to 5 kilometers. Venturing into the realm of strong fluctuation conditions will allow us to predict the benefits of the flattened beam for a FSO system operating at ground level or over longer distances.

The calculations done here are based on a constant refractive index structure parameter, applicable in the case of a horizontal propagation path. In order to determine the benefits of the FGB in a satellite laser communication system, the variable C_n^2 which is inherent in vertical (uplink and downlink) and slant paths must be considered, and theory developed for those cases.

The fade statistics in this paper were based on the lognormal model which is the commonly accepted model under weak fluctuation conditions but which has been shown in the case of simulated data to be highly optimistic in predicting fade probabilities. Although this model allowed us to determine that the flattened Gaussian beam offers advantages in the reduction of fade probability and mean duration of fade over the fundamental mode, with the advent of a model which more accurately reflects field or simulated data, these statistics should be recalculated.

APPENDIX:

CALCULATION OF THE SCINTILLATION INDEX

From equation (6.51), we have

$$\sigma_I^2(L) = 2\,\mathrm{Re}\frac{(0.033)C_n^2 4\pi^2 k^2}{\sum_{n=0}^{N} B_n \sum_{q=0}^{N} B_q^*}\sum_{m=0}^{N} B_m \sum_{p=0}^{N} B_p^* \int_0^1 L d\xi \int_0^\infty d\kappa \kappa^{-8/3}$$
$$\times \exp\left(\frac{-\kappa^2 L\xi}{k}\left(\Lambda_N \xi\right)\right) L_m\left[\frac{i\left|\kappa^2 L\xi^2\right|}{2k\left(1+i\alpha_N L\right)}\right] L_p\left[\frac{-i\left|\kappa^2 L\xi^2\right|}{2k\left(1-i\alpha_N L\right)}\right]$$
$$-\frac{4\pi^2(0.033)k^2 C_n^2}{\sum_{n=0}^{N} B_n \sum_{q=0}^{N} B_q}\sum_{m=0}^{N} B_m \sum_{p=0}^{N} B_p \int_0^1 L d\xi \int_0^\infty \kappa^{-8/3} d\kappa \qquad \text{(A.1)}$$
$$\times \exp\left(\frac{\kappa^2 L\xi\left(1-(\bar{\Theta}_N + i\Lambda_N)\xi\right)}{ik}\right) L_m\left[\frac{i\left|\kappa^2 L\xi^2\right|}{2k\left(1+i\alpha_N L\right)}\right] L_p\left[\frac{i\left|\kappa^2 L\xi^2\right|}{2k\left(1+i\alpha_N L\right)}\right]$$

In order to deal with the integral, we shall rewrite the Laguerre polynomials in their summation form. That is,

$$L_m\left[\frac{i\left|\kappa^2 L\xi^2\right|}{2k\left(1+i\alpha_N L\right)}\right] \equiv \sum_{b=0}^{m} \frac{(-1)^b m!\left(\frac{i\left|\kappa^2 L\xi^2\right|}{2k\left(1+i\alpha_N L\right)}\right)^b}{(b!)^2 (m-b)!} \qquad \text{(A.2)}$$

$$L_p\left[\frac{-i\kappa^2 L\xi^2}{2k\left(1-i\alpha_N L\right)}\right] \equiv \sum_{j=0}^{p} \frac{(-1)^j p!\left(\frac{-i\kappa^2 L\xi^2}{2k\left(1-i\alpha_N L\right)}\right)^j}{(j!)^2 (p-j)!} \qquad \text{(A.3)}$$

$$L_p\left[\frac{i\left|\kappa^2 L\xi^2\right|}{2k\left(1+i\alpha_N L\right)}\right] \equiv \sum_{j=0}^{p} \frac{(-1)^j p!\left(\frac{i\left|\kappa^2 L\xi^2\right|}{2k\left(1+i\alpha_N L\right)}\right)^j}{(j!)^2 (p-j)!} \qquad \text{(A.4)}$$

Substituting (A.2), (A.3), and (A.4) into (A.1), we have

$$\sigma_I^2(L) = 2\,\mathrm{Re}\frac{(0.033)C_n^2 4\pi^2 k^2}{\sum_{n=0}^{N} B_n \sum_{q=0}^{N} B_q^*} \sum_{m=0}^{N} B_m \sum_{p=0}^{N} B_p^* \int_0^1 L d\xi \int_0^\infty \kappa^{-8/3} d\kappa$$

$$\times \exp\left(\frac{-\kappa^2 L\xi}{k}\left(\Lambda_N \xi\right)\right) \sum_{b=0}^{m} \frac{(-1)^b m! \left(\frac{i\left|\kappa^2 L\xi^2\right|}{2k\left(1+i\alpha_N L\right)}\right)^b}{\left(b!\right)^2 (m-b)!} \sum_{j=0}^{p} \frac{(-1)^j p! \left(\frac{-i\kappa^2 L\xi^2}{2k\left(1-i\alpha_N L\right)}\right)^j}{\left(j!\right)^2 (p-j)!}$$

$$-\frac{4\pi^2 (0.033) k^2 C_n^2}{\sum_{n=0}^{N} B_n \sum_{q=0}^{N} B_q} \sum_{m=0}^{N} B_m \sum_{p=0}^{N} B_p \int_0^1 L d\xi \int_0^\infty \kappa^{-8/3} d\kappa \qquad \text{(A.5)}$$

$$\times \exp\left(\frac{\kappa^2 L\xi\left(1-(\bar{\Theta}_N + i\Lambda_N)\xi\right)}{ik}\right) \sum_{b=0}^{m} \frac{(-1)^b m! \left(\frac{i\left|\kappa^2 L\xi^2\right|}{2k\left(1+i\alpha_N L\right)}\right)^b}{\left(b!\right)^2 (m-b)!} \sum_{j=0}^{p} \frac{(-1)^j p! \left(\frac{i\left|\kappa^2 L\xi^2\right|}{2k\left(1+i\alpha_N L\right)}\right)^j}{\left(j!\right)^2 (p-j)!}$$

Reversing the order of summation and integration,

$$\sigma_I^2(L) = 2\,\mathrm{Re}\frac{(0.033)C_n^2 4\pi^2 k^2}{\sum_{n=0}^{N} B_n \sum_{q=0}^{N} B_q^*} \sum_{m=0}^{N} B_m \sum_{p=0}^{N} B_p^*$$

$$\times \int_0^1 L d\xi \sum_{b=0}^{m} \frac{(-1)^b m! \left(\frac{i\left|L\xi^2\right|}{2k\left(1+i\alpha_N L\right)}\right)^b}{\left(b!\right)^2 (m-b)!} \sum_{j=0}^{p} \frac{(-1)^j p! \left(\frac{-iL\xi^2}{2k\left(1-i\alpha_N L\right)}\right)^j}{\left(j!\right)^2 (p-j)!}$$

$$\times \int_0^\infty \kappa^{-8/3+2b+2j} \exp\left(\frac{-\kappa^2 L\xi^2 \Lambda_N}{k}\right) d\kappa$$

$$-\frac{4\pi^2 (0.033) k^2 C_n^2}{\sum_{n=0}^{N} B_n \sum_{q=0}^{N} B_q} \sum_{m=0}^{N} B_m \sum_{p=0}^{N} B_p$$

$$\times \int_0^1 L d\xi \sum_{b=0}^{m} \frac{(-1)^b m! \left(\frac{i\left|L\xi^2\right|}{2k\left(1+i\alpha_N L\right)}\right)^b}{\left(b!\right)^2 (m-b)!} \sum_{j=0}^{p} \frac{(-1)^j p! \left(\frac{i\left|L\xi^2\right|}{2k\left(1+i\alpha_N L\right)}\right)^j}{\left(j!\right)^2 (p-j)!}$$

$$\times \int_0^\infty \kappa^{-8/3+2b+2j} \exp\left(\frac{\kappa^2 L\xi\left(1-(\bar{\Theta}_N + i\Lambda_N)\xi\right)}{ik}\right) d\kappa \qquad \text{(A.6)}$$

The integral $\int_0^\infty \kappa^{-8/3+2b+2j} \exp\left(\frac{\kappa^2 L\xi\left(1-(\bar{\Theta}_N + i\Lambda_N)\xi\right)}{ik}\right) d\kappa$ is equal to

$\frac{1}{2}\left[\frac{ik}{L\xi(\xi(\bar{\Theta}_N + i\Lambda_N)-1)}\right]^{-\frac{5}{6}+j+b} \Gamma\left(-\frac{5}{6}+j+b\right)$, while the integral

$\int_0^\infty \kappa^{-8/3+2b+2j} \exp\left(\frac{-\kappa^2 L\xi^2\Lambda_N}{k}\right) d\kappa$ equals $\frac{1}{2}\left(\frac{k}{L\Lambda_N\xi^2}\right)^{-\frac{5}{6}+j+b} \Gamma\left(-\frac{5}{6}+j+b\right)$. The on-axis scintillation index can thus be written

$$
\begin{aligned}
\sigma_I^2(L) = {} & 2\,\mathrm{Re}\frac{(0.033)C_n^2 2\pi^2 k^2}{\sum_{n=0}^{N} B_n \sum_{q=0}^{N} B_q^*} \sum_{m=0}^{N} B_m \sum_{p=0}^{N} B_p^* \\
& \times \int_0^1 L d\xi \sum_{b=0}^{m} \frac{(-1)^b m! \left(\frac{i\left|L\xi^2\right|}{2k\left(1+i\alpha_N L\right)}\right)^b}{\left(b!\right)^2 (m-b)!} \sum_{j=0}^{p} \frac{(-1)^j p! \left(\frac{-iL\xi^2}{2k\left(1-i\alpha_N L\right)}\right)^j}{\left(j!\right)^2 (p-j)!} \\
& \times \left(\frac{k}{L\Lambda_N\xi^2}\right)^{-\frac{5}{6}+j+b} \Gamma\left(-\frac{5}{6}+j+b\right) \\
& - \frac{2\pi^2(0.033)k^2 C_n^2}{\sum_{n=0}^{N} B_n \sum_{q=0}^{N} B_q} \sum_{m=0}^{N} B_m \sum_{p=0}^{N} B_p \\
& \times \int_0^1 L d\xi \sum_{b=0}^{m} \frac{(-1)^b m! \left(\frac{i\left|L\xi^2\right|}{2k\left(1+i\alpha_N L\right)}\right)^b}{\left(b!\right)^2 (m-b)!} \sum_{j=0}^{p} \frac{(-1)^j p! \left(\frac{i\left|L\xi^2\right|}{2k\left(1+i\alpha_N L\right)}\right)^j}{\left(j!\right)^2 (p-j)!} \\
& \times \left[\frac{ik}{L\xi(\xi(\bar{\Theta}_N + i\Lambda_N)-1)}\right]^{-\frac{5}{6}+j+b} \Gamma\left(-\frac{5}{6}+j+b\right)
\end{aligned}
\tag{A.7}
$$

Dealing with the first term of the difference, we have

$$\frac{(0.033)C_n^2 2\pi^2 k^2 L}{\sum_{n=0}^{N} B_n \sum_{q=0}^{N} B_q^*} \sum_{m=0}^{N} B_m \sum_{p=0}^{N} B_p^* \times \sum_{b=0}^{m} \frac{(-1)^b m! \left(\frac{i|L|}{2k(1+i\alpha_N L)} \right)^b}{(b!)^2 (m-b)!} \sum_{j=0}^{p} \frac{(-1)^j p! \left(\frac{-iL}{2k(1-i\alpha_N L)} \right)^j}{(j!)^2 (p-j)!} \Gamma\left(-\frac{5}{6} + j + b \right) \left(\frac{k}{L\Lambda_N} \right)^{-\frac{5}{6}+j+b} \int_0^1 \xi^{\frac{5}{3}} d\xi \tag{A.8}$$

which can be simplified to

$$\frac{3}{8} \frac{(0.033)C_n^2 2\pi^2 k^2 L}{\sum_{n=0}^{N} B_n \sum_{q=0}^{N} B_q^*} \left(\frac{k}{L\Lambda} \right)^{-\frac{5}{6}} \sum_{m=0}^{N} B_m \sum_{p=0}^{N} B_p^* \times \sum_{b=0}^{m} \frac{(-1)^b m! \left(\frac{i}{2\Lambda_N (1+i\alpha_N L)} \right)^b}{(b!)^2 (m-b)!} \sum_{j=0}^{p} \frac{p! \left(\frac{i}{2\Lambda_N (1-i\alpha_N L)} \right)^j}{(j!)^2 (p-j)!} \Gamma\left(-\frac{5}{6} + j + b \right) \tag{A.9}$$

Now, considering the second term in the difference,

$$\frac{2\pi^2(0.033)k^2C_n^2L}{\sum_{n=0}^{N}B_n\sum_{q=0}^{N}B_q}\sum_{m=0}^{N}B_m\sum_{p=0}^{N}B_p$$
$$\times\sum_{b=0}^{m}\frac{(-1)^b m!\left(\frac{i|L|}{2k(1+i\alpha_N L)}\right)^b}{(b!)^2(m-b)!}\sum_{j=0}^{p}\frac{(-1)^j p!\left(\frac{i|L|}{2k(1+i\alpha_N L)}\right)^j}{(j!)^2(p-j)!}\Gamma\left(-\frac{5}{6}+j+b\right) \quad \text{(A.10)}$$
$$\int_0^1 \xi^{2b+2j}\left[\frac{ik}{L\xi(\xi(\bar{\Theta}_N+i\Lambda_N)-1)}\right]^{-\frac{5}{6}+j+b}d\xi$$

The integral in (A.10) can be rewritten as

$$\left[\frac{ik}{L}\right]^{-\frac{5}{6}+j+b}\int_0^1 \xi^{2b+2j}\left[\xi(\xi(\bar{\Theta}_N+i\Lambda_N)-1)\right]^{\frac{5}{6}-j-b}d\xi =$$
$$\left[\frac{ik}{L}\right]^{-\frac{5}{6}+j+b}\int_0^1 \xi^{\frac{5}{6}+b+j}\left[(\xi(\bar{\Theta}_N+i\Lambda_N)-1)\right]^{\frac{5}{6}-j-b}d\xi \quad \text{(A.11)}$$

Making use of Integral 4 in Appendix 2 of Andrews and Phillips[1], (A.11) is equal to

$$(-1)^{\frac{5}{6}-j-b}\left(\frac{ik}{L}\right)^{-\frac{5}{6}+j+b}\frac{1}{b+j+\frac{11}{6}}\,{}_2F_1\left(-\frac{5}{6}+j+b,\frac{11}{6}+j+b;\frac{17}{6}+j+b;\bar{\Theta}_N+i\Lambda_N\right) \quad \text{(A.12)}$$

Hence, (A.10) is equivalent to

$$\frac{2\pi^2(0.033)k^{\frac{7}{6}}L^{\frac{11}{6}}(i)^{\frac{5}{6}}C_n^2}{\sum_{n=0}^{N}B_n\sum_{q=0}^{N}B_q}\sum_{m=0}^{N}B_m\sum_{p=0}^{N}B_p$$
$$\times\sum_{b=0}^{m}\frac{m!\left(\frac{-1}{2(1+i\alpha_N L)}\right)^b}{(b!)^2(m-b)!}\sum_{j=0}^{p}\frac{p!\left(\frac{-1}{2(1+i\alpha_N L)}\right)^j}{(j!)^2(p-j)!}\Gamma\left(-\frac{5}{6}+j+b\right) \tag{A.13}$$
$$\times\frac{1}{b+j+\frac{11}{6}}\,{}_2F_1\left(-\frac{5}{6}+j+b,\frac{11}{6}+j+b;\frac{17}{6}+j+b;\bar{\Theta}_N+i\Lambda_N\right)$$

We can thus write the on-axis scintillation index as

$$\sigma_I^2=2\,\mathrm{Re}\left[\begin{array}{l}\frac{\frac{3}{8}(0.033)C_n^2 2\pi^2k^{\frac{7}{6}}L^{\frac{11}{6}}\Lambda_N^{\frac{5}{6}}}{\sum_{n=0}^{N}B_n\sum_{q=0}^{N}B_q^*}\sum_{m=0}^{N}\sum_{b=0}^{m}B_m\frac{(-1)^b m!\left(\frac{i}{2\Lambda_N(1+i\alpha_N L)}\right)^b}{(b!)^2(m-b)!}\\ \times\sum_{p=0}^{N}\sum_{j=0}^{p}B_p^*\frac{p!\left(\frac{i}{2\Lambda_N(1-i\alpha_N L)}\right)^j}{(j!)^2(p-j)!}\Gamma\left(-\frac{5}{6}+j+b\right)\\ -\frac{2\pi^2(0.033)k^{\frac{7}{6}}L^{\frac{11}{6}}(i)^{\frac{5}{6}}C_n^2}{\sum_{n=0}^{N}B_n\sum_{q=0}^{N}B_q}\sum_{m=0}^{N}\sum_{b=0}^{m}B_m\frac{m!\left(\frac{-1}{2(1+i\alpha_N L)}\right)^b}{(b!)^2(m-b)!}\\ \times\sum_{p=0}^{N}\sum_{j=0}^{p}B_p\frac{p!\left(\frac{-1}{2(1+i\alpha_N L)}\right)^j}{(j!)^2(p-j)!}\Gamma\left(-\frac{5}{6}+j+b\right)\\ \times\frac{1}{b+j+\frac{11}{6}}\,{}_2F_1\left(-\frac{5}{6}+j+b,\frac{11}{6}+j+b;\frac{17}{6}+j+b;\bar{\Theta}_N+i\Lambda_N\right)\end{array}\right] \tag{A.14}$$

or, factoring out the common coefficients,

$$0.4885C_n^2 k^{\frac{7}{6}} L^{\frac{11}{6}} \operatorname{Re}\left\{ \frac{\Lambda_N^{\frac{5}{6}}}{\sum_{n=0}^{N} B_n \sum_{q=0}^{N} B_q^*} \sum_{m=0}^{N}\sum_{b=0}^{m} B_m \frac{(-1)^b m! \left(\frac{i}{2\Lambda_N (1+i\alpha_N L)} \right)^b}{(b!)^2 (m-b)!} \right.$$

$$\times \sum_{p=0}^{N}\sum_{j=0}^{p} B_p^* \frac{p! \left(\frac{i}{2\Lambda_N (1-i\alpha_N L)} \right)^j}{(j!)^2 (p-j)!} \Gamma\left(-\frac{5}{6} + j + b \right)$$

$$- \frac{(i)^{\frac{5}{6}}}{\sum_{n=0}^{N} B_n \sum_{q=0}^{N} B_q} \sum_{m=0}^{N}\sum_{b=0}^{m} B_m \frac{m! \left(\frac{-1}{2(1+i\alpha_N L)} \right)^b}{(b!)^2 (m-b)!} \sum_{p=0}^{N}\sum_{j=0}^{p} B_p \frac{p! \left(\frac{-1}{2(1+i\alpha_N L)} \right)^j}{(j!)^2 (p-j)!}$$

$$\left. \times \frac{16\Gamma\left(-\frac{5}{6} + j + b \right)}{6b + 6j + 11} {}_2F_1\left(-\frac{5}{6} + j + b, \frac{11}{6} + j + b; \frac{17}{6} + j + b; \overline{\Theta}_N + i\Lambda_N \right) \right\} \qquad \text{(A.15)}$$

REFERENCES

[1] L.C. Andrews and R.L. Phillips, *Laser Beam Propagation Through Random Media, 2nd ed.* (SPIE, Washington,2005).

[2] Y. Baykal, "Correlation and structure functions for multimode-laser-beam incidence in atmospheric turbulence," *Journal of the Optical Society of America A* **4,** 817-819(1987).

[3] Y. Baykal, "Correlation and structure functions of Hermite-sinusoidal-Gaussian laser beams in a turbulent atmosphere," *Journal of the Optical Society of America A* **21**, 1290-1299(2004).

[4] H. T. Eyyuboglu and Y. Baykal, "Analysis of reciprocity of cos-Gaussian and cosh-Gaussian laser beams in a turbulent atmosphere," *Optics Express* **12,** 4569(2004).

[5] W.H. Carter, "Spot size and divergence for Hermite Gaussian beams of any order", *Applied Optics* **19**, 1027-1029 (1980).

[6] S. Saghafi and C.J.R. Sheppard, "Near field and far field of elegant Hermite-Gaussian and Laguerre-Gaussian modes", *Journal of Modern Optics* **45**, 1999-2009 (1998).

[7] C. Y. Young, Y. Gilchrist, and B. R. Macon, "Turbulence induced beam spreading of higher order mode optical waves," *Optical Engineering* **41,** 1097-1103 (2002).

[8] R.L. Phillips and L.C. Andrews, "Spot size and divergence for Laguerre Gaussian beams of any order," *Applied Optics* **22**, 643-644 (1983).

[9] M. Santarsiero and R. Borghi, "Correspondence between super-Gaussian and flattened Gaussian beams," *Journal of the Optical Society of America A* **16,** 188-190 (1999).

[10] B. Lu, S. Luo, and X. Ji, "A further comparative study of flattened Gaussian beams and super-Gaussian beams," *Journal of Modern Optics* **48,** 371-377 (2001).

[11] F. Gori, "Flattened Gaussian beams," *Optics Communications* **107,** 335-341 (1994).

[12] V. Bagini, R. Borghi, F. Gori, A.M. Pacileo, and M. Santarsiero, "Propagation of axially symmetric flattened Gaussian beams," *Journal of the Optical Society of America A* **13,** 1385-1394 (1996).

[13] M. Santarsiero, D. Aiello, R. Borghi, and S. Vicalvi, "Focusing of axially symmetric flattened Gaussian beams," *Journal of Modern Optics* **44**, 633-650 (1997).

[14] A.A. Tovar, "Propagation of flat-topped multi-Gaussian laser beams", *Journal of the Optical Society of America A* **18,** 1897-1904 (2001).

[15] B. Lu, B. Zhang, and S. Luo, "Far-field intensity distribution, M^2 factor, and propagation of flattened Gaussian beams," *Applied optics* **38**, 4581-4584 (1999).

[16] B. Lu and S. Luo, "The pointing stability of flattened Gaussian beams," *Journal of Modern Optics* **49**, 1089-1094(2002).

[17] Y. Baykal and H. T. Eyyuboglu, "Scintillation index of flat-topped Gaussian beams", *Applied Optics* **45**, 3793-3797(2006).

[18] H. Eyyuboglu, C. Arpali, and Y. Baykal, "Flat topped beams and their characteristics in turbulent media", *Optics Express* **14**, 4196-4207(2006).

[19] Y. Cai, "Propagation of various flat-topped beams in a turbulent atmosphere", *Journal of Optics A: Pure and Applied Optics* **8**, 537-545 (2006).

[20] L. C. Andrews, R. L. Phillips, and C. Y. Hopen, *Laser Beam Scintillation with Applications* (SPIE, Washington, 2001).

[21] A.E. Siegman, *Lasers* (University Science, Mill Valley, Calif., 1986).

[22] L.C. Andrews, *Special Functions in Mathematics for Engineers*(SPIE, Washington, 1988).

[23] I.S. Gradshteyn and I.M. Ryzhik, *Table of Integrals, Series, and Products; 5th edition* (Academic Press, San Diego, Calif., 1994).

[24] D.C.Cowan, J. Recolons, L.C. Andrews, and C. Y. Young, "Propagation of flattened Gaussian beams in the atmosphere: a comparison of theory with a computer simulation model", Proc. SPIE **6215** (2006).

[25] Computer simulations courtesy of J. Recolons.

[26] J. Recolons, L.C. Andrews, and R.L. Phillips, "Analysis of beam wander effects for a horizontal-path propagating Gaussian beam wave: Part I – Collimated beam case", *To be published.*